2 (mix)

ABSTRACT

Long, Sheila Ann Thibeault. Triangulation Error Analysis for the Barium Ion Cloud Experiment. (Under the direction of Dr. Edward R. Manring.)

The triangulation method developed at the NASA, Langley Research Center specifically for the Barium Ion Cloud Project is discussed. Expressions for the four displacement errors, the three slope errors, and the curvature error in the triangulation solution due to a probable error in the lines-of-sight from the observation stations to points on the cloud are derived. The triangulation method is then used to determine the effect of the following on these different errors in the solution: the number and location of the stations, the observation duration, east-west cloud drift, the number of input data points, and the addition of extra cameras to one of the stations. The pointing displacement errors are compared, and the pointing slope errors are compared. The displacement errors in the solution due to a probable error in the position of a moving station plus the weighting factors for the data from the moving station are also determined.

TRIANGULATION ERROR ANALYSIS FOR THE BARIUM ION CLOUD EXPERIMENT

by

SHEILA ANN THIBEAULT LONG

A thesis submitted to the Graduate Faculty of
North Carolina State University at Raleigh
in partial fulfillment of the
requirements for the Degree of
Master of Science

DEPARTMENT OF PHYSICS

RALEIGH

1 9 7 3

APPROVED BY:

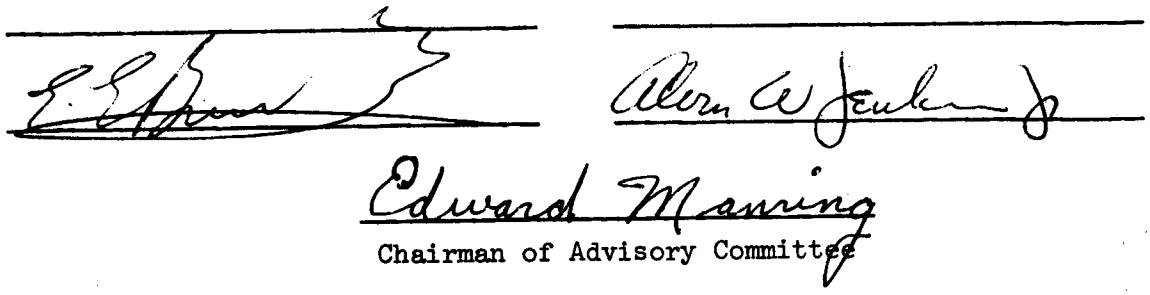

Edward Manning
Chairman of Advisory Committee

BIOGRAPHY

Sheila Ann Thibeault Long was born [redacted] She received her elementary and secondary education in Richmond, Virginia, graduating from John Marshall High School in June 1962.

She entered the College of William and Mary, Williamsburg, Virginia, in September 1962. At William and Mary she received a four-year Virginia State Teacher's Scholarship plus three National Science Foundation Undergraduate Research Grants. She was made a member of the following national collegiate fraternities — Phi Beta Kappa, Sigma Pi Sigma, Kappa Delta Pi, and Delta Delta Delta. She was the president and soloist of Orchesis, the modern dance group at the college. She student-taught the P.S.S.C. physics courses at York High School in Yorktown, Virginia. She received the Bachelor of Science degree with a major in physics and a Virginia State Teacher's Certificate for Secondary Education from William and Mary in June 1966.

Having first worked at the National Aeronautics and Space Administration, Langley Research Center (NASA, LRC) during the summer between her junior and senior years in college, she returned there in August 1966 to become a permanent member of their research staff. At Langley she has helped develop their holographic capability and has also done studies in vision research. Presently she is in their Environmental and Space Sciences Division, Space Physics Branch, Magnetospheric Physics Section doing research on the Barium Ion Cloud Project. She is the

first and present chairman of the Langley Colloquium Series. She is a member of the Optical Society of America and the American Institute of Aeronautics and Astronautics. In the November 1971 issue of "New Woman" magazine, she was saluted as one of the "26 Young Women Who Made It Big In Their Twenties"; and she was chosen to appear in the "1972 Edition of Outstanding Young Women of America."

She began her graduate study in physics on a part-time basis at the College of William and Mary in September 1966. From January 1968 to June 1969, she was on graduate study leave from NASA, LRC to do full-time graduate study in physics at North Carolina State University (NCSU), Raleigh, North Carolina. At NCSU she was made a member of Phi Kappa Phi.

She was married to Edward R. Long, Jr., also a physicist, on June 8, 1968. She and her husband reside in Hampton, Virginia, where they both work at the Langley Research Center. She is a member of the Back River Area Civic League; the Hampton Roads Civic Ballet Company; the Junior Woman's Club of Hampton, Inc.; and the Women's Auxiliary of the Hampton Roads Power Squadron.

ACKNOWLEDGMENTS

The author sincerely thanks Mr. David Adamson and Dr. Clifford L. Fricke - both of the National Aeronautics and Space Administration, Langley Research Center - who formulated the idea for this study and who provided invaluable assistance throughout its entire undertaking.

Sincere appreciation is extended to Dr. Edward R. Manring, chairman of her advisory committee, for all of his guidance and advice and to the other members of the committee, Dr. Alvin W. Jenkins and Dr. Ernest E. Burniston, for their good criticism and helpful suggestions.

This work was funded entirely by the National Aeronautics and Space Administration.

Lastly, many thanks are given to her parents Mr. and Mrs. William R. Thibeault for their faith and to her husband Edward R. Long, Jr., for his patience and inspiration.

TABLE OF CONTENTS

LIST OF TABLES

LIST OF FIGURES

Page

Page

Page

INTRODUCTION

Charged particles radiated from the sun flow toward and enshroud the earth's insulating atmosphere, enclosing the earth's magnetic field within, thus forming the earth's magnetosphere. Up to the present, much data has been collected on the earth's magnetic field within the magnetosphere from satellite-borne magnetometers. However, data on the earth's electric field within the magnetosphere is lacking. In order to understand such dynamic phenomena as geomagnetic storms (which greatly interfer with communications), aurorae, etc., this void must be filled. For this purpose the National Aeronautics and Space Administration (NASA) and the Max Planck Institute, Institute for Physics and Astrophysics, Institute for Extraterrestrial Physics (MPE) jointly formulated the "NASA/MPE Barium Ion Cloud (BIC) Project."

A payload of 1.6 kilograms of neutral barium is released from a four-stage Scout rocket at an altitude of about 31,633 kilometers, or approximately five earth radii. Figure 1 is a photograph of a neutral (spherical) barium cloud. The neutral cloud reaches its peak brightness, which is somewhat brighter than a third magnitude star, in about fifteen to twenty seconds after the release.

The neutral barium rapidly becomes ionized by the incoming solar radiation. The charged particles attach themselves to a magnetic field line and spiral along it, forming an elongated cloud along the direction of the magnetic field. Figure 2 is a photograph of an ionized (elongated) barium cloud. After about four minutes the

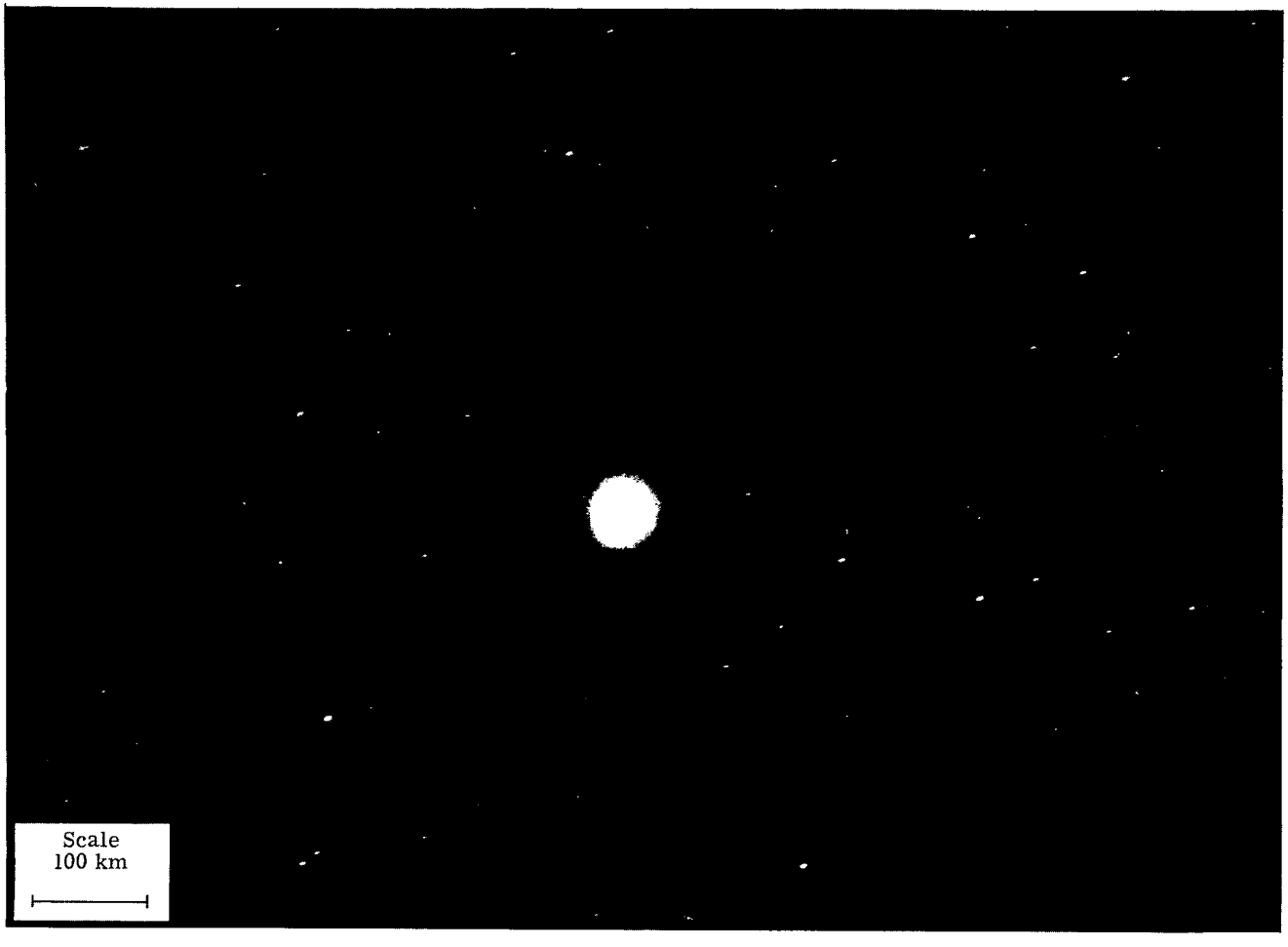

Figure 1.- Neutral barium cloud as seen from Mt. Hopkins Baker Nunn Site, Arizona, on September 21, 1971, at 03 05 13.

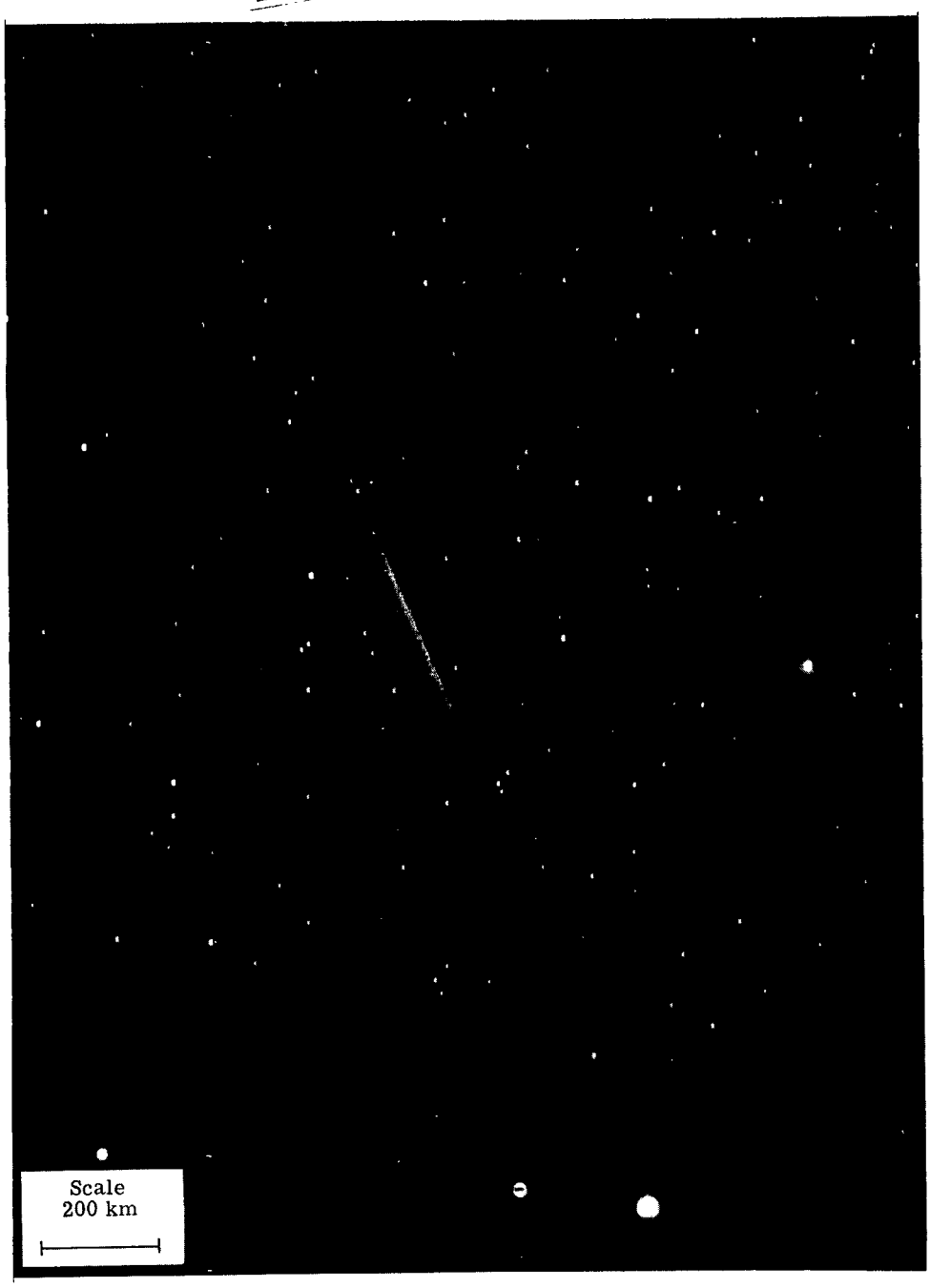

Figure 2.- Ionized barium cloud as seen from Mt. Hopkins Baker Nunn Site, Arizona, on September 21, 1971, at 03 11 14.

elongated cloud subtends an angle of about one half degree, which is approximately the angle subtended by the diameter of the moon. After about thirty minutes the elongated cloud extends to a length of 10,000 kilometers or greater. The observation time is about one hour and fifteen minutes duration.

Initially, the relatively dense cloud of charged particles introduced into the magnetosphere perturbs the weak magnetic field. Also, the initial velocity of the ions, the same as that of the Scout fourth-stage, is greater than that of the ambient plasma.

After an extended time the cloud adopts the velocity of the drifting ambient plasma. The drift velocity $\vec{v}$ for all charged particles is

$$\vec{v} = \frac{\vec{E} \times \vec{\beta}}{\beta^2}, \text{ for } |\vec{E}| < c\,|\vec{\beta}|, \qquad (1)$$

where $\vec{E}$ is the electric field vector, $\vec{\beta}$ is the magnetic induction vector, and c is the speed of light.

Upon vector multiplication of each side of equation 1 by $\vec{\beta}$, it is seen that

$$\vec{E} = -(\vec{v} \times \vec{\beta}) \qquad (2)$$

Using equation 2 the electric field vector can be computed once the drift velocity and the magnetic induction vector are known.

Since the barium is fluorescent against a dark-sky background, it can be photographed from ground-based observation sites. The cameras at the different sites are all synchronized in time. The photographs of the barium cloud are projected onto appropriate star charts, matching the respective star configurations, thus obtaining the coordinates of particular points along the length of the cloud in whatever coordinates were used in constructing the star charts, eg. azimuth and elevation.

By triangulating on the two-dimensional data thus obtained from the various observation sites, the position of the cloud in three-dimensional space as a function of time and, hence, its velocity is determined. From the elongation of the cloud, the geometry of the magnetic field line is deduced. The magnetic field line thus determined can be compared to the magnetic field line resulting from the earth's internal magnetic sources, and any perturbation suffered by the magnetic field line as delineated by the cloud can be deduced. And, from the drift of the cloud, since the magnetic induction is measured by the magnetometer aboard the Scout, the strength and direction of the electric field is computed using equation 2.

It is necessary to know how accurately the position of the cloud in space is determined in order to evaluate the final results of the magnetic field and electric field determinations. It is therefore important to know what errors are introduced into the data through the acquisition and reduction of the data and how these errors are manifested by the triangulation in the solution of locating the barium

cloud in space. This thesis deals with the problem of triangulation and the errors which result from the triangulation for the BIC Experiment.

OBJECTIVES

I. To define what triangulation errors are meaningful to the BIC Experiment.

II. To exercise the triangulation method developed for the BIC Project to obtain data for use in designing the remainder of the experiment.

REVIEW OF LITERATURE

An extensive literature search using the NASA Library facilities yielded no information on triangulation errors which was meaningful to and useful in designing the BIC Experiment.

TRIANGULATION

FOR THE

BIC PROJECT

The Single-Point Two-Station Triangulation Problem

To begin a paper on triangulation errors, it might be illustrative to first consider the simplified triangulation problem of a single point in space observed by two observation stations. Most of what will be stated here concerning this simplified problem is taken from reference 1.

For this two-station triangulation problem, it is convenient to use a relative station coordinate system as shown in Figure 3. The two stations are denoted by A and B. The 1 , 2 , 3 Cartesian coordinate axes are the geocentric coordinate axes defined by: the origin is at the center of the earth; 1 is directed toward the intersection of the Greenwich Meridian with the equator; 2 is directed toward 90° east longitude, 0° latitude; 3 is directed toward the geographic north pole. The radial distance of station A from the earth's center is denoted by r_A; and its 1 , 2 , 3 components, by r_{A_1}, r_{A_2}, r_{A_3}, respectively. The radial distance of station B from the earth's center is denoted by r_B; and its 1 , 2 , 3 components, by r_{B_1}, r_{B_2}, r_{B_3}, respectively. The base line AB, projected onto the 1 , 2 , 3 axes, has the projections AB_1, AB_2, AB_3, respectively, given by

$$AB_1 = r_{B_1} - r_{A_1} \tag{3}$$

$$AB_2 = r_{B_2} - r_{A_2} \tag{4}$$

$$AB_3 = r_{B_3} - r_{A_3} \tag{5}$$

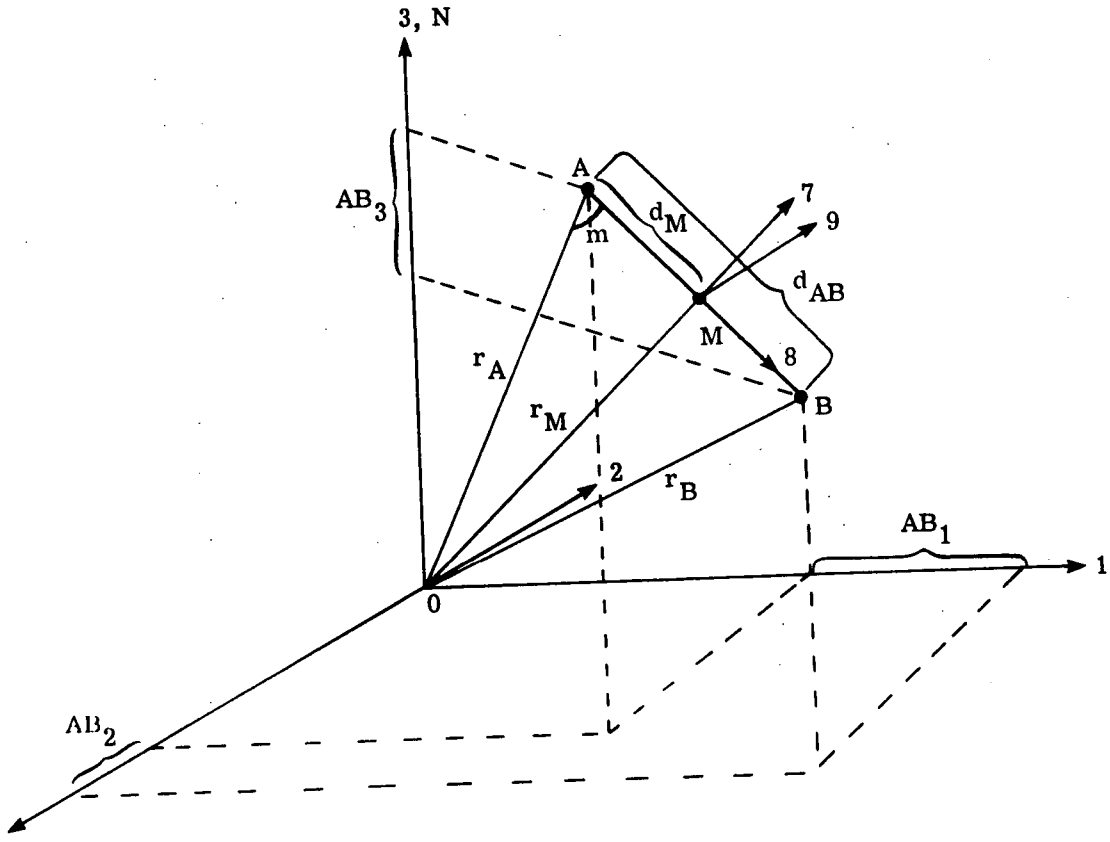

Figure 3.- The relative station coordinate system.

The length d_{AB} of the line AB is then

$$d_{AB} = (AB_1^2 + AB_2^2 + AB_3^2)^{1/2} \tag{6}$$

The radial line from the center of the earth which is perpendicular to the base line AB is denoted by r_M. This perpendicular intersects AB at the point M. The angle m is the angle between r_A and AB and can be found, using the law of cosines, to be

$$m = \cos^{-1}\left(\frac{r_A^2 + d_{AB}^2 - r_B^2}{2\, r_A\, d_{AB}}\right) \tag{7}$$

The point M on AB is located a distance d_M from station A given by

$$d_M = r_A \cos m \tag{8}$$

And, the length of the radial line r_M is given by

$$r_M = r_A \sin m \tag{9}$$

The relative station coordinate system with axes denoted by 7, 8, and 9 is defined by: the origin is at the point M; 7 is directed radially outward along the line r_M; 8 is directed toward station B along the base line AB; 9 is such as to form an orthogonal system. The direction cosines for transforming from the relative station

coordinates to the geocentric coordinates are

$$\gamma_{71} = \frac{r_{A_1} + \frac{d_M \, AB_1}{d_{AB}}}{r_M} \tag{10}$$

$$\gamma_{72} = \frac{r_{A_2} + \frac{d_M \, AB_2}{d_{AB}}}{r_M} \tag{11}$$

$$\gamma_{73} = \frac{r_{A_3} + \frac{d_M \, AB_3}{d_{AB}}}{r_M} \tag{12}$$

$$\gamma_{81} = \frac{AB_1}{d_{AB}} \tag{13}$$

$$\gamma_{82} = \frac{AB_2}{d_{AB}} \tag{14}$$

$$\gamma_{83} = \frac{AB_3}{d_{AB}} \tag{15}$$

$$\gamma_{91} = \gamma_{72} \gamma_{83} - \gamma_{82} \gamma_{73} \tag{16}$$

$$\gamma_{92} = \gamma_{81} \gamma_{73} - \gamma_{71} \gamma_{83} \tag{17}$$

$$\gamma_{93} = \gamma_{71} \gamma_{82} - \gamma_{81} \gamma_{72} \tag{18}$$

The direction cosines for transforming from the relative station coordinate system to the topocentric coordinate system with axes denoted by 4, 5, and 6 can also be found. The topocentric

coordinate system is defined by: the origin is located at a particular location on the surface of the earth, eg. an observation station; 4 is directed along the radial line from the center of the earth to the station, ie vertical from the station; 5 is directed east from the station at 0° elevation perpendicular to 4; 6 is directed north from the station at 0° elevation perpendicular to 4 and 5. The direction cosines for transforming from the relative station coordinates to the topocentric coordinates are then

$$\gamma_{ij} = \sum_{k=1}^{3} \gamma_{jk}\gamma_{ik}, \tag{19}$$

where $i = 7, 8, 9$ and $j = 4, 5, 6$. The γ_{jk} are the direction cosines for transforming from the topocentric coordinates to the geocentric coordinates and are given in reference 1.

Now, the line-of-sight defined by the azimuth and elevation of the point in space from station A may not intersect precisely with the line-of-sight defined by the azimuth and elevation of the point in space from station B. Such could be the result of human error and/or equipment error while acquiring and/or reducing the photographic data.

The lines-of-sight from the two observation stations when projected onto the plane formed by the 7 and 9 axes of the relative station coordinate system form two lines extending from the relative station coordinate system origin M and two angles θ_A and θ_B measured from the 7 axis. To circumvent this problem caused by the non-intersecting lines-of-sight, it is convenient to speak of an angle, say θ, between the two angles θ_A and θ_B. The solution to

the problem of locating the point in space will then lie on the plane which passes through the 8 axis making an angle θ with the 7 axis. The shortest distance between the two lines-of-sight and perpendicular to both is denoted by d_r. The distance from station A to the intersection of d_r and the line-of-sight from station A is denoted by d_A; the distance from station B to the intersection of d_r and the line-of-sight from station B, by d_B. The angles ϕ_A and ϕ_B are measured between the base line AB and the lines-of-sight from station A and station B, respectively. The quantities θ_A, θ_B, θ, d_r, d_A, d_B, ϕ_A, and ϕ_B are all shown in Figure 4.

The 4, 5, and 6 components of the unit lines-of-sight from stations A and B - denoted by i_{A4}, i_{A5}, i_{A6}, i_{B4}, i_{B5}, and i_{B6}, respectively - are given by

$$i_{A4} = \sin el_A \tag{20}$$

$$i_{A5} = \cos el_A \sin az_A \tag{21}$$

$$i_{A6} = \cos el_A \cos az_A \tag{22}$$

$$i_{B4} = \sin el_B \tag{23}$$

$$i_{B5} = \cos el_B \sin az_B \tag{24}$$

$$i_{B6} = \cos el_B \cos az_B \ , \tag{25}$$

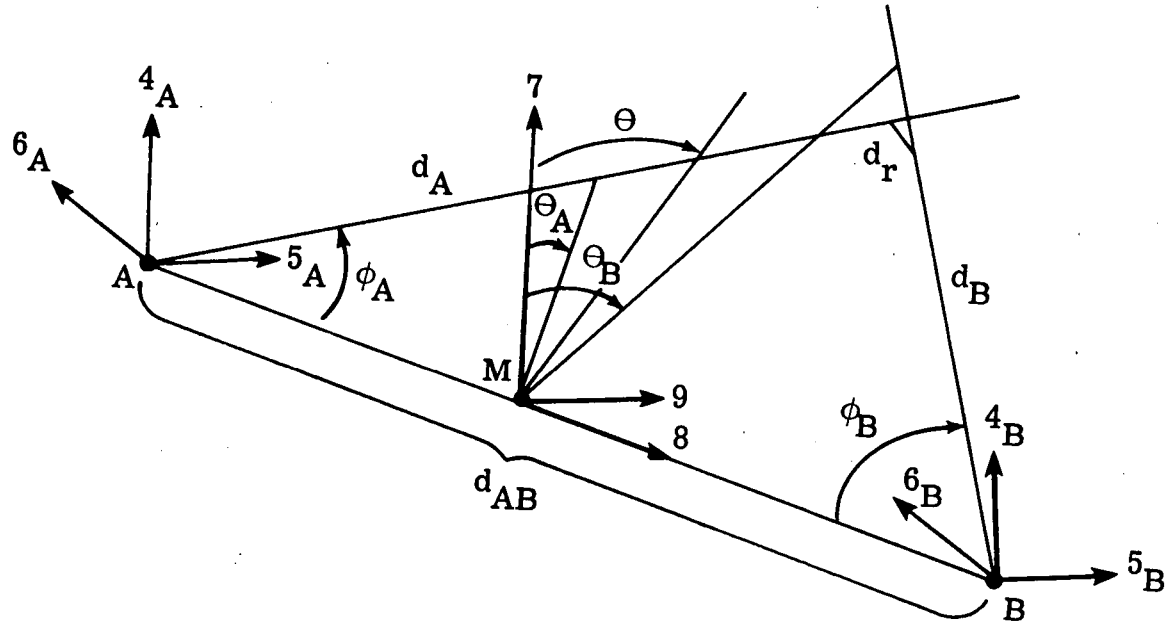

Figure 4.- The line d_r between the two non-intersecting lines-of-sight.

where az_A, el_A, az_B, and el_B are the azimuths and elevations of the point in space from stations A and B, respectively, determined from the photographic data.

The angles ϕ_A and ϕ_B are found from

$$\cos \phi_A = \gamma_{84A} i_{A4} + \gamma_{85A} i_{A5} + \gamma_{86A} i_{A6} \tag{26}$$

$$\cos \phi_B = \gamma_{84B} i_{B4} + \gamma_{85B} i_{B5} + \gamma_{86B} i_{B6}, \tag{27}$$

where γ_{84A}, γ_{85A}, γ_{86A}, γ_{84B}, γ_{85B}, and γ_{86B} are the direction cosines for transforming from the relative station coordinate system to the topocentric coordinate systems centered at stations A and B, respectively, and are found from equation 19.

The angles θ_A and θ_B are found from

$$\tan \theta_A = \frac{\gamma_{94A} i_{A4} + \gamma_{95A} i_{A5} + \gamma_{96A} i_{A6}}{\gamma_{74A} i_{A4} + \gamma_{75A} i_{A5} + \gamma_{76A} i_{A6}} \tag{28}$$

$$\tan \theta_B = \frac{\gamma_{94B} i_{B4} + \gamma_{95B} i_{B5} + \gamma_{96B} i_{B6}}{\gamma_{74B} i_{B4} + \gamma_{75B} i_{B5} + \gamma_{76B} i_{B6}}, \tag{29}$$

where the direction cosines γ_{94A}, γ_{95A}, γ_{96A}, γ_{74A}, γ_{75A}, γ_{76A}, γ_{94B}, γ_{95B}, γ_{96B}, γ_{74B}, γ_{75B}, and γ_{76B} are also found from equation 19.

The distance d_r squared is given by

$$d_r^2 = (d_{AB} - d_A \cos \phi_A - d_B \cos \phi_B)^2$$

$$+ (d_A \sin \phi_A \cos d\theta - d_B \sin \phi_B)^2$$

$$+ (d_A \sin \phi_A \sin d\theta)^2 \quad , \tag{30}$$

where $d\theta = \theta_A - \theta_B$. Minimizing this expression with respect to d_A and d_B by first differentiating it with respect to d_A and d_B and then equating each of these derivatives to zero leads to the following solutions for d_A and d_B

$$d_A = d_{AB} \frac{[\cos \phi_A - (\cos \phi_A \cos \phi_B - \sin \phi_A \sin \phi_B \cos d\theta)\cos \phi_B]}{1 - (\cos \phi_A \cos \phi_B - \sin \phi_A \sin \phi_B \cos d\theta)^2} \tag{31}$$

$$d_B = d_{AB} \frac{[\cos \phi_B - (\cos \phi_A \cos \phi_B - \sin \phi_A \sin \phi_B \cos d\theta)\cos \phi_A]}{1 - (\cos \phi_A \cos \phi_B - \sin \phi_A \sin \phi_B \cos d\theta)^2} \tag{32}$$

The location P of the point in space is assumed to lie on the line d_r. If it is assumed that the angular errors from the two observation sites are equal, then it is reasonable to assume that the location P of the point in space on d_r is at a distance l_A from the line-of-sight from station A and at a distance l_B from the line-of-sight from station B such that

$$\frac{l_A}{d_A} = \frac{l_B}{d_B} = \frac{d_r}{d_A + d_B} \tag{33}$$

Now, the residual angle δ is defined to be the angular deviation between the actual and measured lines-of-sight from an observation station. The location P of the point in space, the distances l_A and l_B, and the residual angle δ are shown in Figure 5. Since the quantities $\frac{l_A}{d_A}$ and $\frac{l_B}{d_B}$ are the tangents of the angular deviations between the actual and measured lines-of-sight from stations A and B, respectively, then δ is determined from

$$\tan \delta = \frac{d_r}{d_A + d_B} \tag{34}$$

The location P of the point in space is at a distance d'_A from station A and at a distance d'_B from station B; the distances d'_A and d'_B are the actual lines-of-sight from stations A and B, respectively, to the location P of the point in space. From Figure 5 it is seen that

$$d'_A = \frac{d_A}{\cos \delta} \tag{35}$$

$$d'_B = \frac{d_B}{\cos \delta} \tag{36}$$

The components of d'_A along the 7 and 9 axes - denoted by d'_{A7} and d'_{A9}, respectively - are

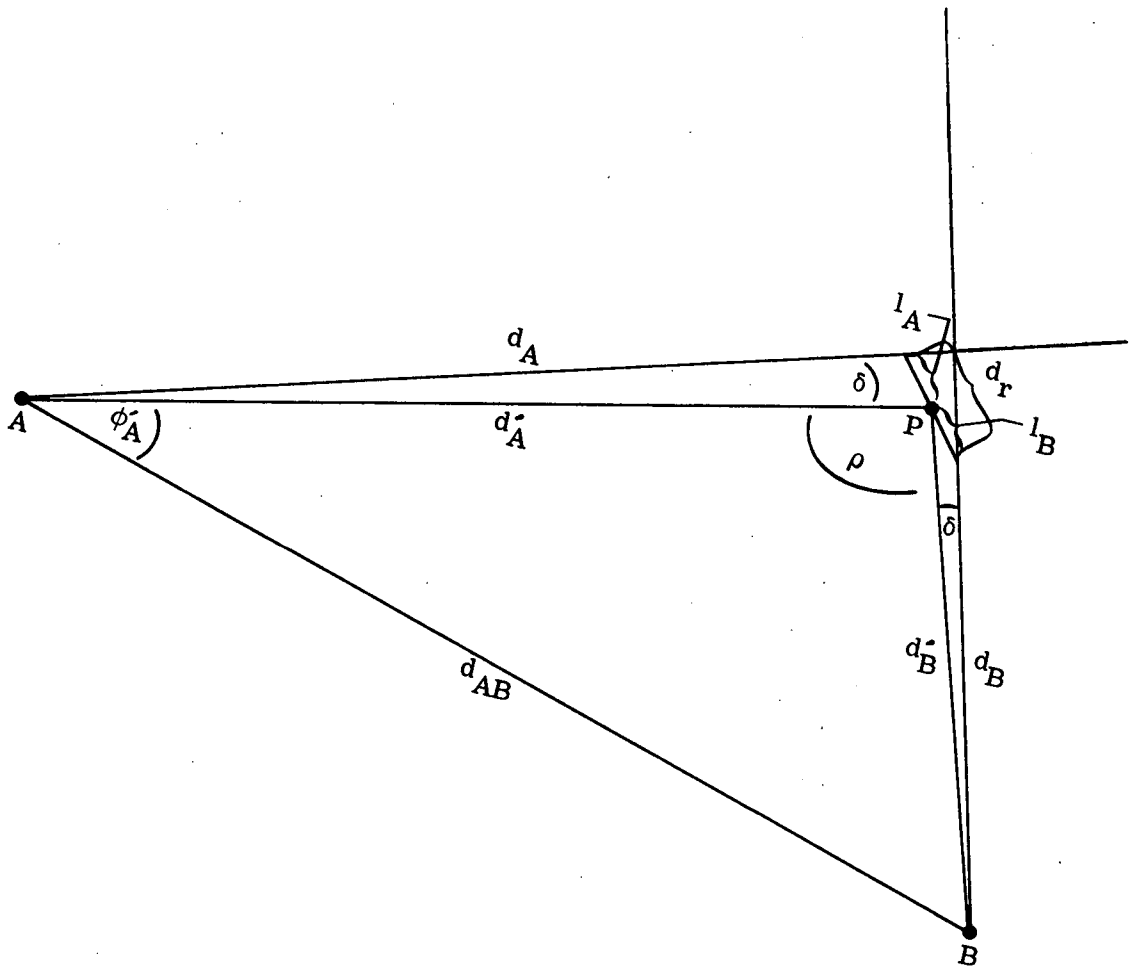

Figure 5.- The residual angle δ.

$$d'_{A7} = d_{A7} + (d_{B7} - d_{A7}) \left(\frac{d_A}{d_A + d_B} \right) \tag{37}$$

$$d'_{A9} = d_{A9} + (d_{B9} - d_{A9}) \left(\frac{d_A}{d_A + d_B} \right) , \tag{38}$$

where d_{A7} and d_{A9} are the 7 and 9 components of d_A and are given by

$$d_{A7} = d_A \sin \phi_A \cos \theta_A \tag{39}$$

$$d_{A9} = d_A \sin \phi_A \sin \theta_A , \tag{40}$$

and where d_{B7} and d_{B9} are the 7 and 9 components of d_B and are given by

$$d_{B7} = d_B \sin \phi_B \cos \theta_B \tag{41}$$

$$d_{B9} = d_B \sin \phi_B \sin \theta_B \tag{42}$$

The component of d'_A along the 8 axis, denoted by d'_{A8}, is given by

$$d'_{A8} = d'_A \cos \phi'_A , \tag{43}$$

where ϕ'_A is the angle between the actual line-of-sight d'_A from station A to the location P and the base line AB and, as seen in

Figure 5, is determined from

$$\sin \phi'_A = \frac{d'_B \sin \rho}{d_{AB}} \quad , \tag{44}$$

where ρ is the angle between the actual line-of-sight from station A to the location P and the actual line-of-sight from station B to the location P and, applying the law of cosines to the geometry of Figure 5, is found to be

$$\rho = \cos^{-1}\left[\frac{(d'_A)^2 + (d'_B)^2 - d_{AB}^2}{2\, d'_A\, d'_B}\right] \tag{45}$$

The angle θ, lying between the angles θ_A and θ_B, which is the angle that the plane through the 8 axis and containing the location P of the point in space makes with the 7 axis is then given by

$$\theta = \tan^{-1}\left(\frac{d'_{A9}}{d'_{A7}}\right), \tag{46}$$

where d'_{A7} and d'_{A9} are given by equations 37 and 38, respectively.

The geocentric components P_1, P_2, P_3 of the location P of the point in space are given by

$$P_1 = r_{A_1} + \gamma_{71A} d'_{A7} + \gamma_{81A} d'_{A8} + \gamma_{91A} d'_{A9} \tag{47}$$

$$P_2 = r_{A_2} + \gamma_{72A} d'_{A7} + \gamma_{82A} d'_{A8} + \gamma_{92A} d'_{A9} \tag{48}$$

$$P_3 = r_{A_3} + \gamma_{73A} d'_{A7} + \gamma_{83A} d'_{A8} + \gamma_{93A} d'_{A9} \quad , \tag{49}$$

where r_{A_1}, r_{A_2}, and r_{A_3} are the geocentric components of station A and where γ_{71A}, γ_{72A}, γ_{73A}, γ_{81A}, γ_{82A}, γ_{83A}, γ_{91A}, γ_{92A}, and γ_{93A} are the direction cosines for transforming from the relative station coordinate system from station A to the geocentric coordinate system.

Finally, the geocentric latitude, the longitude, and the radial distance of the location P of the point in space observed from the two stations - denoted by ϕ'_P, θ_P, and r_P, respectively - are given by

$$\phi'_P = \sin^{-1}\left[\frac{P_3}{(P_1^2 + P_2^2 + P_3^2)^{1/2}}\right] \tag{50}$$

$$\theta_P = \tan^{-1}\left(\frac{P_2}{P_1}\right) \tag{51}$$

$$r_P = (P_1^2 + P_2^2 + P_3^2)^{1/2} \tag{52}$$

Line and Multistation Triangulation Considerations

Now, in this above simplified problem of locating a single point in space using the photographic data from only two observation sites, the solution is not unique unless the lines-of-sight from the two stations to the point in space intersect precisely. In most instances, due to human error and/or equipment error while acquiring and/or reducing the data, the lines-of-sight will not intersect precisely and, hence, the solution of locating the point in space will not be unique. All that can be done is to work in terms of a most probable angle θ lying between the angles θ_A and θ_B, which are the angles measured

from the 7 axis that are made by the projections of the lines-of-sight from stations A and B, respectively, onto the plane formed by the 7 and 9 axes of the relative station coordinate system, as was just done in the above.

In the problem of locating a line, as opposed to a single point, in space using the photographic data from only two observation sites, the surface formed by the lines-of-sight from station A to various points on the line in space will in general intersect with the surface formed by the lines-of-sight from station B to various points on the line in space. If not, then extrapolations of these two surfaces will intersect. Hence, the two surfaces, or their extrapolations, will always intersect in the form of a line; and, therefore, a unique solution to the problem of locating a line in space from two observation stations can always be found.

In the BIC Experiment the barium cloud forms a line, as opposed to a point, in space as the neutral barium becomes ionized and elongates along the magnetic field line. A study of the existing triangulation methods revealed that the existing method most applicable to the BIC Experiment was the one developed by Fred L. Whipple and Luigi G. Jacchia of the Smithsonian Institution Astrophysical Observatory (reference 2). This method, herein referred to as the SAO method, was originally developed for triangulating on photographic meteor trails. It was later used by John E. Hogge of the Langley Research Center for reentry experiments (reference 3). The

SAO method is only for two observation stations and approximates each photographic trail image by a straight line, which as was pointed out above, renders a unique solution always.

However, this author in a separate paper on an analytical study to minimize the triangulation error for an idealized observation site arrangement (reference 4) has shown, for the particular case of 2 or more observation sites symmetrically located on the circumference of a circle with the cloud released on the perpendicular whose foot lies at the center of the circle, that the triangulation error is inversely proportional to the square root of the number of observation sites employed. On the basis of these findings, it was not desired to use only two observation stations for the BIC Project.

Also with regard to the BIC Experiment, the magnetic field lines are not straight, but are curved; hence, the barium cloud images are also curved. It was, hence, not desired to use a straight-line approximation to the curved barium cloud images.

Therefore, it was felt that, although the SAO method has been used for some time with great success for the triangulation of photographic meteor data and of reentry experiment data, it was perhaps not necessarily the best triangulation method for the BIC Project. It was decided to develop an entirely new triangulation method for the BIC Project that would incorporate any number of observation stations and that would accommodate the curved images. The results of the new method could always be compared to the results of the already successful SAO method as a check.

The new triangulation method developed for the BIC Project at the Langley Research Center will be herein referred to as the LaRC method. This author in a separate paper has explained in complete detail for use in computer programs both the SAO and LaRC triangulation methods and has compared the two for their applicability to the BIC Experiment (reference 5). That paper concluded that the LaRC method was the best method for the BIC Experiment; and, hence, it was the method adopted for the project.

It was decided to develop the LaRC method to use the azimuth - elevation coordinates. The azimuth-elevation curve of the cloud image from each observation station can be obtained from the photographic data. This curve from each station defines a conical-like surface in space. For two observation stations, as was pointed out earlier, the intersection of the two cones is unique. For more than two observation stations, however, the intersection of the cones is not unique. Hence, an averaging procedure had to be developed in the LaRC method in order to incorporate the data from more than two observation stations.

The LaRC Triangulation Method

For the reader's convenience a summary of the LaRC method is first given here before it is explained in detail. First, the total arc length of the azimuth - elevation curve from each station is found; and then new azimuth and elevation data points equally spaced along the azimuth - elevation curves are calculated. An initial trial solution in terms of the latitude, longitude, and altitude coordinates -

which are transformed to the azimuth, elevation, and range coordinates - is estimated. The arc lengths between the trial solution and each of the new points on the azimuth - elevation curve from each station are calculated and compared to find the point on each azimuth - elevation curve closest to the initial trial solution. Using the closest point as the origin of a local coordinate system, three residuals, one being the perpendicular distance from the trial solution to the azimuth - elevation curve and the other two being the respective distances from the trial solution to the points lying on either side of the closest point, are found for each station. A residual is the distance from the trial solution to the endpoint of a ray on the surface defined by the azimuth - elevation curve from that station. The minimum residual for each station is found; and the residual sum for all the stations combined, calculated. The initial trial solution is then varied in altitude and in longitude, the incrementing of the longitude being nested within the incrementing of the altitude and each time calculating the residual sum for all the stations combined, until the minimum residual sum from varying both the longitude and altitude is found. Then, the trial latitude is incremented, the altitude and longitude increments decreased by half, and the entire process iterated. Finally, after two iterations the unique solution to the problem of locating the barium cloud in space which minimizes the triangulation error is found.

The LaRC method is discussed in more detail in the following. (The reader interested in using the method might also see reference 6,

a computer program.)

From the photographic data the azimuth and elevation for each point on the image from each observation station is obtained. For N points and L stations, the original azimuths and elevations from the photographic data are denoted by $az''_{\ell,n}$ and $el''_{\ell,n}$, where $n = 1,2,\ldots,N$ and $\ell = 1,2,\ldots,L$. The arc length $ds_{\ell,n}$ in degrees between points n and $n-1$ is

$$ds_{\ell,n} = \left[\left(el''_{\ell,n}-el''_{\ell,n-1}\right)^2 + \left(az''_{\ell,n} - az''_{\ell,n-1}\right)^2 \cos^2\left(\frac{el''_{\ell,n} + el''_{\ell,n-1}}{2}\right)\right]^{1/2}, \tag{53}$$

where $ds_{\ell,1} = 0$, $el''_{\ell,0} = az''_{\ell,0} = 0$.

The total arc length $sarc_\ell$ in degrees of the azimuth-elevation curve from the $\ell^{\underline{th}}$ station is

$$sarc_\ell = \sum_{n=1}^{N} ds_{\ell,n} \tag{54}$$

Since it is desirable to have the points on the azimuth-elevation curves equally spaced, BN is defined as the spacing desired in degrees between consecutive points on the azimuth-elevation curves. For the present, BN is set equal to 0.28 degrees. The total number of points NB_ℓ along the azimuth-elevation curve from the $\ell^{\underline{th}}$ station is then

$$NB_\ell = \frac{sarc_\ell}{BN} \tag{55}$$

New azimuth and elevation data points spaced $BN = 0.28^{\circ}$ apart along the azimuth-elevation curves are then calculated using FTLUP, a Langley Research Center systems computer subroutine which calculates $y = F(x)$ from a table of values using second-order interpolation. A second-degree least squares curve is then fitted through these new azimuth and elevation data points from each observation station, based on three points and centered symmetrically about the point n where $n = 1,2,\ldots,NB_{\ell}$, obtaining the coefficients $bc_{m,\ell,n}$ where $m = 1,2,3$. This is accomplished using the following equations and procedure.

$$c_{i,j} = c_{i,j-1}(az_{\ell,nv} - az_{\ell,n}) \cos\left(\frac{el_{\ell,nv} + el_{\ell,n}}{2}\right); \tag{56}$$

$i = 1,2,3$; $j = 2,3$; $nv = nm-2+i$; $nm = 2$, if $n < 2$, and $nm = NB_{\ell} - 1$, if $n > NB_{\ell} - 1$; $c_{1,1} = c_{2,1} = c_{3,1} = 1$

$$a_{i,m} = \sum_{k=1}^{3} c_{k,i}\, c_{k,m} \tag{57}$$

$$b_{i} = \sum_{k=1}^{3} c_{k,i}\, (el_{\ell,nm-2+k} - el_{\ell,n}) \tag{58}$$

The problem is to solve the matrix equation $a_{i,m}bc_{m} = b_{i}$, where $a_{i,m}$ is a square coefficient matrix and b_{i} is a matrix of constant vectors. The solution is found using SIMEQ, a Langley Research Center systems computer subroutine which solves a set of simultaneous equations and obtains the determinant. The bc_{m} values found are the coefficients $bc_{m,\ell,n}$, which are stored for later use.

An initial trial solution in terms of latitude, longitude, and altitude coordinates—denoted by plat, plon, and pr, respectively—is estimated. These coordinates are then transformed to the azimuth, elevation, and range coordinates—denoted by paz, pel, and pra, respectively—according to the transformation in the appendix. Then the arc lengths $dsn_{\ell,n}$ in degrees between the trial solution (paz, pel, pra) and each of the n equally-spaced points on the azimuth-elevation curve $(az_{\ell,n}, el_{\ell,n})$ from each station are calculated.

$$dsn_{\ell,n} = \left[(pel - el_{\ell,n})^2 + (paz - az_{\ell,n})^2 \cos^2\left(\frac{pel + el_{\ell,n}}{2}\right)\right]^{1/2} \tag{59}$$

For a given station these arc lengths to the n points are compared to find the one which is the shortest or, in other words, to find the point on each azimuth-elevation curve which is the closest to the initial trial solution. The value of n for this closest point is denoted by t, as indicated in Figure 6. Suppressing the subscript t in the following, as it is for a particular point, the horizontal and vertical components—denoted by x_ℓ and y_ℓ, respectively—of dsn_ℓ are

$$x_\ell = (paz - az_\ell) \cos\left(\frac{pel + el_\ell}{2}\right) \tag{60}$$

$$y_\ell = pel - el_\ell \tag{61}$$

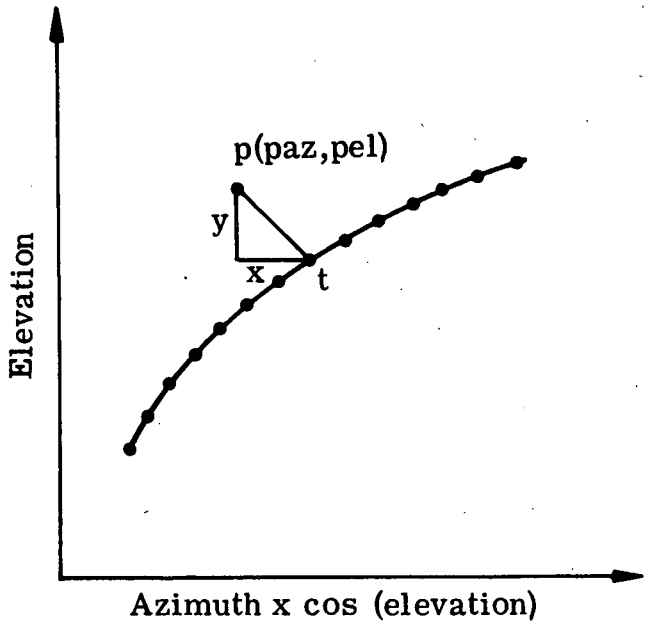

Figure 6.- The point t on the azimuth-elevation curve closest to the trial solution (paz, pel).

The coordinate system of Figure 7 is a local coordinate system with the point t as the origin. The coordinates of the point p in this system are x_ℓ and y_ℓ as given by equations 60 and 61, respectively. The coordinates of the point r in this system are xl_ℓ and yl_ℓ, where xl_ℓ and yl_ℓ are given by

$$xl_\ell = x_\ell \tag{62}$$

$$yl_\ell = bc_{1,\ell} + bc_{2,\ell} xl_\ell + bc_{3,\ell} xl_\ell^2 , \tag{63}$$

using the bc coefficients found from the least squares curve fit that correspond to n = t.

The slope of the tangent to the curve at the point t is given by the change in yl_ℓ with respect to xl_ℓ.

$$\frac{d(yl_\ell)}{d\ xl_\ell} = bc_{2,\ell} + 2\ bc_{3,\ell} xl_\ell \tag{64}$$

The angle θ_ℓ as seen in Figure 7 is just

$$\theta_\ell = \tan^{-1}\left(\frac{d(yl_\ell)}{d\ xl_\ell}\right)$$

$$= \tan^{-1}\ (bc_{2,\ell} + 2\ bc_{3,\ell}\ xl_\ell) , \tag{65}$$

using equation 64.

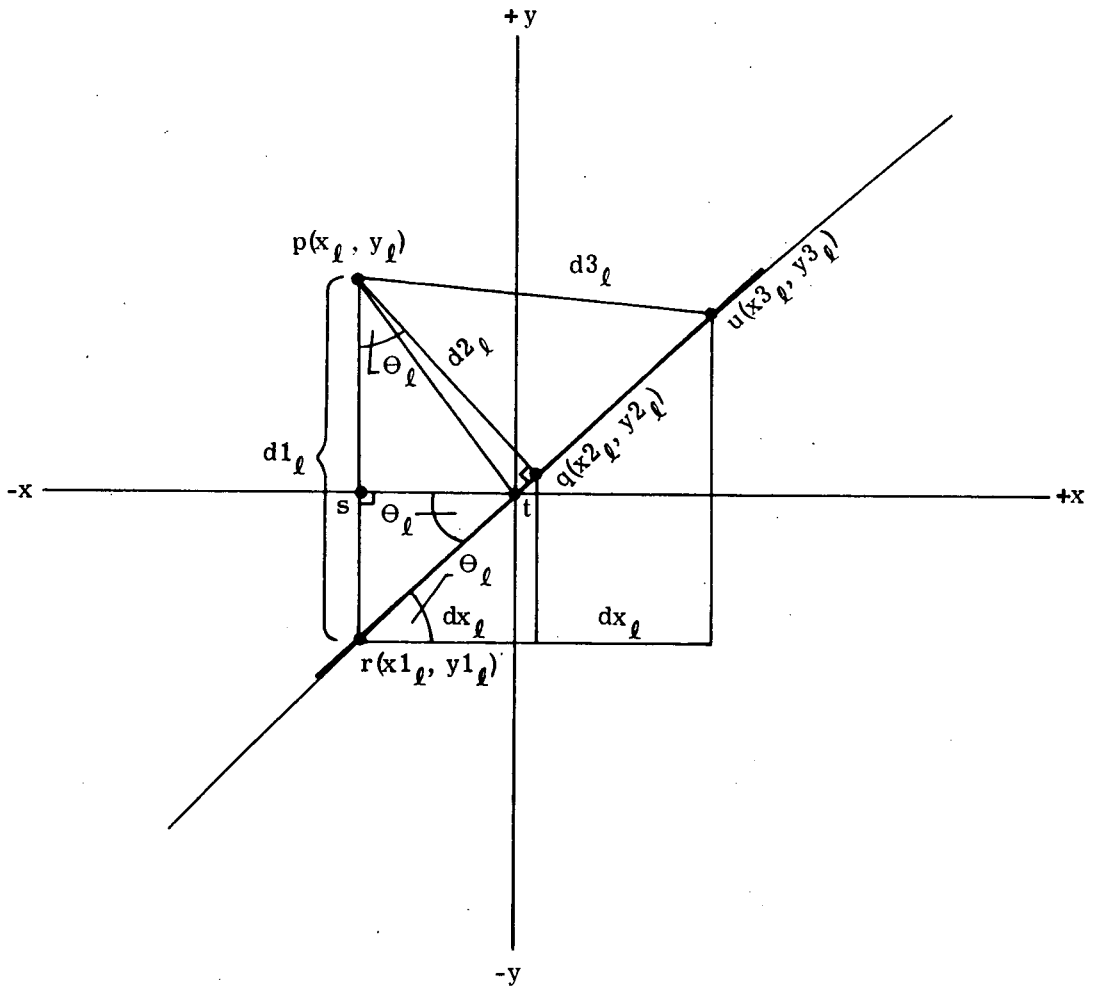

Figure 7.- The local coordinate system centered at the point t plus the three residuals $d1_\ell$, $d2_\ell$, and $d3_\ell$.

The three residuals dl_ℓ, $d2_\ell$, and $d3_\ell$ as shown in Figure 7 are computed according to the following. From Figure 7 it is seen that

$$dl_\ell = [(y_\ell - yl_\ell)^2 + (x_\ell - xl_\ell)^2]^{1/2}$$

$$= [(y_\ell - yl_\ell)^2]^{1/2}, \text{ using equation 62}$$

$$= y_\ell - yl_\ell \tag{66}$$

From Figure 7 it is also seen that the triangle pqr is similar to the triangle tsr; hence, the angle rpq is equal to θ_ℓ. The distance qr is then

$$qr = (y_\ell - yl_\ell) \sin \theta_\ell \tag{67}$$

The distance dx_ℓ is then

$$dx_\ell = qr \cos \theta_\ell$$

$$= (y_\ell - yl_\ell) \sin \theta_\ell \cos \theta_\ell , \tag{68}$$

using equation 67 for qr.

The coordinates of the point q, which is very near to or the same as the closest point t, are $x2_\ell$ and $y2_\ell$ and are given by

$$x2_{\ell} = x1_{\ell} + dx_{\ell} \tag{69}$$

$$y2_{\ell} = bc_{1,\ell} + bc_{2,\ell} x2_{\ell} + bc_{3,\ell} x2_{\ell}^2 \tag{70}$$

And,

$$d2_{\ell} = [(y_{\ell} - y2_{\ell})^2 + (x_{\ell} - x2_{\ell})^2]^{1/2} \tag{71}$$

The coordinates of the point u are $x3_{\ell}$ and $y3_{\ell}$ and are given by

$$x3_{\ell} = x2_{\ell} + dx_{\ell} \tag{72}$$

$$y3_{\ell} = bc_{1,\ell} + bc_{2,\ell}\, x3_{\ell} + bc_{3,\ell}\, x3_{\ell}^2 \tag{73}$$

And,

$$d3_{\ell} = [(y_{\ell} - y3_{\ell})^2 + (x_{\ell} - x3_{\ell})^2]^{1/2} \tag{74}$$

The origin of the coordinate system is then shifted from the point t to the point q to make the calculation of the minimum residual d_{ℓ} from the $\ell^{\underline{th}}$ station simpler. This shift does not affect the final expression for d_{ℓ}.

The minimum residual d_{ℓ} can be written in the following general form

$$d_{\ell} = C_o + C_1\, dx_{\ell} + C_2\, dx_{\ell}^2 \ , \tag{75}$$

where the coefficients C_o,C_1, and C_2 need to be determined. Taking the first derivative of d_ℓ with respect to dx_ℓ,

$$\frac{d(d_\ell)}{d\ dx_\ell} = C_1 + 2C_2\ dx_\ell \tag{76}$$

The condition for a minimum d_ℓ with respect to dx_ℓ is then

$$0 = C_1 + 2C_2\ dx_\ell \tag{77}$$

Hence,

$$dx_{\ell_{min}} = -\frac{C_1}{2C_2} \tag{78}$$

The three residuals $d1_\ell$, $d2_\ell$, and $d3_\ell$ can be written in the following forms, respectively, using this new coordinate system

$$d1_\ell = C_o - C_1\ dx_\ell + C_2\ dx_\ell^2 \tag{79}$$

$$d2_\ell = C_o \tag{80}$$

$$d3_\ell = C_o + C_1\ dx_\ell + C_2\ dx_\ell^2 \tag{81}$$

Solving these three equations simultaneously, the coefficients C_o, C_1, and C_2 can be found. The coefficient C_o is just equal to

$d2_\ell$ because of the origin of the new coordinate system. Subtracting equation 79 from equation 81,

$$d3_\ell - d1_\ell = 2\ C_1\ dx_\ell \tag{82}$$

Hence,

$$C_1 = \frac{d3_\ell - d1_\ell}{2\ dx_\ell} \tag{83}$$

Adding equations 79 and 81,

$$d3_\ell + d1_\ell = 2\ C_o + 2\ C_2\ dx_\ell^2$$

$$= 2\ d2_\ell + 2\ C_2 dx_\ell^2\ , \text{ using equation 80} \tag{84}$$

Hence,

$$C_2 = \frac{d3_\ell + d1_\ell - 2\ d2_\ell}{2\ dx_\ell^2} \tag{85}$$

Then, equation 78 for $dx_{\ell_{min}}$ becomes, using equations 83 and 85 for C_1 and C_2, respectively,

$$dx_{\ell_{min}} = \frac{-C_1}{2\,C_2} \tag{78}$$

$$= \frac{-(d3_\ell - d1_\ell)/2\,dx_\ell}{2(d3_\ell + d1_\ell - 2\,d2_\ell)/2\,dx_\ell^2}$$

$$= \frac{-(d3_\ell - d1_\ell)\,dx_\ell}{2(d3_\ell + d1_\ell - 2\,d2_\ell)} \tag{86}$$

Substituting equations 80, 83, 85, and 86 for C_o, C_1, C_2, and dx_ℓ, respectively, into equation 75 for d_ℓ, it becomes

$$d_\ell = C_o + C_1\,dx_\ell + C_2\,dx_\ell^2 \tag{75}$$

$$= d2_\ell + \frac{(d3_\ell - d1_\ell)}{2\,dx_\ell}\left[\frac{-(d3_\ell - d1_\ell)\,dx_\ell}{2(d3_\ell + d1_\ell - 2\,d2_\ell)}\right]$$

$$+ \frac{(d3_\ell + d1_\ell - 2\,d2_\ell)}{2\,dx_\ell^2}\left[\frac{-(d3_\ell - d1_\ell)\,dx_\ell}{2(d3_\ell + d1_\ell - 2\,d2_\ell)}\right]^2$$

$$= d2_\ell - \frac{(d3_\ell - d1_\ell)^2}{4(d3_\ell + d1_\ell - 2\,d2_\ell)} + \frac{(d3_\ell - d1_\ell)^2}{8(d3_\ell + d1_\ell - 2\,d2_\ell)}$$

$$= d2_\ell - \frac{(d3_\ell - d1_\ell)^2}{8(d3_\ell + d1_\ell - 2\,d2_\ell)} \tag{87}$$

Therefore, the minimum residual d_ℓ between the trial solution and the azimuth-elevation curve from station ℓ is

$$d_\ell = d2_\ell - \frac{(d3_\ell - d1_\ell)^2}{8(d3_\ell + d1_\ell - 2\,d2_\ell)} \tag{87}$$

Then the square root of the sum of the squares of the residuals, called the residual sum and denoted by E, is calculated.

$$E = \left[\sum_{\ell=1}^{L} (d_\ell)^2 \right]^{1/2} \tag{88}$$

This first value of E is denoted by $E1_a$.

The initial trial longitude plon is incremented by da_+. From Figure 8 it is seen that

$$da_+ = \frac{dr}{pr \cos (plat)} , \tag{89}$$

where pr and plat are the trial altitude and latitude, respectively. Initially, dr is set equal to 80 km. The incremented longitude is

$$plon'_+ = plon + da_+ \tag{90}$$

Using this new value $plon'_+$ for the longitude, E is again calculated. This value of E is denoted by $E2_a$. The residual sums $E1_a$ and $E2_a$ are compared.

A1. If $E2_a < E1_a$, $plon'_+$ is incremented by da_+ ($plon''_+ = plon'_+ + da_+$), E is calculated, and this value of E is denoted by $E3_a$.

B1. If $E2_a > E1_a$, the values of $E1_a$ and $E2_a$ are interchanged, the sign of da_+ is changed and this new increment is denoted by da_-, plon is incremented by da_- ($plon'_- =$

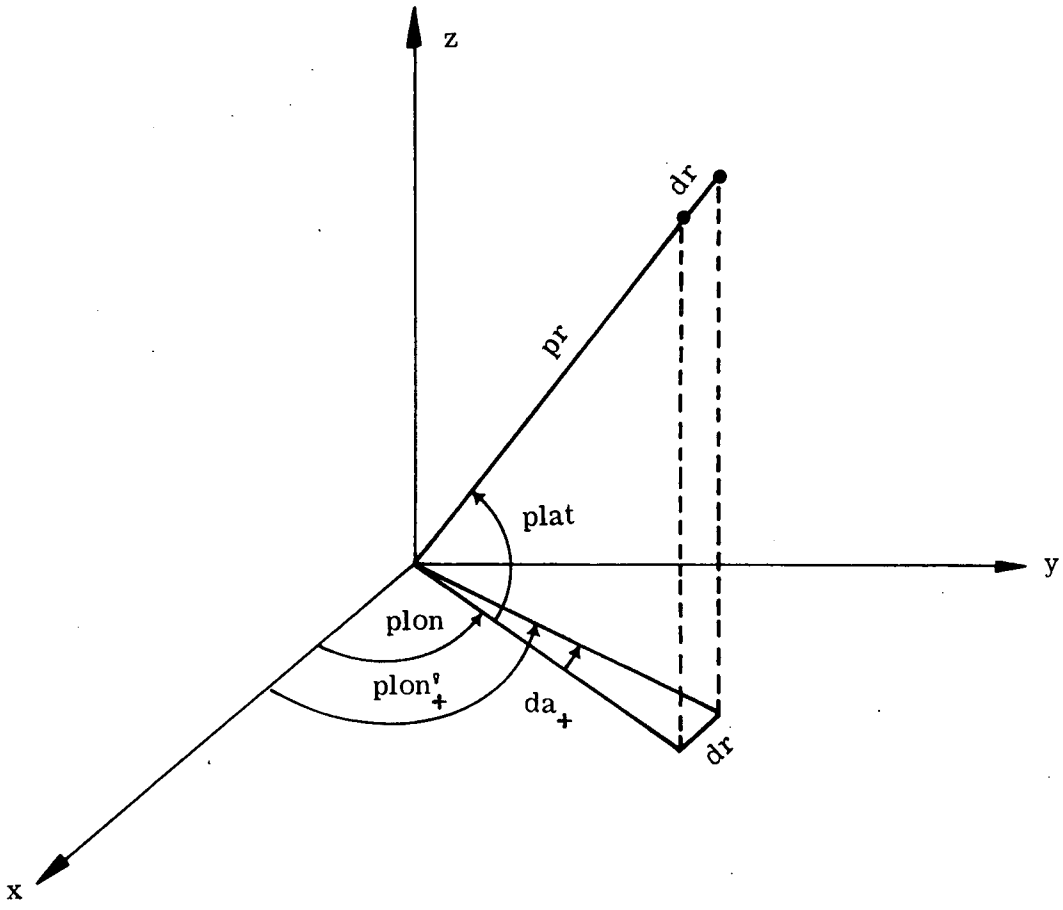

Figure 8.- The increment da_+.

plon + da_-), E is calculated, and this value of E is denoted by $E3_a$.

The residual sums $E2_a$ and $E3_a$ are compared.

A2. If $E2_a < E3_a$, the comparing terminates.

B2. If $E2_a > E3_a$, the old value of $E2_a$ is given to El_a, the old value of $E3_a$ is given to $E2_a$, $plon''_+$ is incremented by da_+ ($plon'''_+ = plon''_+ + da_+$) or $plon'_-$ is incremented by da_- ($plon''_- = plon'_- + da_-$) depending on whether route A1 or route B1 was used, E is calculated, this value of E is denoted by $E3_a$, $E3_a$ is again compared to $E2_a$, and this is continued until an $E3_a$ is found such that $E2_a < E3_a$.

This procedure is carried out until an $E2_a$ is found such that $E2_a < El_a$ and $E2_a < E3_a$, where El_a, $E2_a$, and $E3_a$ are three consecutive residual sums. Then, using these three residual sums the approximate value of the longitude $plon_a$ which gives the minimum residual sum E_a from varying the longitude, as shown in Figure 9, is calculated. For the purpose of simplifying this calculation of $plon_a$, the origin is shifted to the point $plon_2$, shown in Figure 9; this shift does not affect the final expression for $plon_a$. The points $plon_1$, $plon_2$, and $plon_3$ are the longitudes which correspond to the three residual sums El_a, $E2_a$, and $E3_a$, respectively.

The shift in origin requires a change in the longitudinal variable to dlon, where

$$dlon = plon - plon_2 \ , \tag{91}$$

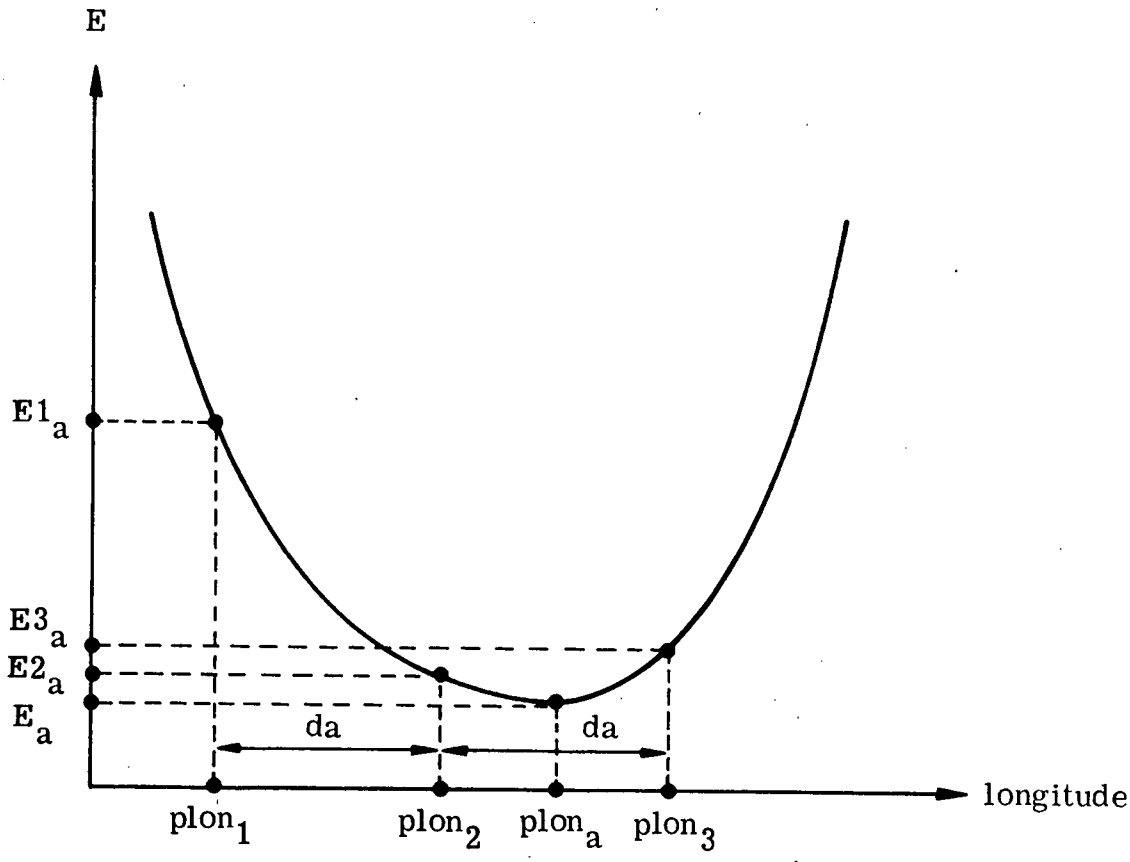

Figure 9.- The longitude $plon_a$ which gives the minimum residual sum E_a.

where plon is the longitude of the trial solution and $plon_2$ is the longitude which gives the residual sum $E2_a$. The residual sum E can be written in the following general form

$$E = A_o + A_1 \, dlon + A_2 \, dlon^2, \tag{92}$$

where the coefficients A_o, A_1, and A_2 need to be determined. The first derivative of E with respect to dlon is

$$\frac{d\,E}{d\,dlon} = A_1 + 2\,A_2 \, dlon \tag{93}$$

The condition for a minimum E with respect to dlon is

$$0 = A_1 + 2\,A_2 \, dlon \tag{94}$$

Hence,

$$dlon_{min} = \frac{-\,A_1}{2\,A_2} \tag{95}$$

The three residual sums $E1_a$, $E2_a$, and $E3_a$ can be written in the following respective forms using this new coordinate system.

$$E1_a = A_o - A_1\ da + A_2\ da^2 \tag{96}$$

$$E2_a = A_o \tag{97}$$

$$E3_a = A_o + A_1\ da + A_2\ da^2 \tag{98}$$

Solving these three equations simultaneously gives the coefficients A_o, A_1, and A_2. From equation 97 it is seen that $A_o = E2_a$ already because of the choice of origin of the new coordinate system. Subtracting equation 96 from equation 98 gives

$$E3_a - E1_a = 2\ A_1\ da \tag{99}$$

Therefore,

$$A_1 = \frac{E3_a - E1_a}{2\ da} \tag{100}$$

Adding equations 96 and 98 gives

$$E3_a + E1_a = 2\ A_o + 2\ A_2\ da^2$$

$$= 2\ E2_a + 2\ A_2\ da^2, \text{ using equation 97} \tag{101}$$

Therefore,

$$A_2 = \frac{E3_a + E1_a - 2\ E2_a}{2\ da^2} \tag{102}$$

Hence, equation 95 for $dlon_{min}$ becomes, using equations 100 and 102 for A_1 and A_2, respectively,

$$dlon_{min} = \frac{-\ A_1}{2\ A_2} \tag{95}$$

$$= \frac{-\ (E3_a - E1_a)/2\ da}{2(E3_a + E1_a - 2\ E2_a)/2\ da^2}$$

$$= \frac{-\ (E3_a - E1_a)\ da}{2(E3_a + E1_a - 2\ E2_a)} \tag{103}$$

From equation 91 it is seen that

$$dlon_{min} = plon_a - plon_2\ , \tag{104}$$

where $plon_a$ is the longitude that gives the minimum residual sum E_a. Hence,

$$plon_a = dlon_{min} + plon_2 \tag{104}$$

$$= \frac{-\ (E3_a - E1_a)\ da}{2(E3_a + E1_a - 2\ E2_a)} + plon_2\ , \tag{105}$$

using equation 103 for $dlon_{min}$.

Therefore,

$$plon_a = plon_2 - \frac{(E3_a - E1_a)\, da}{2(E3_a + E1_a - 2\, E2_a)} \quad , \tag{105}$$

where da is da_+ or da_- depending on whether routes A1 or B1 were taken. The longitude $plon_a$ is used to again calculate E. This value of E is denoted by E_a and is the minimum residual sum from varying the longitude.

This value of E_a is denoted by $E1_r$. Then the initial trial altitude pr is incremented by $dr = 80$ km, and the entire procedure of incrementing the longitude by da and finding a second value for E_a using this new value of the altitude is carried out. This new value of E_a is denoted by $E2_r$. The procedure for incrementing the altitude by dr and finding E_r, the minimum residual sum from varying the altitude, is identical to the procedure for incrementing the longitude by da and finding E_a, the minimum residual sum from varying the longitude. The incrementing of the longitude, after finding the first value of E_a, is nested within the incrementing of the altitude. The overall procedure of incrementing the altitude is carried out until an $E2_r$ is found such that $E2_r < E1_r$ and $E2_r < E3_r$, where $E1_r$, $E2_r$, and $E3_r$ are three consecutive residual sums. Using these three residual sums the approximate value of the altitude pr_r which gives the minimum residual sum E_r from varying the altitude is calculated, using an equation completely analogous to equation 105 for $plon_a$. The altitude pr_r is then used to calculate

E_r. The value of E_r is denoted by E_m, since it is actually the minimum residual sum from varying both the longitude and altitude.

Then using the values of $plon_a$ and pr_r which gave the minimum residual sum E_m and incrementing the initial trial latitude plat by dna = 1° and decreasing the value of dr by half (dr = 40 km), the entire procedure of varying the longitude and altitude to find the minimum residual sum E_m is repeated. Then using the new values of $plon_a$ and pr_r found from the first iteration and incrementing the trial latitude again by dna = 1° and decreasing the value of dr again by half (dr = 20 km), the entire procedure of varying the longitude and altitude to find the minimum residual sum E_m is again repeated. With dr = 20 km this procedure is repeated over the range of latitude, in increments of dna = 1°, desired. The final values of the longitude and altitude, corresponding to the given values of latitude, which give the final minimum residual sums provide the unique solution to the problem of locating a barium cloud in space which minimizes the error. For the LaRC triangulation output this geodetic coordinate solution is finally transformed to geocentric coordinates, according to equations derived by this author in a separate paper on the transformation from geocentric to geodetic coordinates and vice versa in powers of the earth's flattening (reference 7).

Triangulation Errors

For The

BIC Experiment

Observation Stations for the BIC Project

For the BIC Project, use had to be made, as much as possible, of existing observation stations. Table 1 is a list of the observation stations chosen for the BIC Project and their respective coordinates. These stations were chosen on the basis of their availability, facilities, relative location, and weather conditions during the launch-window periods for the experiment. The two prime sites, ones that have to be clear for the "go" launch condition, are Mt. Hopkins and Cerro Morado. The Wallops station is actually the NASA CV-990 High Altitude Research Aircraft (NASA-711), which is equipped as an airborne optical observatory and which flies between Bermuda and Wallops Station at an altitude of 35,000 feet or higher for the experiment. It was decided to have a north-eastern station to improve the triangulation accuracy; and since the east coast is frequently plagued by cloud cover, it was decided to use an aircraft to fly above the clouds. The Baker-Nunn sites are extra sites included to improve the triangulation accuracy.

The observatories at Byrd Station, Antarctica, and Great Whale, Canada, were included to obtain data on the geophysical condition at the time of the release and to monitor any induced changes that might occur, but not to obtain data for triangulation purposes.

Pointing Displacement Errors

The two-dimensional input data to the triangulation program could have, and probably will have, errors which occurred during the

Table 1: The BIC observation stations and their respective coordinates.

Station	Geodetic Latitude (deg)	East Longitude (deg)	Altitude (km)
Byrd Station, Antarctica	-80.0167	-119.5167	0
Cerro Morado, Chile	-30.1657	-70.7673	2.1346
Edwards Air Force Base Baker-Nunn, California	34.9641	-117.9146	0.0781
Great Whale, Canada	55.2700	-77.7800	0
Mt. Hopkins, Arizona	31.6853	-110.8774	2.3640
Mt. Hopkins Baker-Nunn, Arizona	31.6853	-110.8774	2.3640
Natal Baker-Nunn, Brazil	-5.9306	-35.1617	0.0421
Wallops Station, Virginia	37.9324	-75.4717	0.0106
White Sands, New Mexico	32.4238	-106.5528	1.6500

data acquisition and data reduction phases of the experiment. It is important to know how such errors are manifested by the triangulation in the three-dimensional solution of locating the barium cloud in space. A reasonable error to assume for the total error occurring during the acquisition and reduction of the data is a probable error ed of 0.01 degrees in the lines-of-sight from the observation stations to the points on the cloud.

The probable error $ed = 0.01$ degrees is introduced into the lines-of-sight from one observation station at a time. The perturbed azimuth and elevation coordinates, $az'_{\lambda,n}$ and $el'_{\lambda,n}$, corresponding to the probable error $ed = 0.01^{\circ}$ in the n lines-of-sight from station λ are

$$az'_{\lambda,n} = az_{\lambda,n} - \frac{ed}{\cos el'_{\lambda,n}} \frac{del}{dae} \tag{106}$$

$$el'_{\lambda,n} = el_{\lambda,n} + ed \frac{daz}{dae} \quad , \tag{107}$$

where $az_{\lambda,n}$ is the unperturbed azimuth and $el_{\lambda,n}$ is the unperturbed elevation of the $n^{\underline{th}}$ point on the cloud from station λ and where

$$daz = (az_{\lambda,n+1} - az_{\lambda,n}) \cos\left(\frac{el_{\lambda,n+1} + el_{\lambda,n}}{2}\right) \tag{108}$$

$$del = el_{\lambda,n+1} - el_{\lambda,n} \tag{109}$$

$$dae = [(daz)^2 + (del)^2]^{1/2} \tag{110}$$

First, the solution of locating the barium cloud in space is found, using points along the magnetic field line which passes through the chosen BIC nominal release point for the input data; the solution in latitude, longitude, and range coordinates is denoted by ϕ_N, θ_N, and r_N. The solution is then found, using the same input data but introducing the probable error ed = 0.01° into the lines-of-sight from one station, say station λ; this perturbed solution is denoted by $\phi'_{\lambda,N}$, $\theta'_{\lambda,N}$, and $r'_{\lambda,N}$. The two solutions are then compared by finding the displacement between the two respective curves in space according to the following.

Initially, for the unperturbed solution a least squares polynominal fit of fourth degree is found for $\theta_N = \theta_N(\phi_N)$ and also for $r_N = r_N(\phi_N)$ using LSQPOL, a Langley Research Center systems computer subroutine which determines the M coefficients of the polynomial of degree M-1 which gives the best fit in the least squares sense. The coefficients of the polynomial for $\theta_N = \theta_N(\phi_N)$ are denoted by $b\ell_{M,N}$, where M = 1,2,3,4,5; the coefficients of the polynomial for $r_N = r_N(\phi_N)$, by $br_{M,N}$.

The polynomial for $\theta_N = \theta_N(\phi_N)$ using the $b\ell$ coefficients is

$$\theta_N = b\ell_{1,N} + b\ell_{2,N}\phi_N + b\ell_{3,N}\phi_N^2 + b\ell_{4,N}\phi_N^3 + b\ell_{5,N}\phi_N^4 \qquad (111)$$

The polynomial for $r_N = r_N(\phi_N)$ using the br coefficients is, similarly,

$$r_N = br_{1,N} + br_{2,N}\phi_N + br_{3,N}\phi_N^2 + br_{4,N}\phi_N^3 + br_{5,N}\phi_N^4 \qquad (112)$$

The first derivative $\dot{\theta}_N$ of θ_N with respect to ϕ_N is

$$\dot{\theta}_N = b\ell_{2,N} + 2\, b\ell_{3,N}\phi_N + 3\, b\ell_{4,N}\phi_N^2 + 4\, b\ell_{5,N}\phi_N^3 \qquad (113)$$

The first derivative $\dot{r}_N$ of r_N with respect to ϕ_N is, similarly,

$$\dot{r}_N = br_{2,N} + 2\, br_{3,N}\phi_N + 3\, br_{4,N}\phi_N^2 + 4\, br_{5,N}\phi_N^3 \qquad (114)$$

From Figure 10 it is seen that the vector $\vec{B}$, which is tangent to the unperturbed solution curve at the point C, is given by

$$\begin{aligned}\vec{B} &= B_\phi \hat{i}_\phi + B_\theta \hat{i}_\theta + B_r \hat{i}_r \\ &= r_c \delta\phi_c \hat{i}_\phi + r_c \cos\phi_c \dot{\theta}_c \delta\phi_c \hat{i}_\theta + \dot{r}_c \delta\phi_c \hat{i}_r \\ &= (r_c \hat{i}_\phi + r_c \cos\phi_c \dot{\theta}_c \hat{i}_\theta + \dot{r}_c \hat{i}_r)\delta\phi_c \quad , \end{aligned} \qquad (115)$$

where $\delta\phi_c$ is the difference in latitude between the point C and the nearby point C' on the same curve and $\hat{i}_\phi$, $\hat{i}_\theta$, and $\hat{i}_r$ are unit vectors in the directions of increasing latitude, longitude, and range, respectively, and θ_c, r_c, $\dot{\theta}_c$, and $\dot{r}_c$ are given by equations 111, 112, 113, and 114, respectively, for the point N = C. The point A in Figure 10 is the point on the perturbed solution curve,

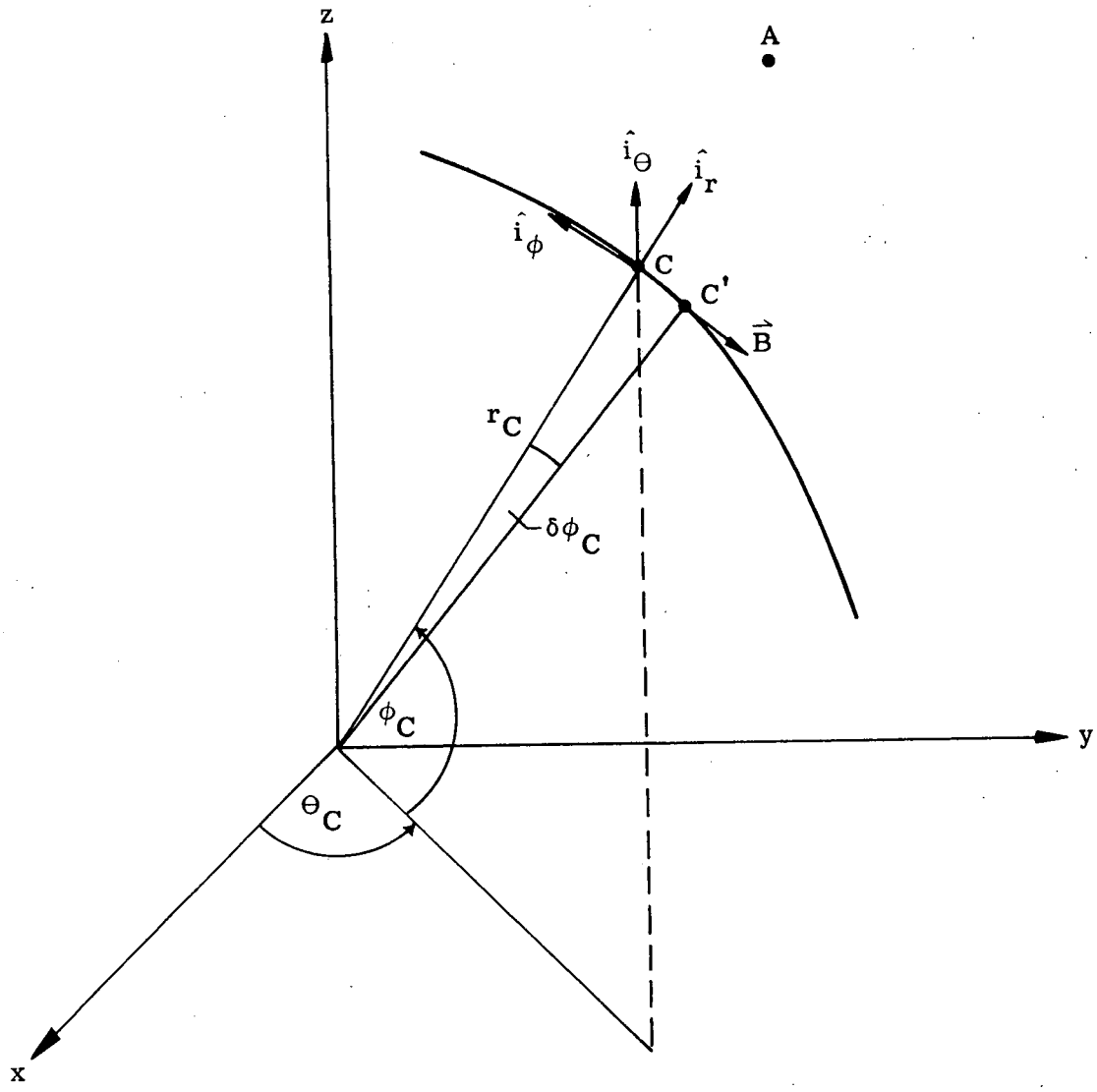

Figure 10.- The vector $\vec{B}$.

due to a probable error ed = 0.01° in the lines-of-sight from station λ, having the same latitude ϕ_c as the point C on the unperturbed solution curve.

As is shown in Figure 11 the vector from the point A to the point C is $\vec{A}$. The vector from the point A which is perpendicular to $\vec{B}$ is $\vec{C}$. It is assumed that the vector distance from the point A to the unperturbed solution curve is $\vec{C}$. From Figure 11 it is seen that

$$\vec{C} = \vec{A} + F\vec{B}, \tag{116}$$

where F needs to be determined. Dotting both sides of equation 116 with $\vec{B}$ gives

$$\vec{B} \cdot \vec{C} = \vec{B} \cdot \vec{A} + F\vec{B} \cdot \vec{B} \tag{117}$$

But, $\vec{B} \cdot \vec{C} = 0$, as $\vec{C}$ is perpendicular to $\vec{B}$; so

$$0 = \vec{B} \cdot \vec{A} + F\vec{B} \cdot \vec{B} \tag{118}$$

Therefore,

$$F = -\frac{\vec{A} \cdot \vec{B}}{\vec{B} \cdot \vec{B}} \tag{119}$$

Substituting equation 119 for F into equation 116, the expression

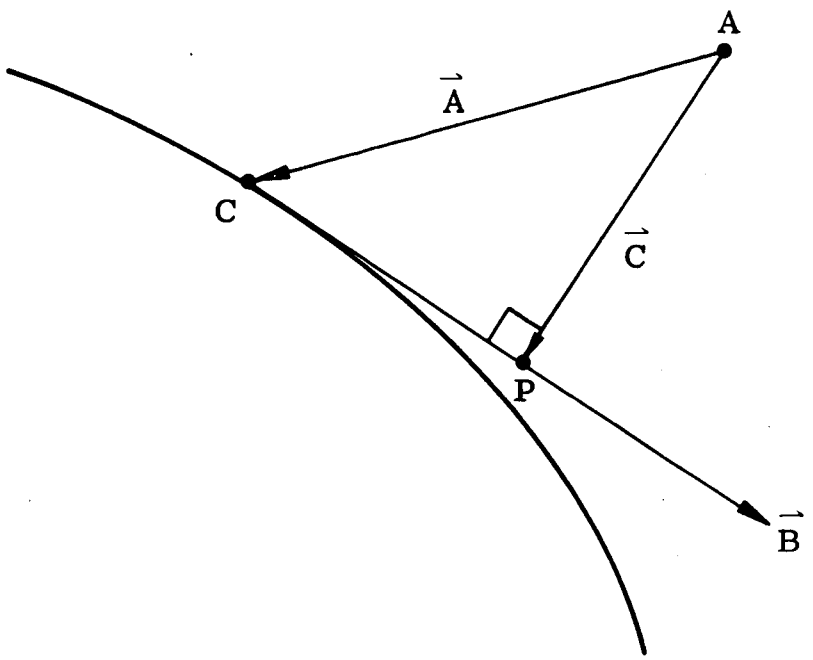

Figure 11.- The vectors $\vec{A}$, $\vec{B}$, and $\vec{C}$.

for $\vec{C}$ becomes

$$\vec{C} = \vec{A} + F\vec{B} \tag{116}$$

$$= \vec{A} - \frac{\vec{A} \cdot \vec{B}}{\vec{B} \cdot \vec{B}} \vec{B}$$

$$= \vec{A} - \frac{\vec{A} \cdot (r_c \hat{i}_\phi + r_c \cos \phi_c \dot{\theta}_c \hat{i}_\theta + \dot{r}_c \hat{i}_r)\delta\phi_c}{(r_c^2 + r_c^2 \cos^2 \phi_c \dot{\theta}_c^2 + \dot{r}_c^2)\delta\phi_c^2}$$

$$\times (r_c \hat{i}_\phi + r_c \cos \phi_c \dot{\theta}_c \hat{i}_\theta + \dot{r}_c \hat{i}_r)\delta\phi_c$$

$$= \vec{A} - \frac{\vec{A} \cdot (r_c \hat{i}_\phi + r_c \cos \phi_c \dot{\theta}_c \hat{i}_\theta + \dot{r}_c \hat{i}_r)}{(r_c^2 + r_c^2 \cos^2 \phi_c \dot{\theta}_c^2 + \dot{r}_c^2)}$$

$$\times (r_c \hat{i}_\phi + r_c \cos \phi_c \dot{\theta}_c \hat{i}_\theta + \dot{r}_c \hat{i}_r) \tag{120}$$

Now, as can be seen from Figures 10 and 11, the vector $\vec{A}$ is given by

$$\vec{A} = r_{\lambda,A}(\theta_c - \theta_{\lambda,A}) \cos \phi_c \hat{i}_\theta + (r_c - r_{\lambda,A})\hat{i}_r \ , \tag{121}$$

where $\theta_{\lambda,A}$ and $r_{\lambda,A}$ are the longitude and range, respectively, of the point A, which is on the perturbed solution curve due to a probable error ed = 0.01° in the lines-of-sight from station λ. Substituting equation 121 for $\vec{A}$ into equation 120, the expression for $\vec{C}$ becomes

$$\vec{C} = r_{\lambda,A}\,(\theta_c - \theta_{\lambda,A})\cos\phi_c \hat{i}_\theta + (r_c - r_{\lambda,A})\hat{i}_r$$

$$- \frac{[r_{\lambda,A}(\theta_c-\theta_{\lambda,A})\cos\phi_c \hat{i}_\theta + (r_c-r_{\lambda,A})\hat{i}_r]\cdot[r_c\hat{i}_\phi + r_c\cos\phi_c\dot{\theta}_c\hat{i}_\theta + \dot{r}_c\hat{i}_r]}{(r_c^2 + r_c^2\cos^2\phi_c\dot{\theta}_c^2 + \dot{r}_c^2)}$$

$$\times (r_c\hat{i}_\phi + r_c\cos\phi_c\dot{\theta}_c\hat{i}_\theta + \dot{r}_c\hat{i}_r)$$

$$= r_{\lambda,A}(\theta_c - \theta_{\lambda,A})\cos\phi_c\hat{i}_\theta + (r_c - r_{\lambda,A})\hat{i}_r$$

$$- \frac{[r_{\lambda,A}\, r_c(\theta_c - \theta_{\lambda,A})\cos^2\phi_c\dot{\theta}_c + (r_c - r_{\lambda,A})\dot{r}_c]}{(r_c^2 + r_c^2\cos^2\phi_c\dot{\theta}_c^2 + \dot{r}_c^2)}$$

$$\times (r_c\hat{i}_\phi + r_c\cos\phi_c\dot{\theta}_c\hat{i}_\theta + \dot{r}_c\hat{i}_r)$$

$$= \frac{[r_{\lambda,A}(\theta_c-\theta_{\lambda,A})\cos\phi_c - r_{\lambda,A}r_c^2(\theta_c-\theta_{\lambda,A})\cos^3\phi_c\dot{\theta}_c^2 - r_c(r_c-r_{\lambda,A})\cos\phi_c\dot{\theta}_c\dot{r}_c]\hat{i}_\theta}{(r_c^2 + r_c^2\cos^2\phi_c\dot{\theta}_c^2 + \dot{r}_c^2)}$$

$$+ \frac{[-r_{\lambda,A}\, r_c^2\,(\theta_c-\theta_{\lambda,A})\cos^2\phi_c\dot{\theta}_c - r_c(r_c-r_{\lambda,A})\,\dot{r}_c]\,\hat{i}_\phi}{(r_c^2 + r_c^2\cos^2\phi_c\dot{\theta}_c^2 + \dot{r}_c^2)}$$

$$+ \frac{[(r_c-r_{\lambda,A}) - r_{\lambda,A}r_c(\theta_c-\theta_{\lambda,A})\cos^2\phi_c\dot{\theta}_c\dot{r}_c - (r_c-r_{\lambda,A})\,\dot{r}_c^2]\,\hat{i}_r}{(r_c^2 + r_c^2\cos^2\phi_c\dot{\theta}_c^2 + \dot{r}_c^2)} \qquad (122)$$

Therefore, the east-west, north-south, and vertical components—denoted by $d1_{\lambda,A}$, $d2_{\lambda,A}$, and $d3_{\lambda,A}$, respectively—of the total pointing displacement error in the solution point A due to a probable error ed = 0.01° in the lines-of-sight from station λ are, respectively,

$$dl_{\lambda,A} = \cos\phi_c \frac{[r_{\lambda,A}(\theta_c-\theta_{\lambda,A})-r_c(r_c-r_{\lambda,A})\dot{\theta}_c\dot{r}_c-r_{\lambda,A}r_c^2(\theta_c-\theta_{\lambda,A})\cos^2\phi_c\dot{\theta}_c^2]}{(r_c^2 + r_c^2\cos^2\phi_c\dot{\theta}_c^2 +\dot{r}_c^2)} \tag{123}$$

$$d2_{\lambda,A} = -r_c \frac{[r_{\lambda,A}r_c(\theta_c-\theta_{\lambda,A})\cos^2\phi_c\dot{\theta}_c + (r_c-r_{\lambda,A})\dot{r}_c]}{(r_c^2 + r_c^2\cos^2\phi_c\dot{\theta}_c^2 + \dot{r}_c^2)} \tag{124}$$

$$d3_{\lambda,A} = \frac{[(r_c-r_{\lambda,A})-r_{\lambda,A}r_c(\theta_c-\theta_{\lambda,A})\cos^2\phi_c\dot{\theta}_c\dot{r}_c-(r_c-r_{\lambda,A})\dot{r}_c^2]}{(r_c^2 + r_c^2\cos^2\phi_c\dot{\theta}_c^2 + \dot{r}_c^2)} \tag{125}$$

It is recalled that in the above expressions for $dl_{\lambda,A}$, $d2_{\lambda,A}$, and $d3_{\lambda,A}$ the subscript C is for the point on the unperturbed solution curve which has the same latitude as the point A on the perturbed solution curve.

Therefore, the east-west, north-south, and vertical components — denoted by $dS1_{NA}$, $dS2_{NA}$, and $dS3_{NA}$, respectively - of the total pointing displacement error in the $NA^{\underline{th}}$ solution point due to a probable error ed = 0.01° in the lines-of-sight from the observation stations to the points on the cloud are, respectively,

$$dS1_{NA} = \left[\sum_{\lambda=1}^{L} (dl_{\lambda,NA})^2\right]^{1/2} \tag{126}$$

$$dS2_{NA} = \left[\sum_{\lambda=1}^{L} (d2_{\lambda,NA})^2\right]^{1/2} \tag{127}$$

$$dS3_{NA} = \left[\sum_{\lambda=1}^{L} (d3_{\lambda,NA})^2 \right]^{1/2} , \quad 1 \leq NA \leq NT, \tag{128}$$

where NT is the total number of points on the solution curve and the summation over λ means that the error in the lines-of-sight is only put into the data from one station, station λ, at a time.

The total pointing displacement error dST_{NA} in the $NA^{\underline{th}}$ solution point due to a probable error $ed = 0.01^{\circ}$ in the lines-of-sight from the observation stations to the points on the cloud is then

$$dST_{NA} = [(dS1_{NA})^2 + (dS2_{NA})^2 + (dS3_{NA})^2]^{1/2} \tag{129}$$

The dimensions of $dS1_{NA}$, $dS2_{NA}$, $dS3_{NA}$, and dST_{NA} are kilometers.

Pointing Displacement Errors as a Function of the Number and Location of the Observation Stations

It was decided to exercise the LaRC triangulation method to its fullest in order to extract meaningful information to aid in designing the remainder of the experiment. To begin with, the errors in the triangulation solution as a function of the number and the location of the observation stations were desired. These were important to know for the formulation of the "go"-"no go" launch criteria for the experiment in the event of unfavorable weather or equipment malfunction at one or more of the stations. Eight cases - which were composed of all the possible combinations of from two to five stations, always keeping the two prime sites Mt. Hopkins and Cerro Morado - plus a ninth case - which

was composed of just Mt. Hopkins and Cerro Morado, but with two cameras at Mt. Hopkins — were investigated. These nine cases of different station combinations are listed in Table 2. Figures 12, 13, 14, and 15 are plots of the pointing displacement errors—east-west, north-south, vertical, and total, respectively—as functions of the latitude for the nine cases of different station combinations. It is seen from the figures that case 9, with just the two prime stations, is the worst and that case 1, with all five stations, is the best. The cases composed of three and four observation stations give intermediate results. Case 8, which denotes the case of one camera at Cerro Morado and two cameras at Mt. Hopkins, is considerably better than case 9, which denotes the case of just one camera at each of these same two stations.

Pointing Slope Errors

In addition to determining what pointing displacement errors to expect in the triangulation solution of the cloud position, it was decided to determine what pointing errors in slope and curvature to also expect. First, it is necessary to find the latitude, longitude, and range coordinates of the line between two points in geocentric coordinates. In Figure 16 the points P_{N-1} and P_N denote the two points in question.

If the point P_N is the point P in Figure 11, where the vector $\vec{C}$ drawn from the point A on the perturbed solution curve perpendicularly intersects the vector $\vec{B}$ which is tangent to the point C on the

Table 2: The nine cases of different station combinations.

Case 1:	Cerro Morado Mt. Hopkins Natal Baker Nunn Wallops White Sands
Case 2:	Cerro Morado Mt. Hopkins Natal Baker Nunn White Sands
Case 3:	Cerro Morado Mt. Hopkins Natal Baker Nunn Wallops
Case 4:	Cerro Morado Mt. Hopkins Wallops White Sands
Case 5:	Cerro Morado Mt. Hopkins White Sands
Case 6:	Cerro Morado Mt. Hopkins Wallops
Case 7:	Cerro Morado Mt. Hopkins Natal Baker Nunn
Case 8:	Cerro Morado Mt. Hopkins Mt. Hopkins Baker Nunn
Case 9:	Cerro Morado Mt. Hopkins

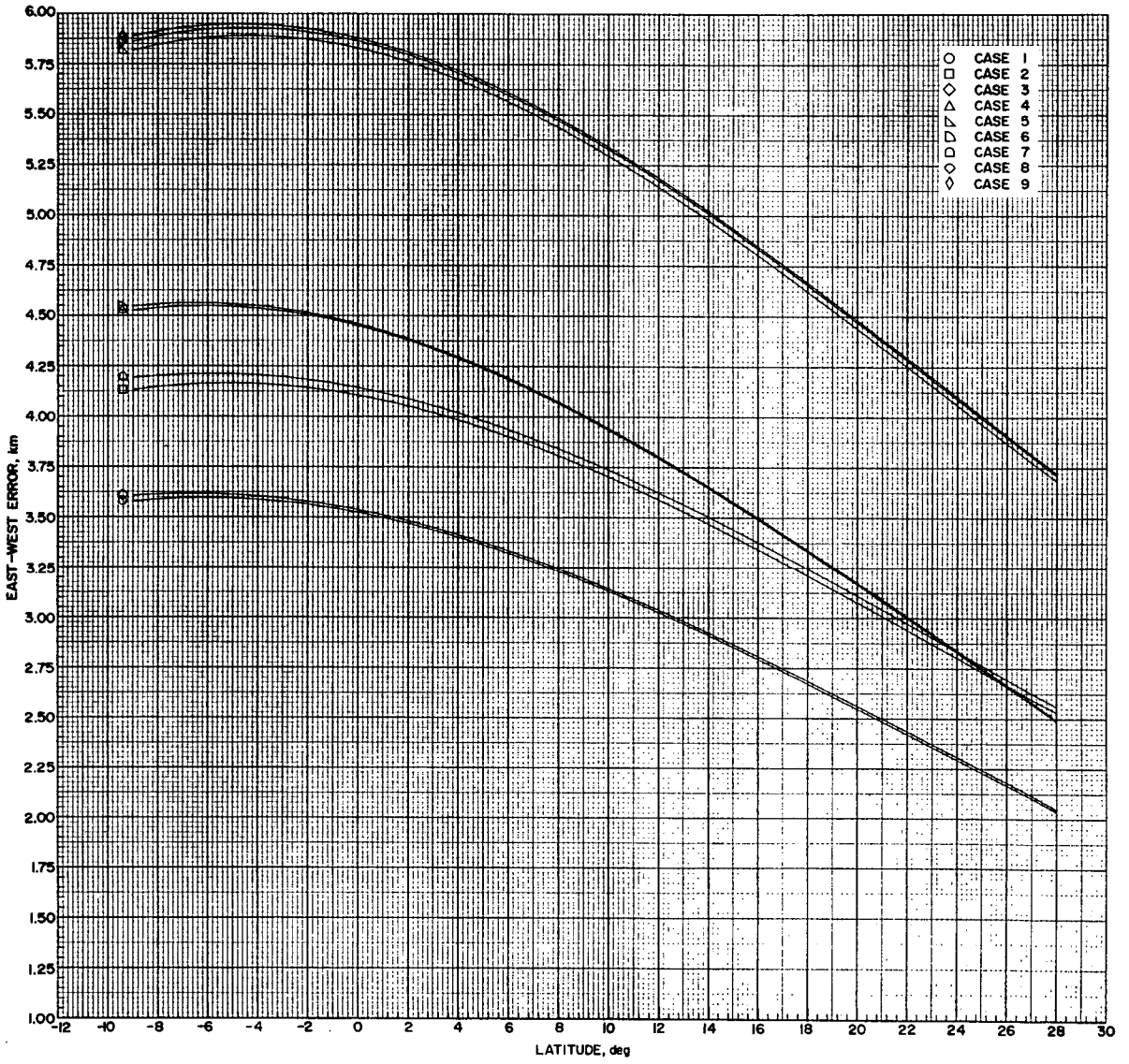

Figure 12.- East-west pointing displacement error as a function of latitude for the different station cases.

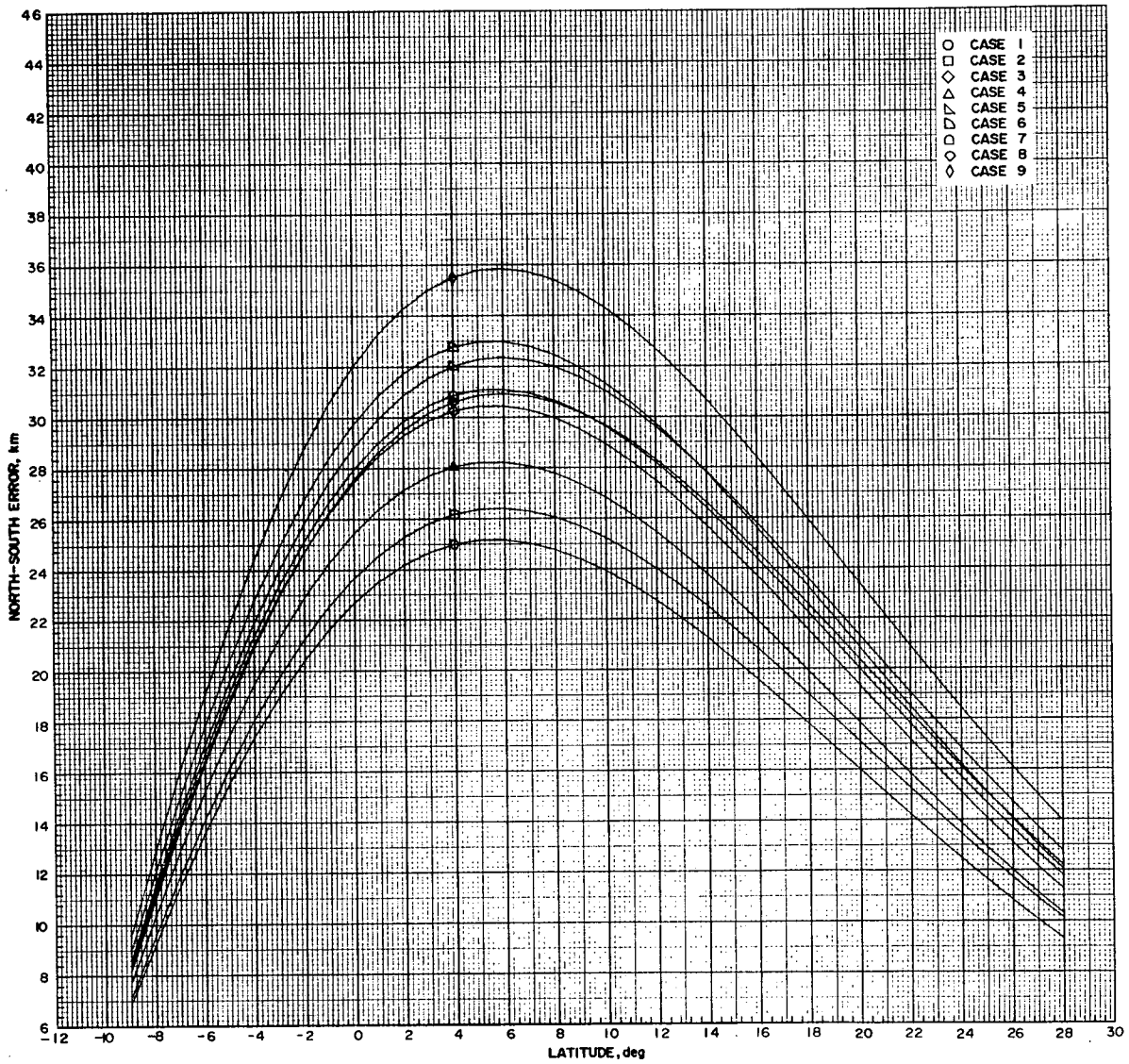

Figure 13.- North-south pointing displacement error as a function of latitude for the different station cases.

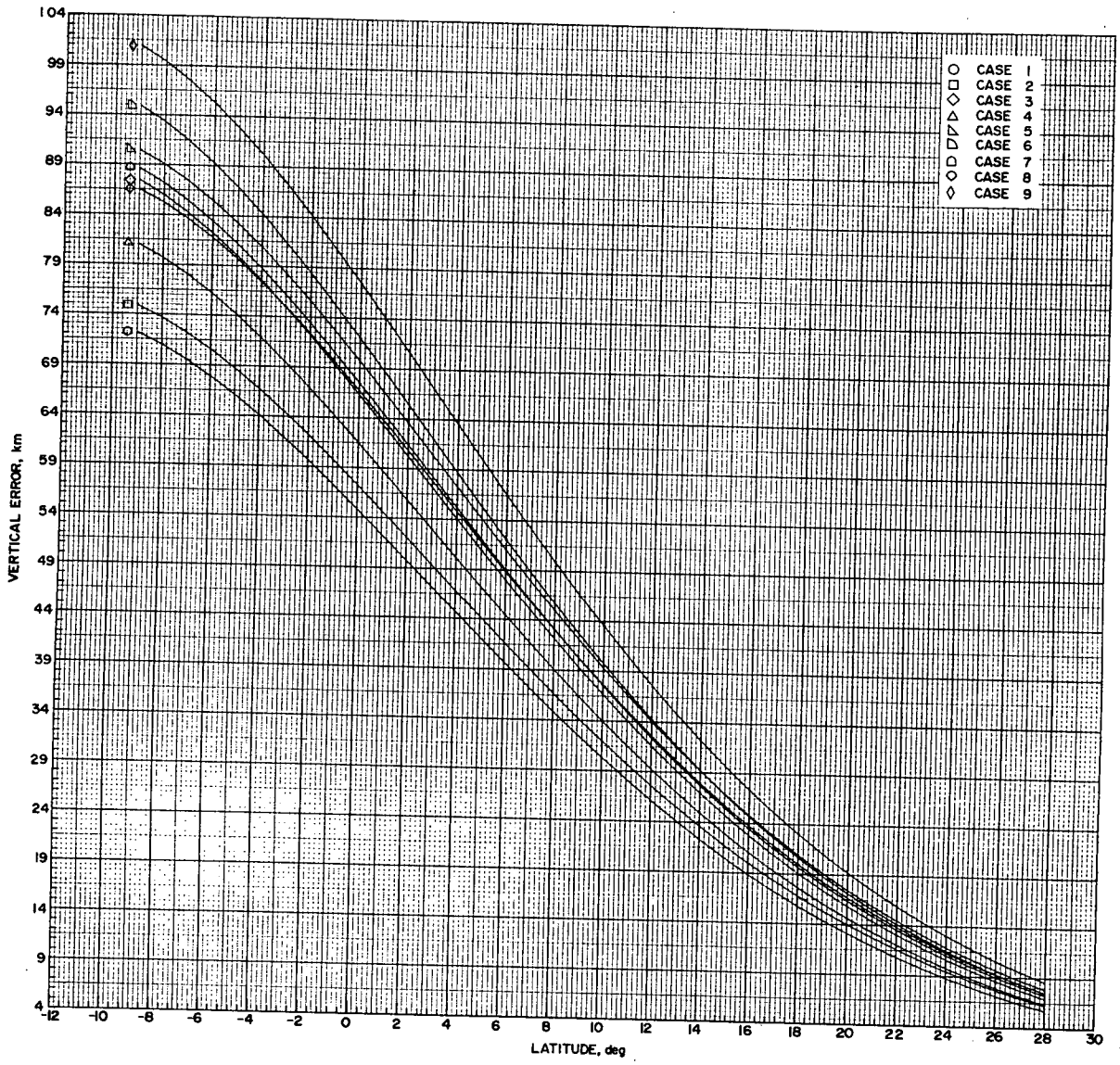

Figure 14.- Vertical pointing displacement error as a function of latitude for the different station cases.

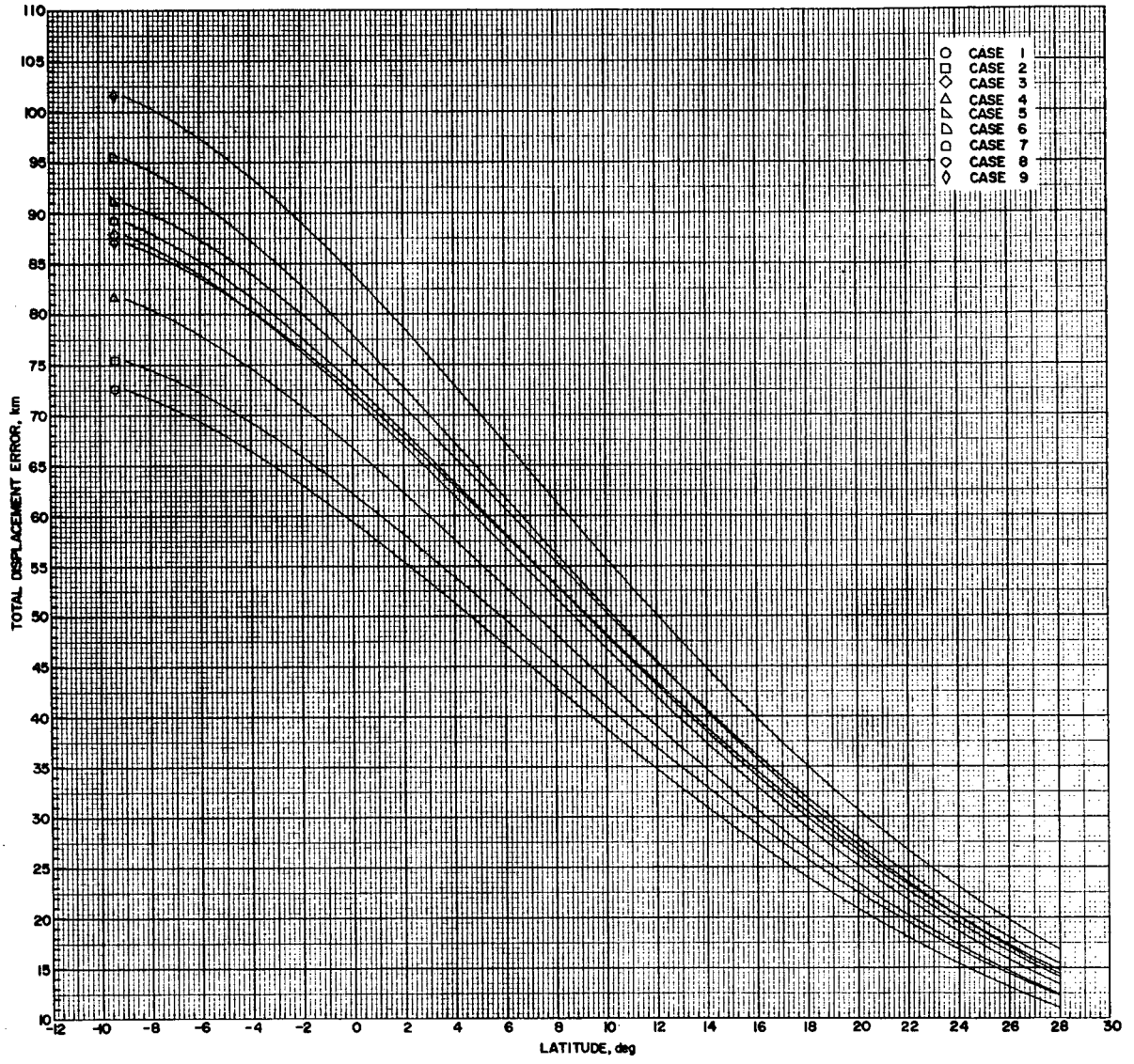

Figure 15.- Total pointing displacement error as a function of latitude for the different station cases.

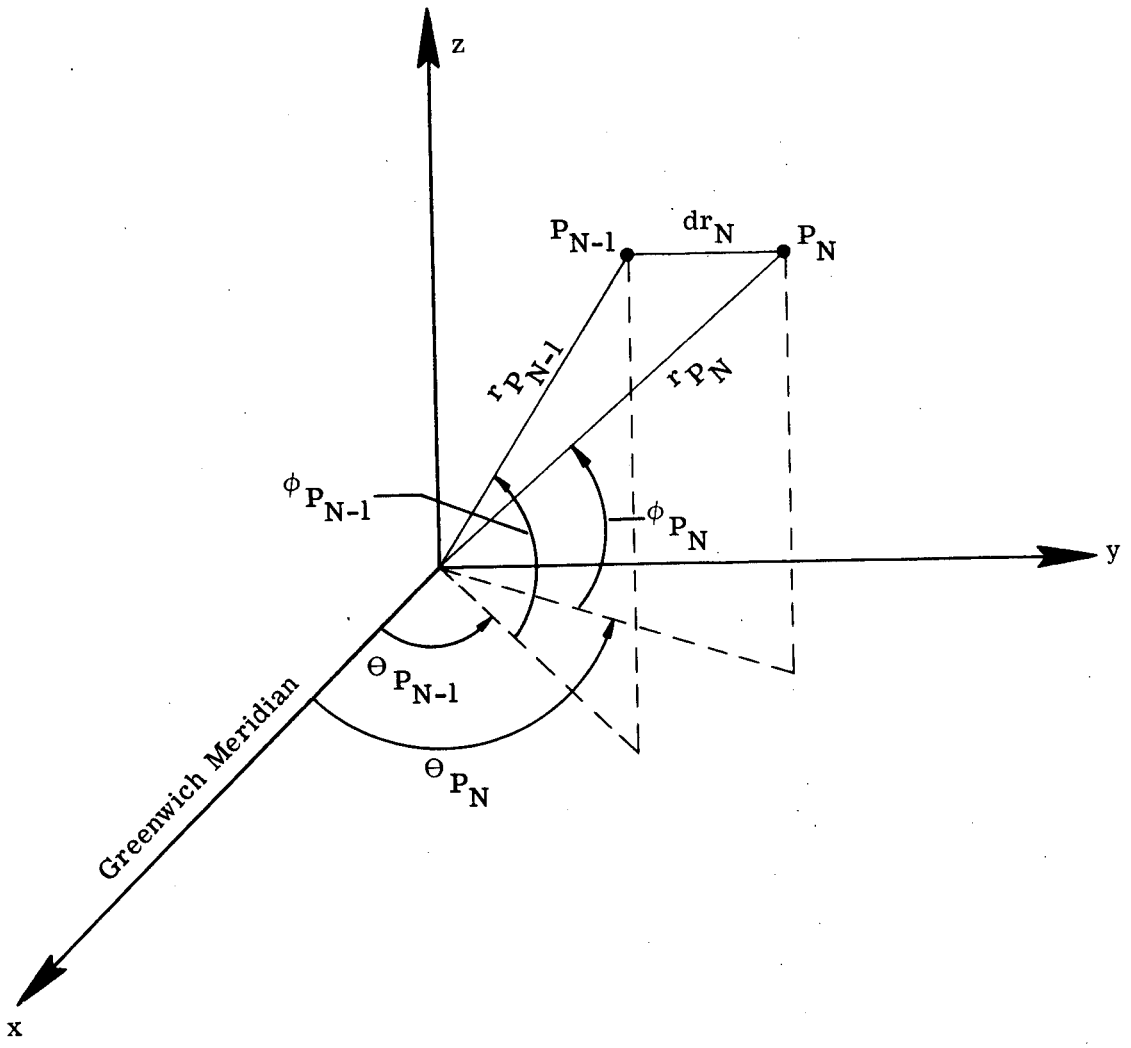

Figure 16.- The latitude, longitude, and range of the points P_{N-1} and P_N.

unperturbed solution curve, then the latitude, longitude, and range of the point P_N—denoted by ϕ_{P_N}, θ_{P_N}, and r_{P_N}, respectively—are given by

$$\phi_{P_N} = \phi_c + F \tag{130}$$

$$\theta_{P_N} = \theta_c + F \dot{\theta}_c \tag{131}$$

$$r_{P_N} = r_c + F \dot{r}_c , \tag{132}$$

where ϕ_c is the latitude of the point C, which is the same as the latitude of the point A. The quantities θ_c, r_c, $\dot{\theta}_c$, and $\dot{r}_c$ are the longitude, range, change in longitude with respect to latitude, and change in range with respect to latitude, respectively, of the point C and are given by equations 111-114, respectively, for N = C.

Analogous expressions also exist for the latitude, longitude, and range of the point P_{N-1}—which are denoted by $\phi_{P_{N-1}}$, $\theta_{P_{N-1}}$, and $r_{P_{N-1}}$, respectively.

From Figure 16 it is seen that the x,y,z components of P_N and P_{N-1}—denoted by x_{P_N}, y_{P_N}, z_{P_N} and $x_{P_{N-1}}$, $y_{P_{N-1}}$, $z_{P_{N-1}}$, respectively—are

$$x_{P_N} = r_{P_N} \cos \phi_{P_N} \cos \theta_{P_N} \tag{133}$$

$$y_{P_N} = r_{P_N} \cos \phi_{P_N} \sin \theta_{P_N} \tag{134}$$

$$z_{P_N} = r_{P_N} \sin \phi_{P_N} \tag{135}$$

$$x_{P_{N-1}} = r_{P_{N-1}} \cos \phi_{P_{N-1}} \cos \theta_{P_{N-1}} \tag{136}$$

$$y_{P_{N-1}} = r_{P_{N-1}} \cos \phi_{P_{N-1}} \sin \theta_{P_{N-1}} \tag{137}$$

$$z_{P_{N-1}} = r_{P_{N-1}} \sin \phi_{P_{N-1}} \tag{138}$$

The differences between the respective rectangular components of P_N and P_{N-1}—denoted by dx_N, dy_N, and dz_N—are

$$dx_N = x_{P_N} - x_{P_{N-1}} \tag{139}$$

$$dy_N = y_{P_N} - y_{P_{N-1}} \tag{140}$$

$$dz_N = z_{P_N} - z_{P_{N-1}} \tag{141}$$

Therefore, the line between P_{N-1} and P_N in latitude, longitude, and range coordinates—denoted by $d\phi_N$, $d\theta_N$, and dr_N, respectively—is given by

$$d\phi_N = \sin^{-1}\left(\frac{dz_N}{(dx_N^2 + dy_N^2 + dz_N^2)^{1/2}}\right) \tag{142}$$

$$d\theta_N = \tan^{-1}\left(\frac{dy_N}{dx_N}\right) \tag{143}$$

$$dr_N = (dx_N^2 + dy_N^2 + dz_N^2)^{1/2} \tag{144}$$

As is seen in Figure 17 there is a line solution through the points P_{N-1} and P_N and also a line solution through the points P_{N-1} and $P'_{\lambda,N}$, where $P'_{\lambda,N}$ is the perturbed solution point due to the probable error $ed = 0.01^{\circ}$ in the lines-of-sight from station λ. Just as the latitude, longitude, and range of the line between P_{N-1} and P_N were found, the latitude, longitude, and range of the line between P_{N-1} and $P'_{\lambda,N}$ can similarly be found. The rectangular components of $P'_{\lambda,N}$—denoted by $x'_{\lambda,N}$, $y'_{\lambda,N}$, and $z'_{\lambda,N}$—are

$$x'_{\lambda,N} = r'_{\lambda,N} \cos \phi'_{\lambda,N} \cos \theta'_{\lambda,N} \tag{145}$$

$$y'_{\lambda,N} = r'_{\lambda,N} \cos \phi'_{\lambda,N} \sin \theta'_{\lambda,N} \tag{146}$$

$$z'_{\lambda,N} = r'_{\lambda,N} \sin \phi'_{\lambda,N} \quad , \tag{147}$$

where $\phi'_{\lambda,N}$, $\theta'_{\lambda,N}$, and $r'_{\lambda,N}$ are the latitude, longitude, and range, respectively, of the perturbed solution point $P'_{\lambda,N}$. The differences between the respective rectangular components of $P'_{\lambda,N}$ and P_{N-1}—

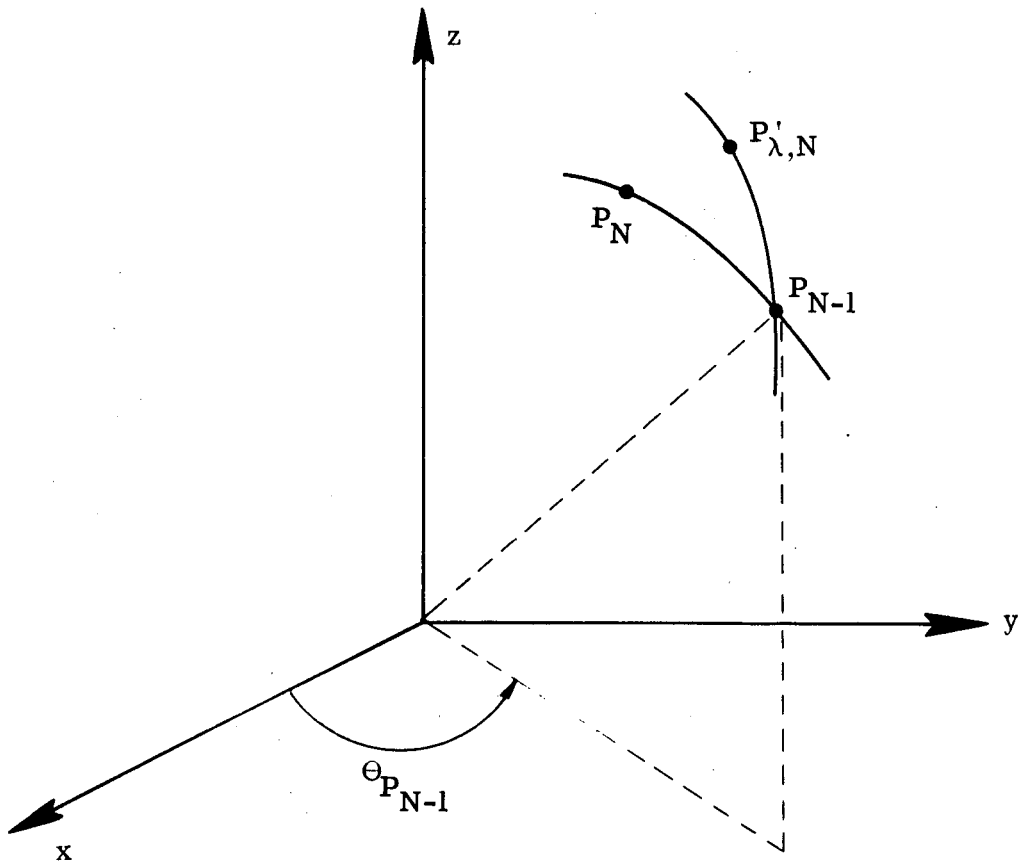

Figure 17.- A line solution through P_{N-1} and P_N and a line solution through P_{N-1} and $P'_{\lambda,N}$.

denoted by $dx'_{\lambda,N}$, $dy'_{\lambda,N}$, and $dz'_{\lambda,N}$—are

$$dx'_{\lambda,N} = x'_{\lambda,N} - x_{P_{N-1}} \tag{148}$$

$$dy'_{\lambda,N} = y'_{\lambda,N} - y_{P_{N-1}} \tag{149}$$

$$dz'_{\lambda,N} = z'_{\lambda,N} - z_{P_{N-1}} \tag{150}$$

Therefore, the line between P_{N-1} and $P'_{\lambda,N}$ in latitude, longitude, and range coordinates—denoted by $d\phi'_{\lambda,N}$, $d\theta'_{\lambda,N}$, and $dr'_{\lambda,N}$, respectively—is given by

$$d\phi'_{\lambda,N} = \sin^{-1}\left(\frac{dz'_{\lambda,N}}{\left[(dx'_{\lambda,N})^2 + (dy'_{\lambda,N})^2 + (dz'_{\lambda,N})^2\right]1/2}\right) \tag{151}$$

$$d\theta'_{\lambda,N} = \tan^{-1}\left(\frac{dy'_{\lambda,N}}{dx'_{\lambda,N}}\right) \tag{152}$$

$$dr'_{\lambda,N} = \left[(dx'_{\lambda,N})^2 + (dy'_{\lambda,N})^2 + (dz'_{\lambda,N})^2\right]^{1/2} \tag{153}$$

Since the magnetic field lines of the earth lie approximately in planes of constant longitude, the longitude $d\theta_N$ of the line between P_{N-1} and P_N is very nearly equal to $\theta_{P_{N-1}}$, the longitude of the point P_{N-1}. Since the slope error is small, the longitude $d\theta'_{\lambda,N}$ of the line between P_{N-1} and $P'_{\lambda,N}$ is also very nearly equal to $\theta_{P_{N-1}}$.

It is convenient to construct a new coordinate system x', y', z'—with its origin at P_{N-1}, x' axis in the plane of constant longitude $\theta_{P_{N-1}}$, z' axis the same as the z axis in Figure 17, and y' axis to form a right-handed orthogonal set—as shown in Figure 18. The vector from P_{N-1} to P_N is denoted by $\vec{dP}$; and the vector from P_{N-1} to $P'_{\lambda,N}$, by $\vec{dP}'$. The latitude, longitude, range components of $\vec{dP}$ are $d\phi_N$, $d\theta_N$, dr_N as given by equations 142-144, respectively; and the latitude, longitude, range components of $\vec{dP}'$ are $d\phi'_{\lambda,N}$, $d\theta'_{\lambda,N}$, $dr'_{\lambda,N}$ as given by equations 151-153, respectively. The total output pointing slope error $aST_{\lambda,N}$ is the angle between the vectors $\vec{dP}$ and $\vec{dP}'$. The total output pointing slope error can be resolved into two components—one in the plane of constant longitude and the other perpendicular to this plane. The parallel component is called the latitude output pointing slope error and is denoted by $aS1_{\lambda,N}$; the perpendicular component is called the longitude output pointing slope error and is denoted by $aS2_{\lambda,N}$.

The rectangular coordinates of the unit vector $\hat{dP}$ in the primed coordinate system of Figure 18—denoted by ddx_N, ddy_N, and ddz_N—are

$$ddx_N = \cos d\phi_N \cos\left(d\theta_N - \theta_{P_{N-1}}\right) \tag{154}$$

$$ddy_N = \cos d\phi_N \sin\left(d\theta_N - \theta_{P_{N-1}}\right) \tag{155}$$

$$ddz_N = \sin d\phi_N \quad , \tag{156}$$

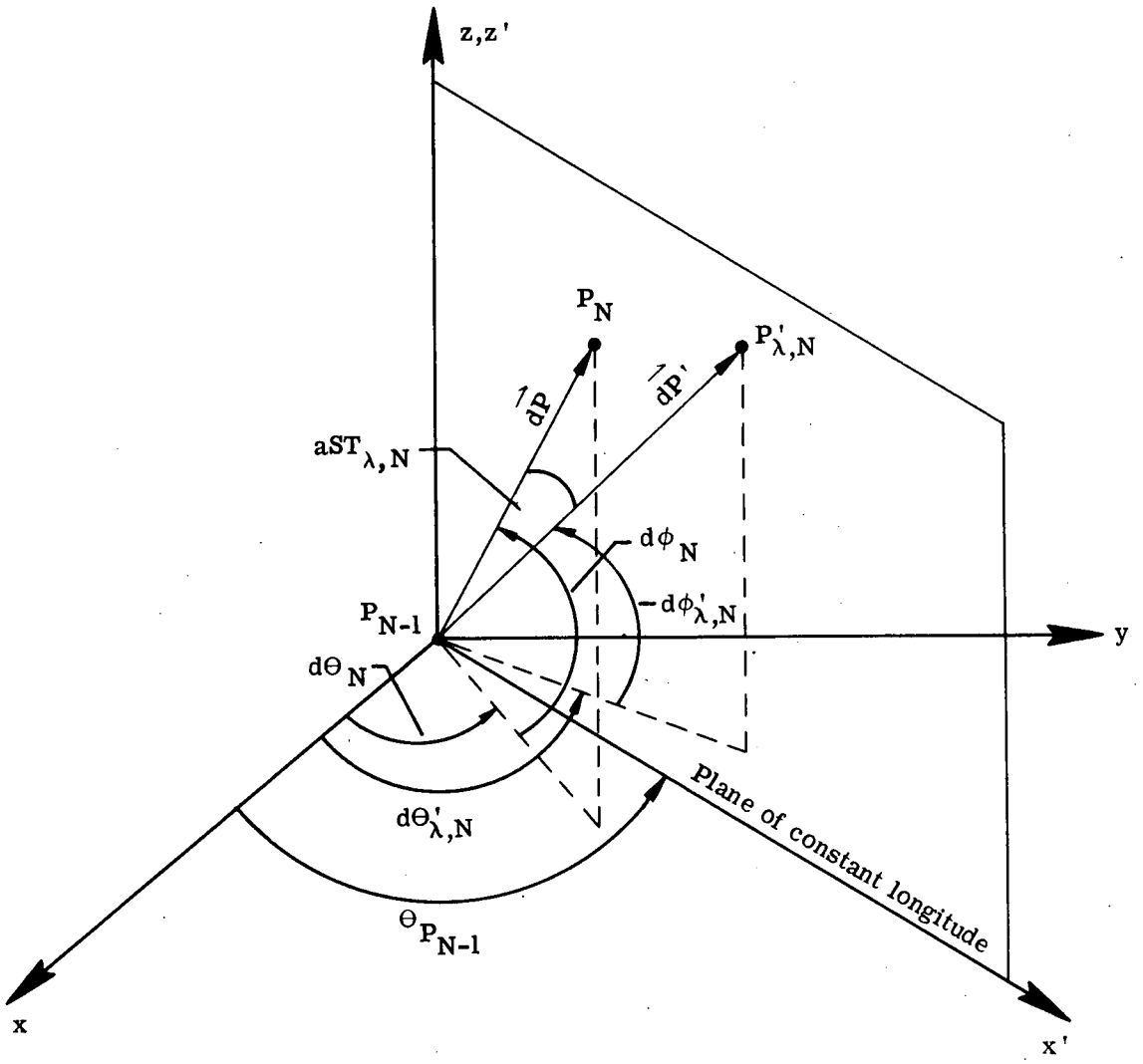

Figure 18.- The vectors $\vec{dP}$ and $\vec{dP'}$ and the total output pointing slope error $aST_{\lambda,N}$.

where $\theta_{P_{N-1}}$ is the longitude of the point P_{N-1} and $d\phi_N$ and $d\theta_N$ are given by equations 142 and 143. Similarly, the rectangular coordinates of the unit vector $\hat{dP}'$ in the primed coordinate system of Figure 18 - denoted by $ddx'_{\lambda,N}$, $ddy'_{\lambda,N}$, and $ddz'_{\lambda,N}$ - are

$$ddx'_{\lambda,N} = \cos d\phi'_{\lambda,N} \cos \left(d\theta'_{\lambda,N} - \theta_{P_{N-1}}\right) \tag{157}$$

$$ddy'_{\lambda,N} = \cos d\phi'_{\lambda,N} \sin \left(d\theta'_{\lambda,N} - \theta_{P_{N-1}}\right) \tag{158}$$

$$ddz'_{\lambda,N} = \sin d\phi'_{\lambda,N} \quad , \tag{159}$$

where $d\phi'_{\lambda,N}$ and $d\theta'_{\lambda,N}$ are given by equations 151 and 152.

Hence, the latitude and longitude components of the total output pointing slope error, denoted by $aS1_{\lambda,N}$ and $aS2_{\lambda,N}$, and the total output pointing slope error $aST_{\lambda,N}$ in the $N^{\underline{th}}$ solution point due to a probable error $ed = 0.01^{\circ}$ in the lines-of-sight from station λ are, respectively,

$$aS1_{\lambda,N} = \tan^{-1}\left(\frac{ddz'_{\lambda,N}}{ddx'_{\lambda,N}}\right) - \tan^{-1}\left(\frac{ddz_N}{ddx_N}\right) \tag{160}$$

$$aS2_{\lambda,N} = ddy'_{\lambda,N} - ddy_N \tag{161}$$

$$aST_{\lambda,N} = \left[(aS1_{\lambda,N})^2 + (aS2_{\lambda,N})^2\right]^{1/2} \tag{162}$$

The latitude and longitude components of the total output pointing slope error, denoted by $aS1_{NA}$ and $aS2_{NA}$, and the total output

pointing slope error aST_{NA} in the $NA^{\underline{th}}$ solution point due to a probable error $ed = 0.01^{\circ}$ in the lines-of-sight from the observation stations to the points on the cloud are, respectively,

$$aS1_{NA} = \left[\sum_{\lambda=1}^{L} (aS1_{\lambda,NA})^2 \right] 1/2 \tag{163}$$

$$aS2_{NA} = \left[\sum_{\lambda=1}^{L} (aS2_{\lambda,NA})^2 \right] 1/2 \tag{164}$$

$$aST_{NA} = \left[(aS1_{NA})^2 + (aS2_{NA})^2 \right]^{1/2}, \quad 1 \leq NA \leq NT , \tag{165}$$

where NT is the total number of points on the solution curve and the summation over λ means that the error in the lines-of-sight is only put into the data from one station, station λ, at a time.

The total pointing slope error AST is defined as the ratio of the total output pointing slope error aST to the total input pointing slope error sa. In Figure 19, the points p_{n-1} and p_n are consecutive points spaced BN degrees apart on the unperturbed azimuth-elevation curve. It is recalled that $BN = 0.28^{\circ}$. The point p_n', a line from which perpendicularly intersects the unperturbed curve at the point p_n, is on the perturbed azimuth-elevation curve due to a probable error $ed = 0.01^{\circ}$ in the line-of-sight from the station to the point p_n. The total input pointing slope error sa is given by

$$\tan sa = \frac{ed}{BN} \tag{166}$$

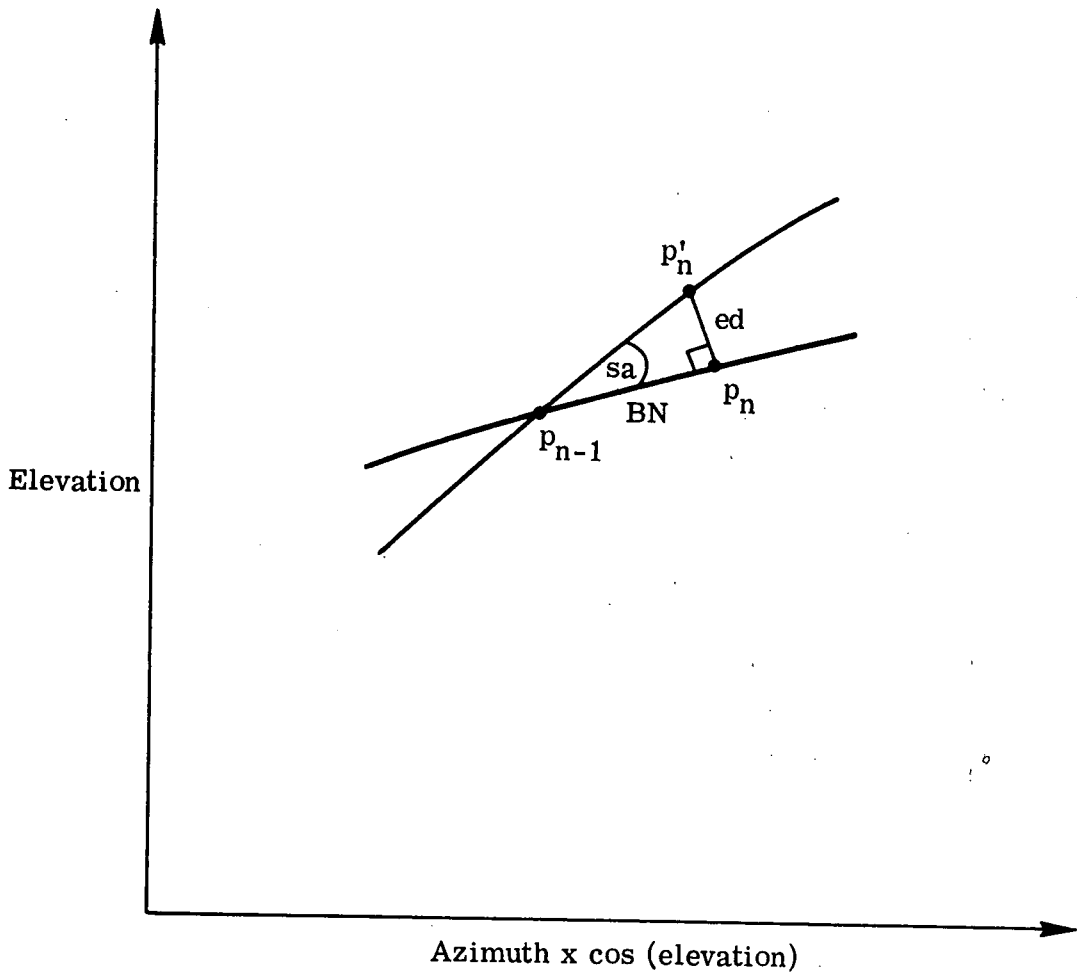

Figure 19.- The total input pointing slope error sa.

Since ed = 0.01° and BN = 0.28°, tan sa is small and, hence, is approximately equal to sa. Hence,

$$sa = \frac{ed}{BN} \tag{167}$$

Therefore, the total pointing slope error AST_{NA} in the $NA^{\underline{th}}$ solution point due to a probable error ed = 0.01° in the lines-of-sight from the observation stations to the points on the cloud is

$$AST_{NA} = \frac{aST_{NA}}{sa} , \tag{168}$$

where aST_{NA} is given by equation 165 and sa is given by equation 167.

Now,

$$AST_{NA} = \frac{aST_{NA}}{sa} \tag{168}$$

$$= \frac{\left[(aS1_{NA})^2 + (aS2_{NA})^2\right]^{1/2}}{sa} \text{ , using equation 165}$$

$$= \left[\left(\frac{aS1_{NA}}{sa}\right)^2 + \left(\frac{aS2_{NA}}{sa}\right)^2\right]^{1/2} \tag{169}$$

Therefore, from equation 169 it is seen that the latitude pointing slope error $AS1_{NA}$, the component of the total pointing slope error in the plane of constant longitude, and the longitude pointing slope error $AS2_{NA}$, the component of the total pointing slope error

perpendicular to the plane of constant longitude, in the $NA^{\underline{th}}$ solution point due to a probable error $ed = 0.01^{\circ}$ in the lines-of-sight from the observation stations to the points on the cloud are, respectively,

$$ASl_{NA} = \frac{aSl_{NA}}{sa} \tag{170}$$

$$AS2_{NA} = \frac{aS2_{NA}}{sa} , \tag{171}$$

where aSl_{NA}, $aS2_{NA}$, and sa are given by equations 163, 164, and 167, respectively.

The three slope errors ASl_{NA}, $AS2_{NA}$, and AST_{NA} are all dimensionless.

Pointing Slope Errors as a Function of the Number and Location of the Observation Stations

Figures 20, 21, and 22 are plots of the latitude pointing slope error, the longitude pointing slope error, and the total pointing slope error, respectively, as functions of the latitude for the nine different station combinations. As for the pointing displacement errors, the greatest accuracy is for the five-station case, case 1, and the least accuracy is for the two-station case, case 9, the combinations of four and three stations giving intermediate accuracies. Again, case 8, with two cameras at Mt. Hopkins and one at Cerro Morado, is considerably more accurate than case 9, with just one camera at each of these same two stations.

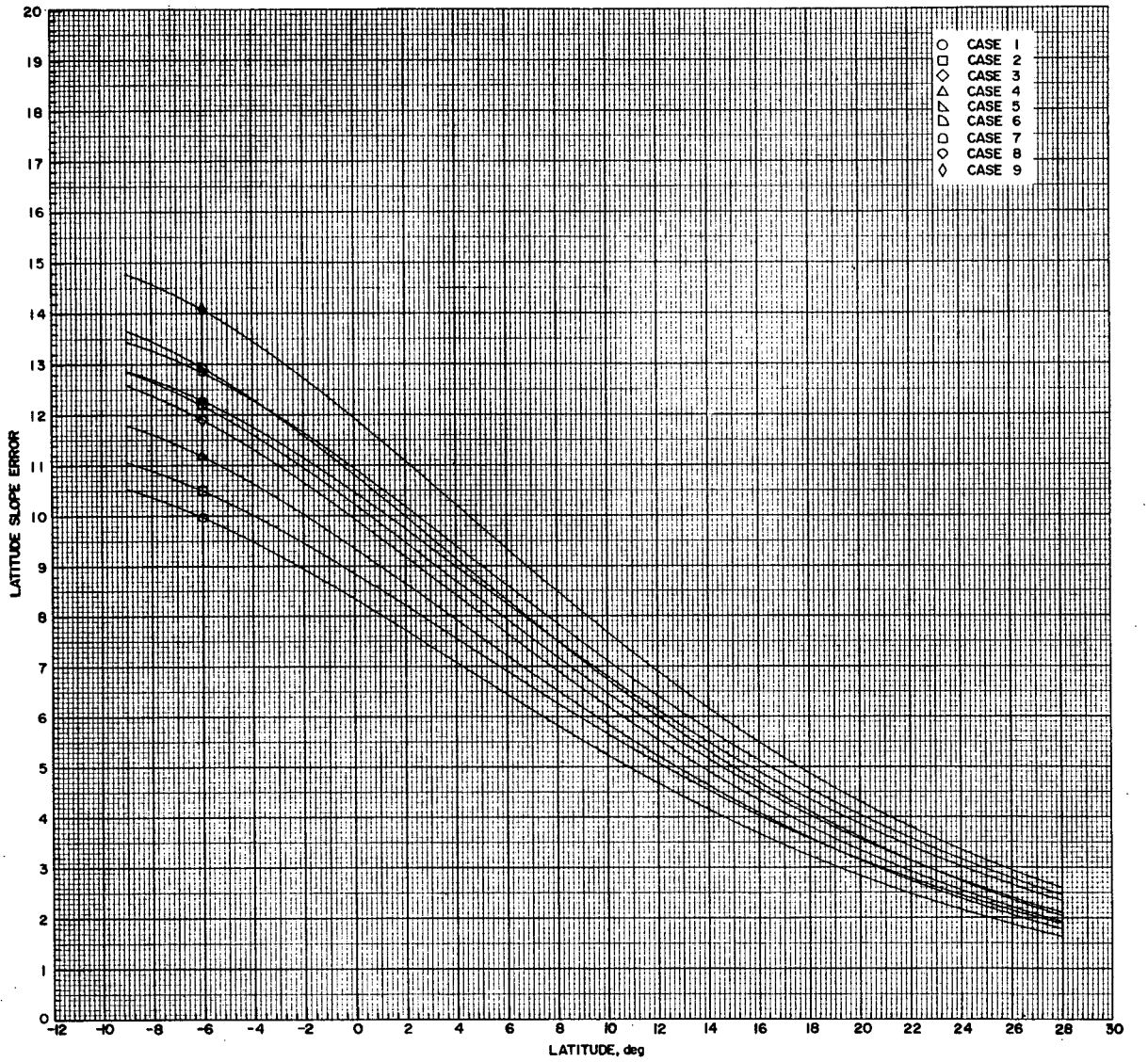

Figure 20.- Latitude pointing slope error as a function of latitude for the different station cases.

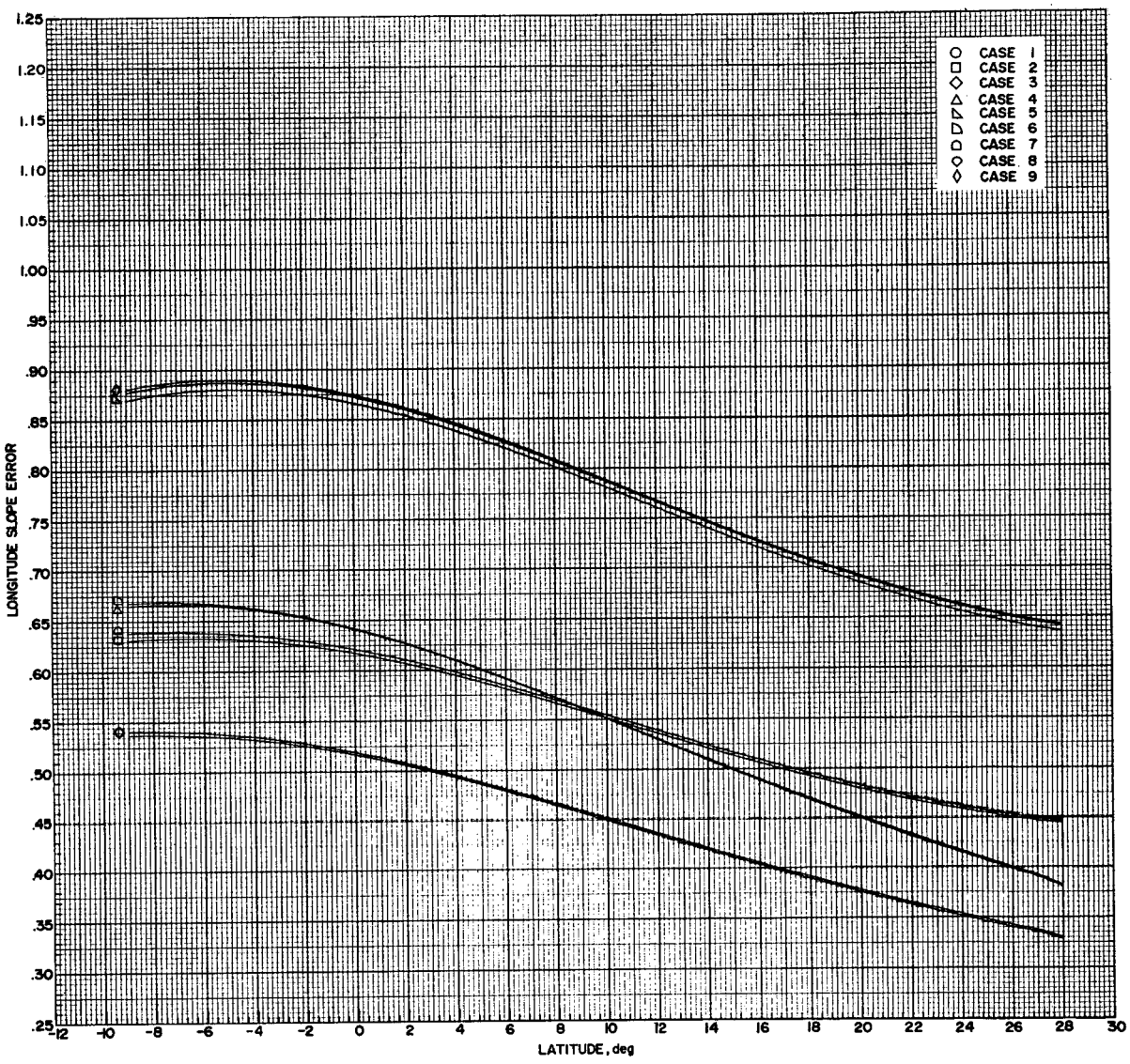

Figure 21.- Longitude pointing slope error as a function of latitude for the different station cases.

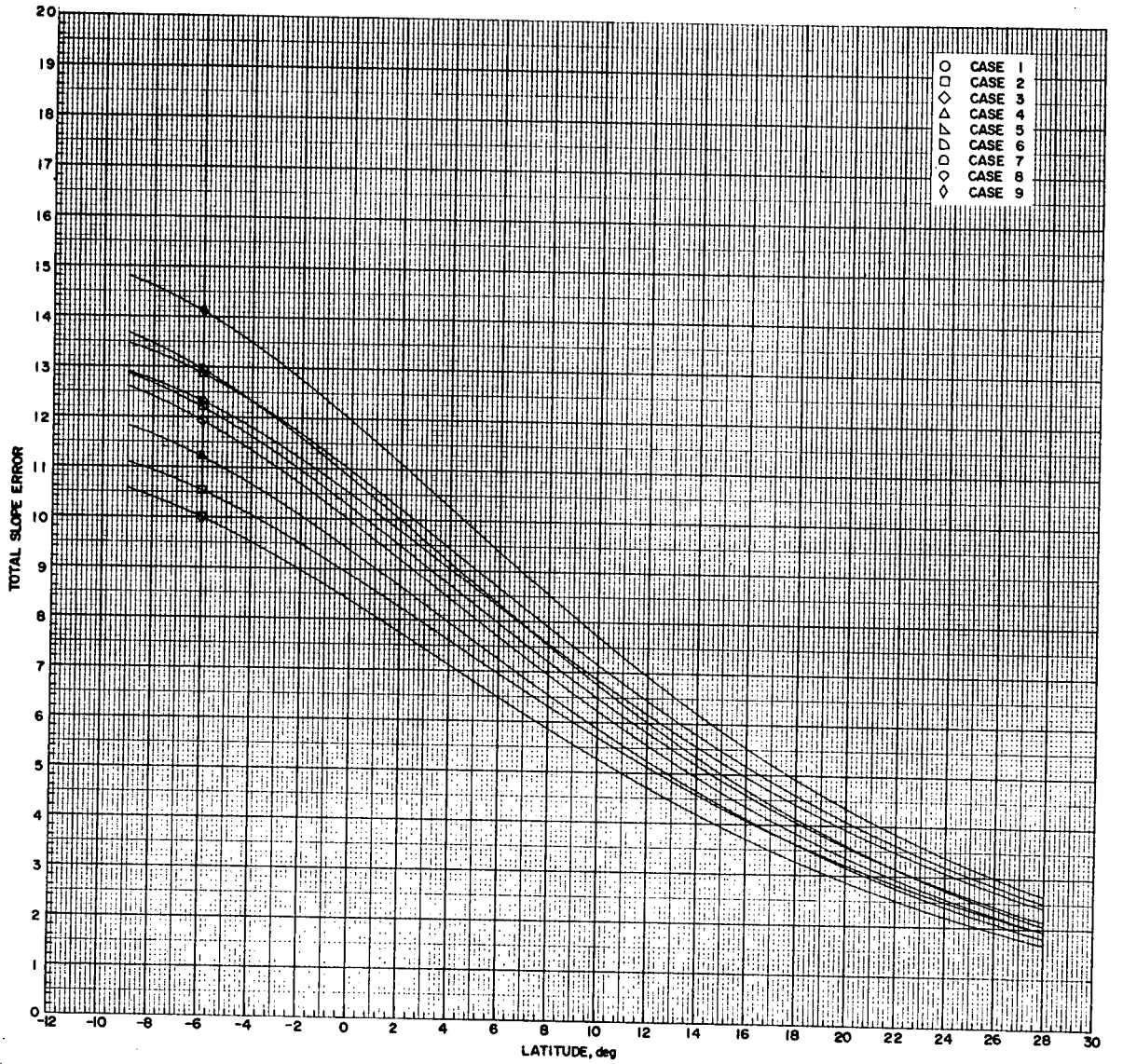

Figure 22.- Total pointing slope error as a function of latitude for the different station cases.

Pointing Curvature Error

The pointing curvature error is defined as the ratio of the output pointing curvature error to the input pointing curvature error. For defining the input pointing curvature error, consider Figure 23, in which R is the radius of curvature of the perturbed azimuth-elevation curve through the three consecutive points p'_{n-2}, p'_{n-1}, and p'_n due to a probable error $ed = 0.01^\circ$ in the line-of-sight from the station to the point p_{n-1} on the unperturbed azimuth-elevation curve through the three consecutive points p_{n-2}, p_{n-1}, and p_n spaced $BN = 0.28^\circ$ apart. The angle α is small, as BN is small. From Figure 23 it is seen that

$$\cos \alpha = \frac{R - ed}{R} \tag{172}$$

$$R \cos \alpha = R - ed$$

$$R\left(1 - \frac{\alpha^2}{2} \pm \ldots\right) = R - ed, \quad \text{expanding } \cos \alpha$$

$$R - R\frac{\alpha^2}{2} = R - ed, \text{ as } \alpha \text{ is small}$$

$$R\frac{\alpha^2}{2} = ed$$

Hence,

$$R = \frac{2\ ed}{\alpha^2} \tag{173}$$

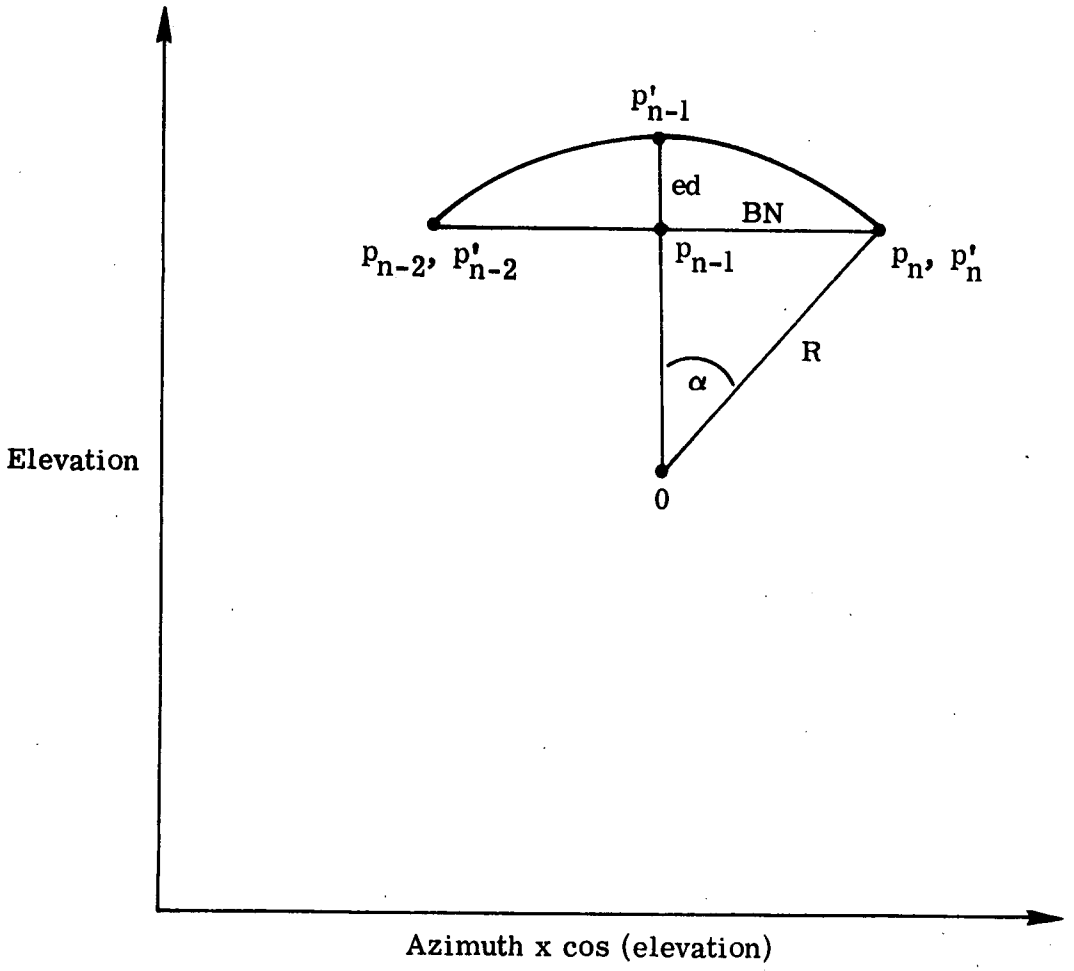

Figure 23.- The radius of curvature R.

Also from Figure 23 it is seen that

$$\sin \alpha = \frac{BN}{R} \tag{174}$$

Hence,

$$\alpha = \frac{BN}{R} \text{ , as } \alpha \text{ is small} \tag{175}$$

Substituting equation 175 for α into equation 173 for R, it becomes

$$R = \frac{2\ ed}{\alpha^2} \tag{173}$$

$$= \frac{2\ ed}{(BN/R)^2} \text{ , using equation 175}$$

$$= \frac{2\ ed\ R^2}{BN^2}$$

Hence,

$$R = \frac{BN^2}{2\ ed} \tag{176}$$

Therefore, the input pointing curvature error c_i, defined as the reciprocal of the radius of curvature of the perturbed azimuth-elevation curve , is given by

$$c_i = \frac{1}{R}$$

$$= \frac{2\ ed}{BN^2}\ , \qquad (177)$$

using equation 176 for R.

Analogously, the output pointing curvature error $c_{o_{\lambda,N}}$ in the $N^{\underline{th}}$ solution point due to a probable error $ed = 0.01^o$ in the lines-of-sight from station λ is

$$c_{o_{\lambda,N}} = \frac{2[(dl_{\lambda,N})^2 + (d2_{\lambda,N})^2 + (d3_{\lambda,N})^2]^{1/2}}{dr_N^2}\ , \qquad (178)$$

where $dl_{\lambda,N}$, $d2_{\lambda,N}$, and $d3_{\lambda,N}$ are given by equations 123, 124, and 125 for the point N, respectively, and dr_N is given by equation 144.

The pointing curvature error $CS_{\lambda,N}$ in the $N^{\underline{th}}$ solution point due to a probable error $ed = 0.01^o$ in the lines-of-sight from station λ, defined as the ratio of $c_{o_{\lambda,N}}$ to c_i, is then

$$CS_{\lambda,N} = \frac{c_{o_{\lambda,N}}}{c_i} \qquad (179)$$

$$= \frac{2[(dl_{\lambda,N})^2 + (d2_{\lambda,N})^2 + (d3_{\lambda,N})^2]^{1/2}/dr_N^2}{2\ ed/BN^2}$$

$$= \frac{[(dl_{\lambda,N})^2 + (d2_{\lambda,N})^2 + (d3_{\lambda,N})^2]^{1/2}\ BN^2}{ed\ dr_N^2}\ , \qquad (180)$$

using equations 177 and 178 for c_i and $c_{o_{\lambda,N}}$, respectively.

Therefore, the pointing curvature error CS_{NA} in the $NA^{\underline{th}}$ solution point due to a probable error ed = 0.01° in the lines-of-sight from the observation stations to the points on the cloud is

$$CS_{NA} = \left[\sum_{\lambda=1}^{L} (CS_{\lambda,NA})^2 \right]^{1/2} , \quad 1 \leq NA \leq NT, \tag{181}$$

where NT is the total number of points on the solution curve and the summation over λ means that the error in the lines-of-sight is only put into the data from one station, station λ, at a time. The dimensions of the pointing curvature error are degrees/kilometers.

Pointing Curvature Error as a Function of the Number and Location of the Observation Stations

Figure 24 is a plot of the pointing curvature error as a function of the latitude for the nine different station combinations. As for the pointing displacement errors and the pointing slope errors, the greatest accuracy is for the five-station case and the least accuracy is for the two-station case. The cases of four and three stations give intermediate accuracies in the following decreasing order - 2, 4, 3, 7, 8, 6, and 5. Also, as for the pointing displacement errors and the pointing slope errors, case 8, with two cameras at Mt. Hopkins and one at Cerro Morado, is considerably more accurate than case 9, with just one camera at each of these same two stations.

Therefore, from Figures 12, 13, 14, 15, 20, 21, 22, and 24, the different error components - east-west displacement, north-south displacement, vertical displacement, total displacement, latitude slope,

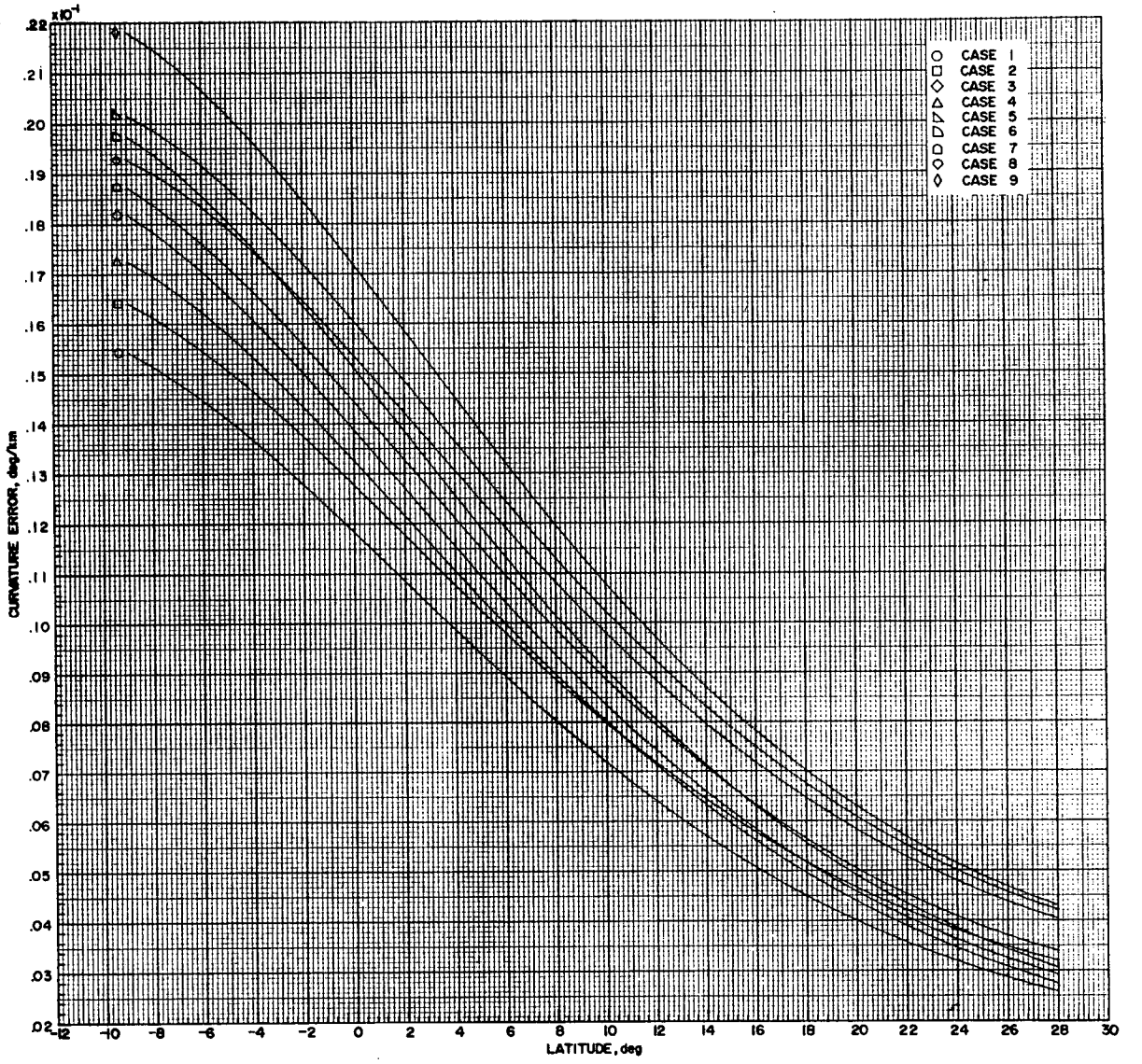

Figure 24.- Pointing curvature error as a function of latitude for the different station cases.

longitude slope, total slope, and curvature, respectively - in the triangulation solution due to a probable error ed = 0.01° in pointing can be seen as functions of the number and location of the observation stations. In the event of unfavorable weather or equipment malfunction at one or more of the stations, these plots can be consulted to see if the respective errors can be tolerated or not before deciding whether or not to launch.

Comparison of Pointing Displacement Errors

It was decided of interest to compare the three pointing displacement error components to each other to determine which component is the greatest. Figure 25 is a plot of the east-west pointing displacement error, the north-south pointing displacement error, the vertical pointing displacement error, and the total pointing displacement error as functions of the latitude for case 1. Case 1, which is the case composed of five stations, was chosen for this comparison because it is the case which gives the smallest values for all three displacement error components. As can be seen from Figure 25, the vertical component is the largest component throughout the latitudinal region of -9° to 15°, whereas the north-south component is the largest component throughout the latitudinal region of 16° to 28°.

Comparison of Pointing Slope Errors

Also of interest is a comparison of the two pointing slope error components. Figure 26 is a plot of the latitude pointing slope error, the longitude pointing slope error, and the total

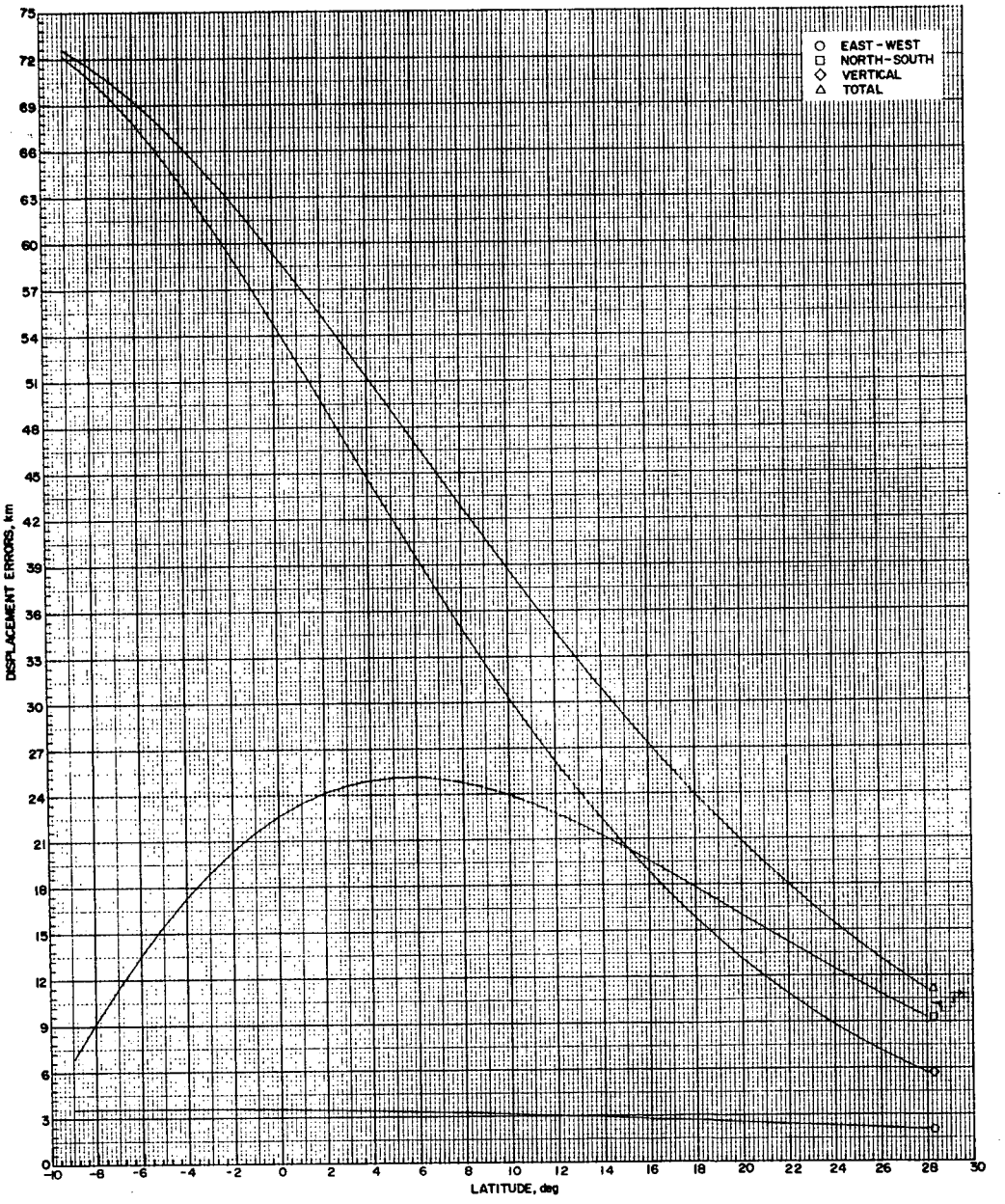

Figure 25.- Pointing displacement errors as a function of latitude for the five-station case.

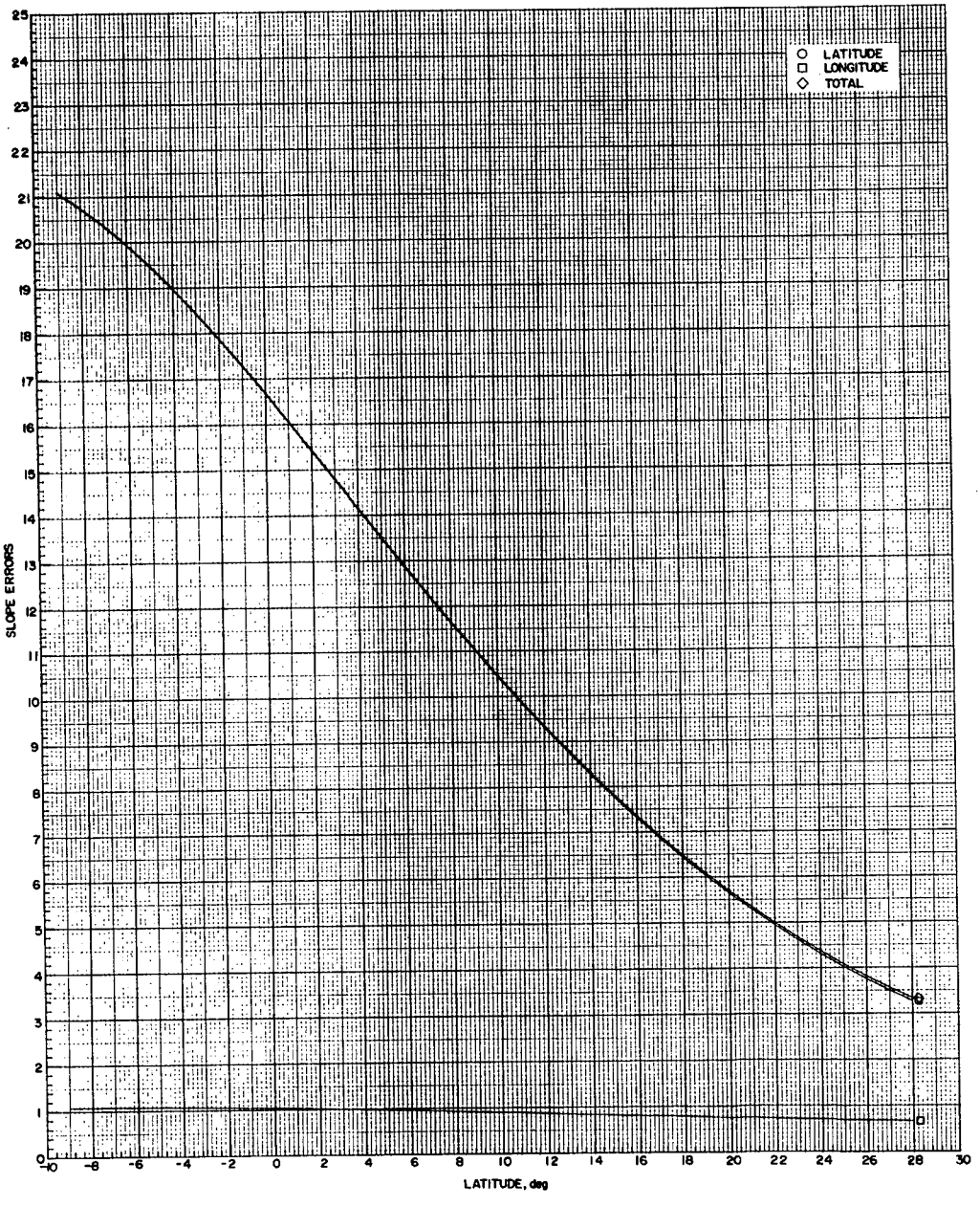

Figure 26.- Pointing slope errors as a function of latitude for the five-station case.

pointing slope error as functions of the latitude for case 1, which gives the smallest values for both slope error components. As can be seen from Figure 26, the latitude component is much larger than the longitude component and the total pointing slope error very closely approximates the latitude component.

Pointing Errors as a Function of Observation Duration

The barium cloud elongates along the length of the magnetic field line. Since the magnetic field lines are approximately constant in longitude, the barium cloud is essentially elongating in latitude. Looking back to Figures 25, 26, and 24, the four pointing displacement errors, the three pointing slope errors, and the pointing curvature error, respectively, as functions of the latitude for the five-station case can be seen. Since the position in latitude of the elongating cloud is a function of the time after the barium is released, these pointing errors are also functions of the time after release. From Figures 25, 26, and 24, then, the pointing errors as functions of the observation time after release can be obtained.

The rate of elongation of the cloud was predicted to be about 1.2 km/sec in each direction. Observation durations of 10,000 sec, 6,000 sec, and 1,000 sec would then correspond to total cloud lengths of 24,000 km, 14,400 km and 2,400 km, respectively. The angle of latitude ϕ_t that the cloud length subtends at the time t after release is approximately

$$\phi_t = \tan^{-1} \left(\frac{L_t}{H}\right) , \qquad (182)$$

where L_t is the length of the cloud at the time t after release and $H = 31{,}633.008$ km is the altitude of the nominal release point. Using equation 182 the angles of latitude subtended for the cloud lengths of 24,000 km, 14,400 km, and 2,400 km—which correspond to the observation durations of 10,000 sec, 6,000 sec, and 1,000 sec, respectively—are 37.188°, 24.476°, and 4.339°, respectively. Centering these three angles of latitude about the nominal release point latitude, which is 9.229°, gives the regions of latitude covered by the elongating cloud during these respective observation durations. The regions of latitude corresponding to the observation durations of 10,000 sec, 6,000 sec, and 1,000 sec are (-9.365° to 27.823°), (-3.009° to 21.467°), and (7.060° to 11.398°), respectively. By examining these three regions of latitude in Figures 25, 26, and 24, the pointing displacement errors, the pointing slope errors, and the pointing curvature error can be seen, respectively, as functions of these three observation durations.

From Figure 25 it is seen that the east-west pointing displacement error practically remains constant throughout the three observation durations, that the north-south pointing displacement error increases toward the lower-latitude end and decreases toward the higher-latitude end over the 1,000-sec observation duration and first increases and then decreases toward the lower-latitude end and decreases toward the

higher-latitude end over the 6,000-sec and 10,000-sec observation durations, and that the vertical and total pointing displacement errors increase toward the lower-latitude end and decrease toward the higher-latitude end over all three of the observation durations. From Figure 26 it is seen that the longitude pointing slope error practically remains constant throughout the three observation durations and that the latitude and total pointing slope errors increase toward the lower-latitude end and decrease toward the higher-latitude end over all three of the observation durations. From Figure 24 it is seen that the pointing curvature error also increases toward the lower-latitude end and decreases toward the higher-latitude end over all three of the observation durations.

Pointing Errors as a Function of East-West Cloud Drift

The barium cloud is expected to drift eastward or westward. It was decided to investigate how the triangulation results are affected if the cloud drifts in such a fashion into other areas of the sky. An east-west drift corresponds to a longitudinal drift; hence, it is convenient for this investigation to look at, actually, the effect of using different release points—release points having the same latitude and altitude, but different longitudes.

It is reasonable to assume that in order to observe the barium cloud at an altitude of 32,000 kilometers from a particular observation station the elevation angle from that station to the cloud should not

be less than 20 degrees. From the equations derived in the appendix, the elevations were calculated for all integer values of the longitude between 0° and 180° and between 0° and -180° for the five observation stations—Mt. Hopkins, Cerro Morado, Wallops, Arequipa, and White Sands. It was found for the range of longitudes between -49° and -119° that the elevation angles were approximately greater than or equal to 20 degrees for all five stations simultaneously. Six different release points—each having latitude equal to 9.229 degrees and altitude equal to 31,633.008 kilometers, with longitudes equal to -49°, -63°, -77°, -91°, -105°, and -119°, respectively—were chosen for the investigation. Points along the respective magnetic field lines through these particular release points were used for the input data to the LaRC method.

Figures 27, 28, 29, 30, 31, 32, 33, and 34, respectively, are plots of the pointing errors—east-west displacement, north-south displacement, vertical displacement, total displacement, latitude slope, longitude slope, total slope, and curvature—as functions of the latitude for the five-station case for different release points varying in longitude. Now, the coordinates of the nominal release point chosen for the BIC Experiment are latitude = 9.229°, longitude = -75.000°, and altitude = 31,633.008 km. Hence, these plots can be examined to see if the triangulation errors increase or decrease as the cloud drifts eastward or westward from this chosen nominal release point. From Figures 27-34 it is seen that all of the pointing errors increase as the cloud drifts eastward into the longitudinal

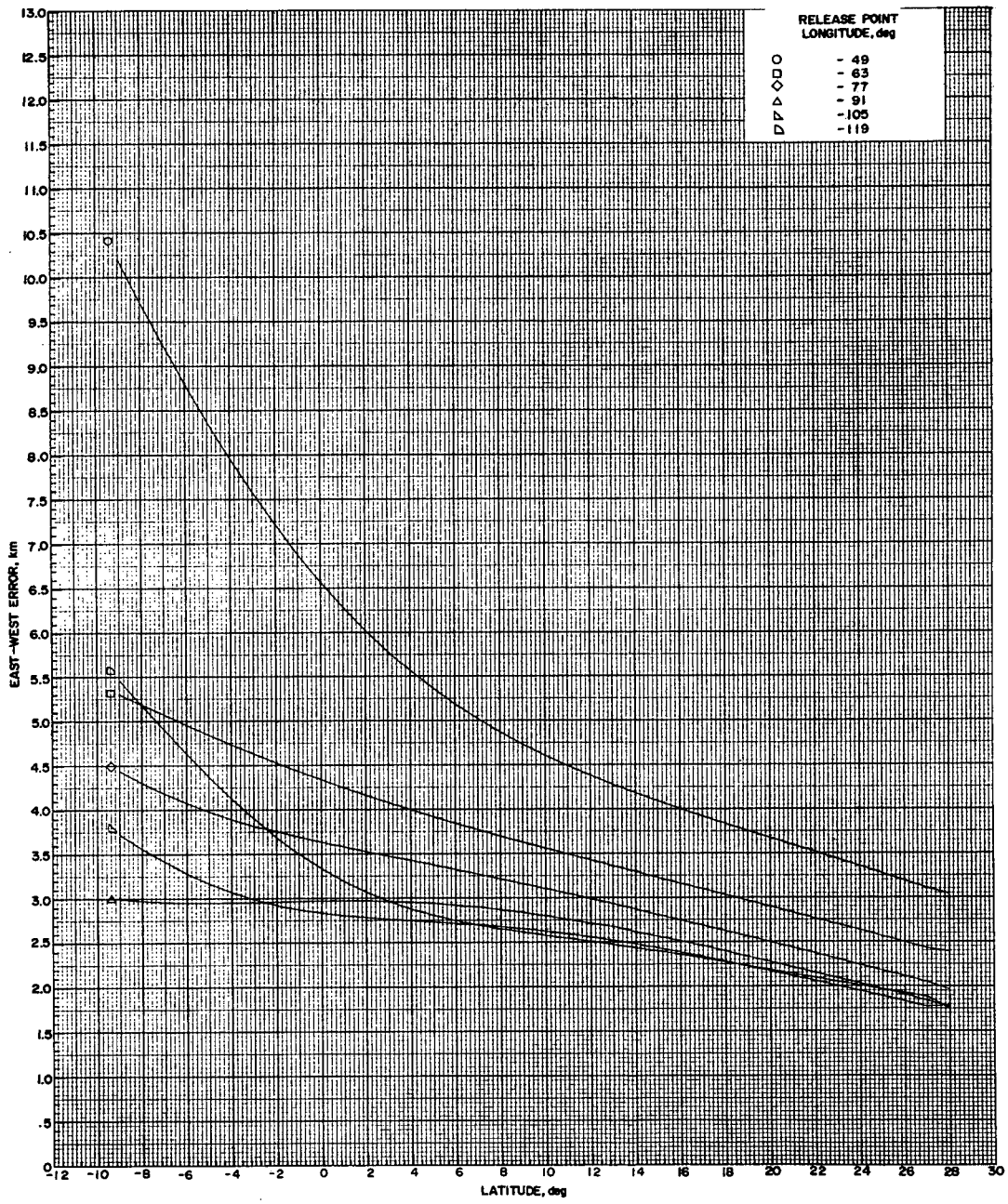

Figure 27.- East-west pointing displacement error as a function of latitude for the five-station case for different release points varying in longitude.

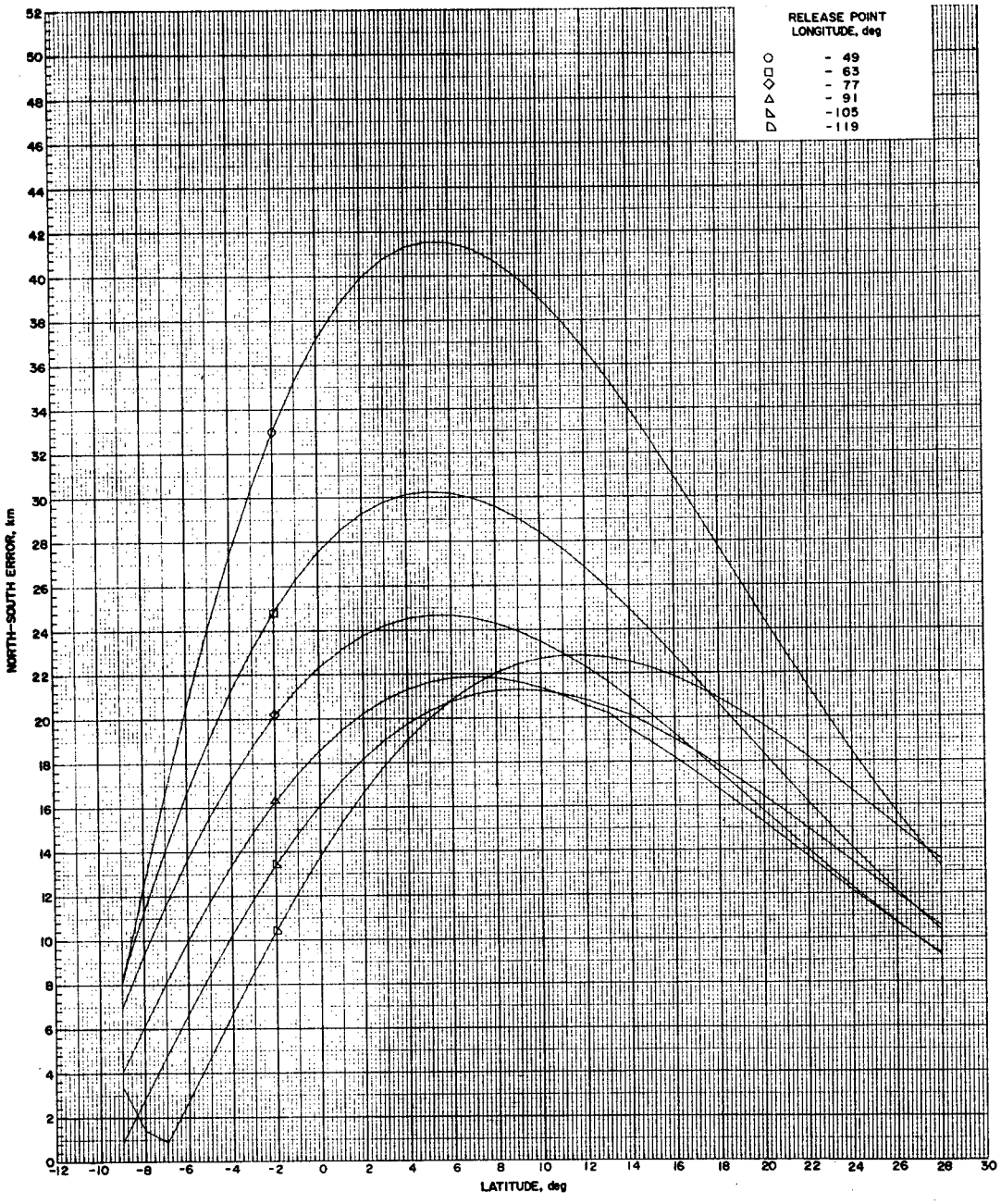

Figure 28.- North-south pointing displacement error as a function of latitude for the five-station case for different release points varying in longitude.

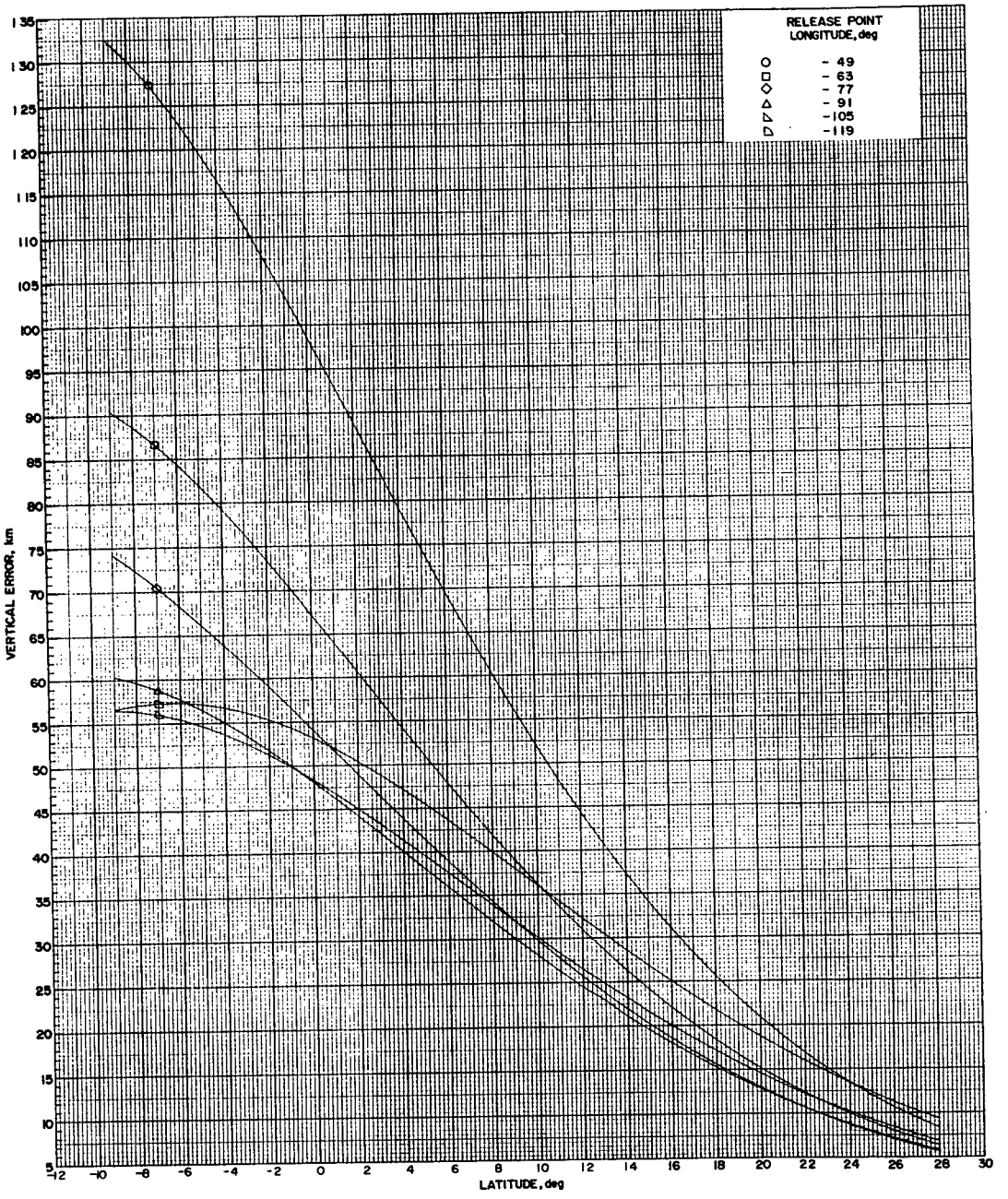

Figure 29.- Vertical pointing displacement error as a function of latitude for the five-station case for different release points varying in longitude.

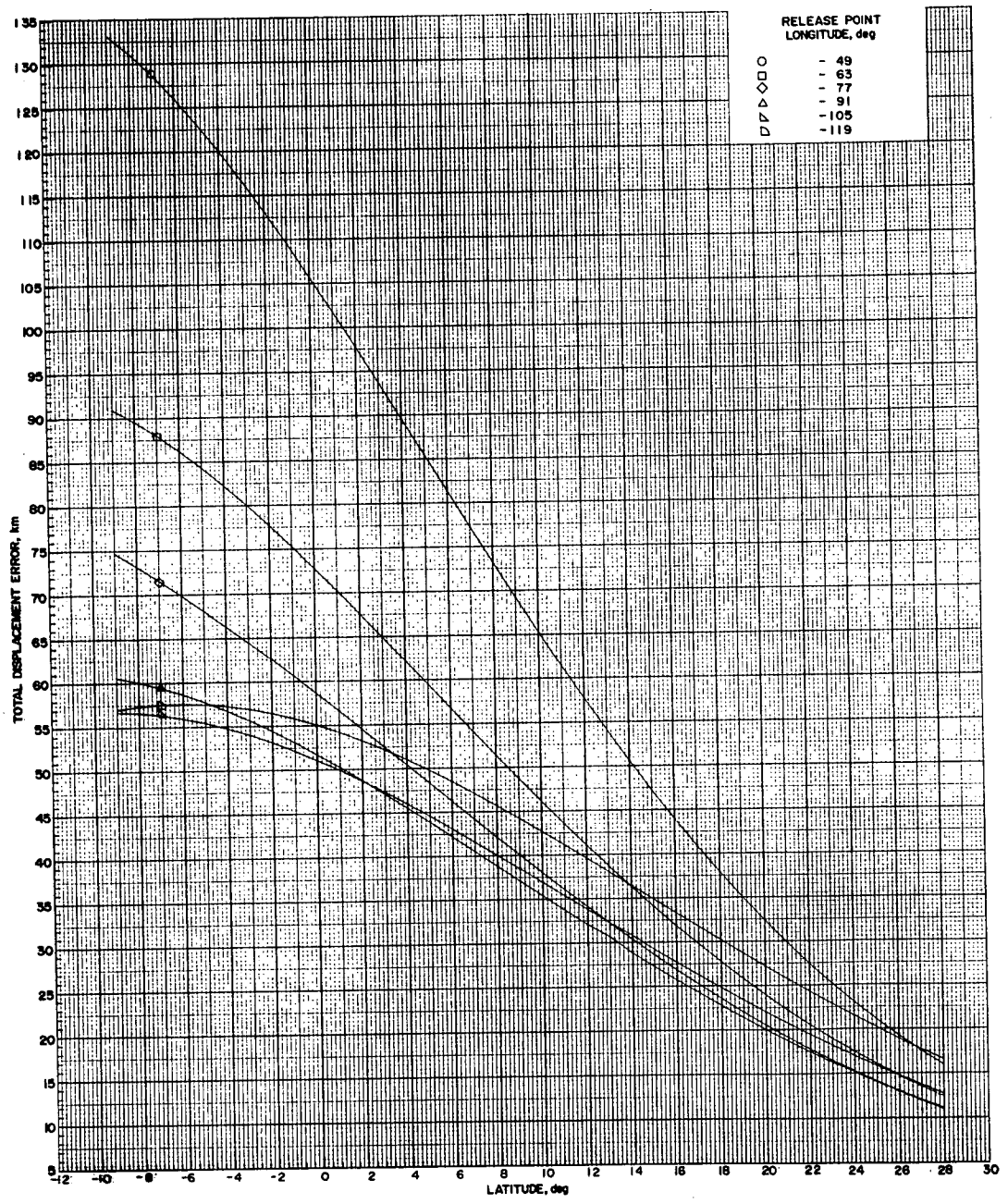

Figure 30.- Total pointing displacement error as a function of latitude for the five-station case for different release points varying in longitude.

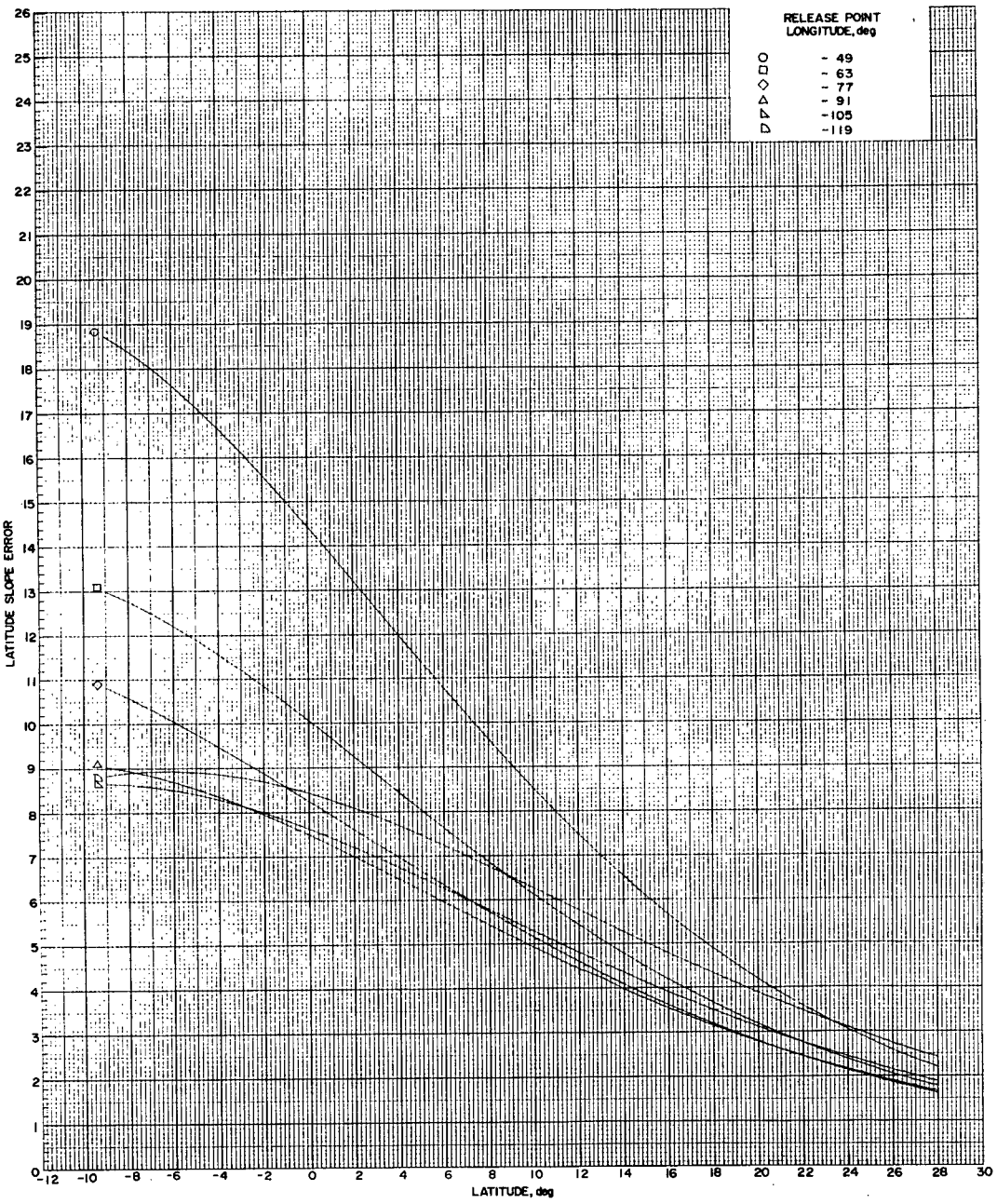

Figure 31.- Latitude pointing slope error as a function of latitude for the five-station case for different release points varying in longitude.

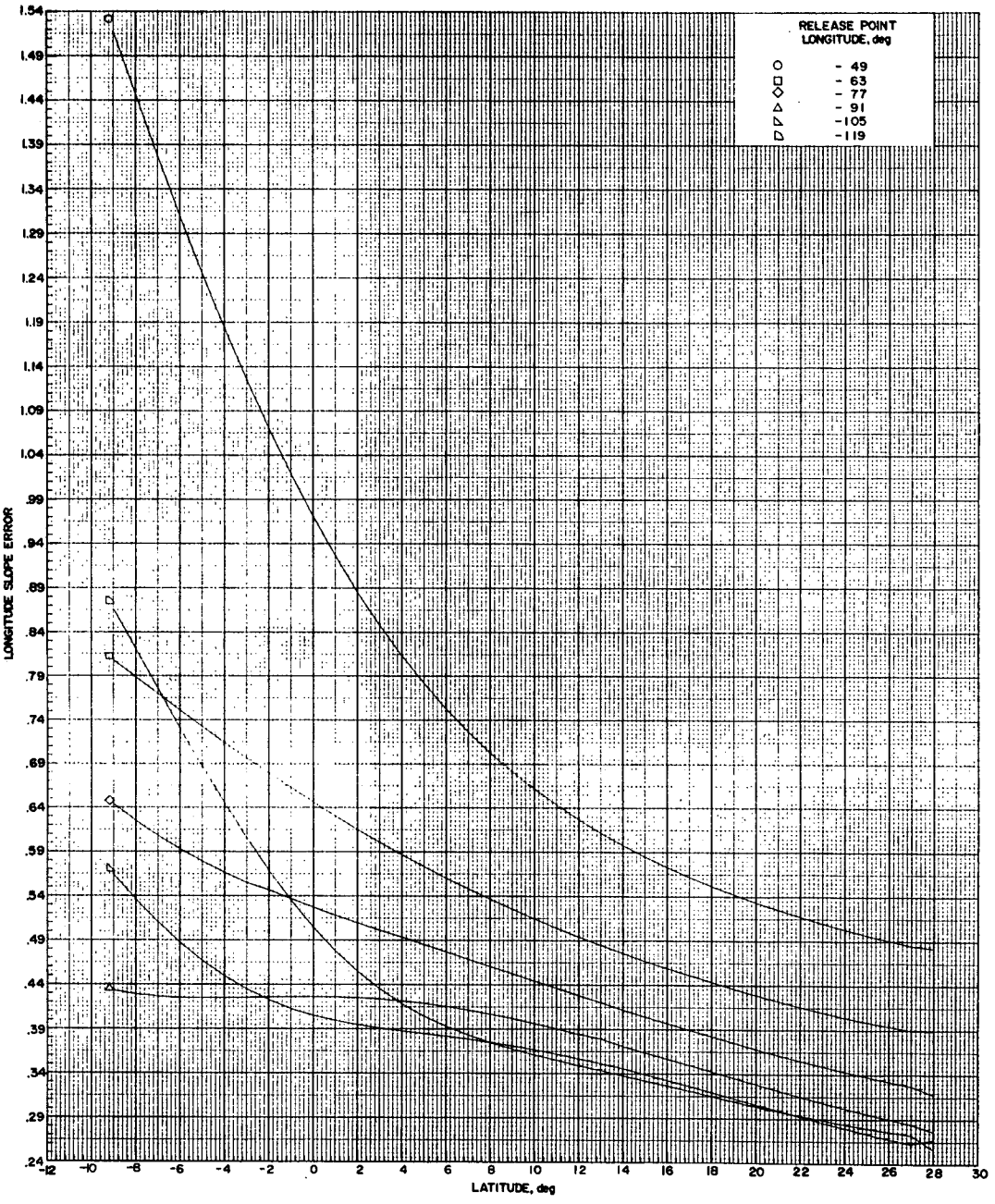

Figure 32.- Longitude pointing slope error as a function of latitude for the five-station case for different release points varying in longitude.

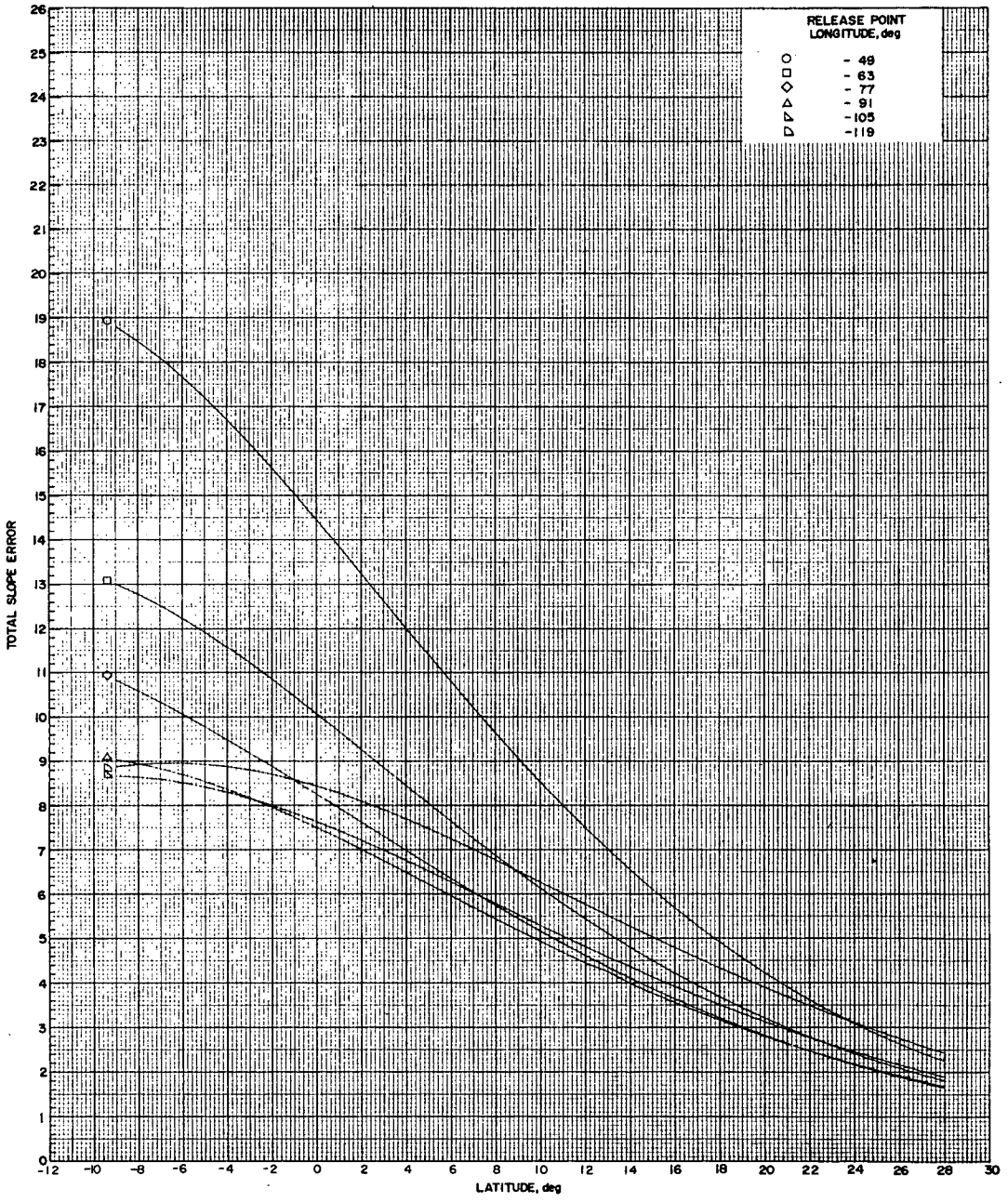

Figure 33.- Total pointing slope error as a function of latitude for the five-station case for different release points varying in longitude.

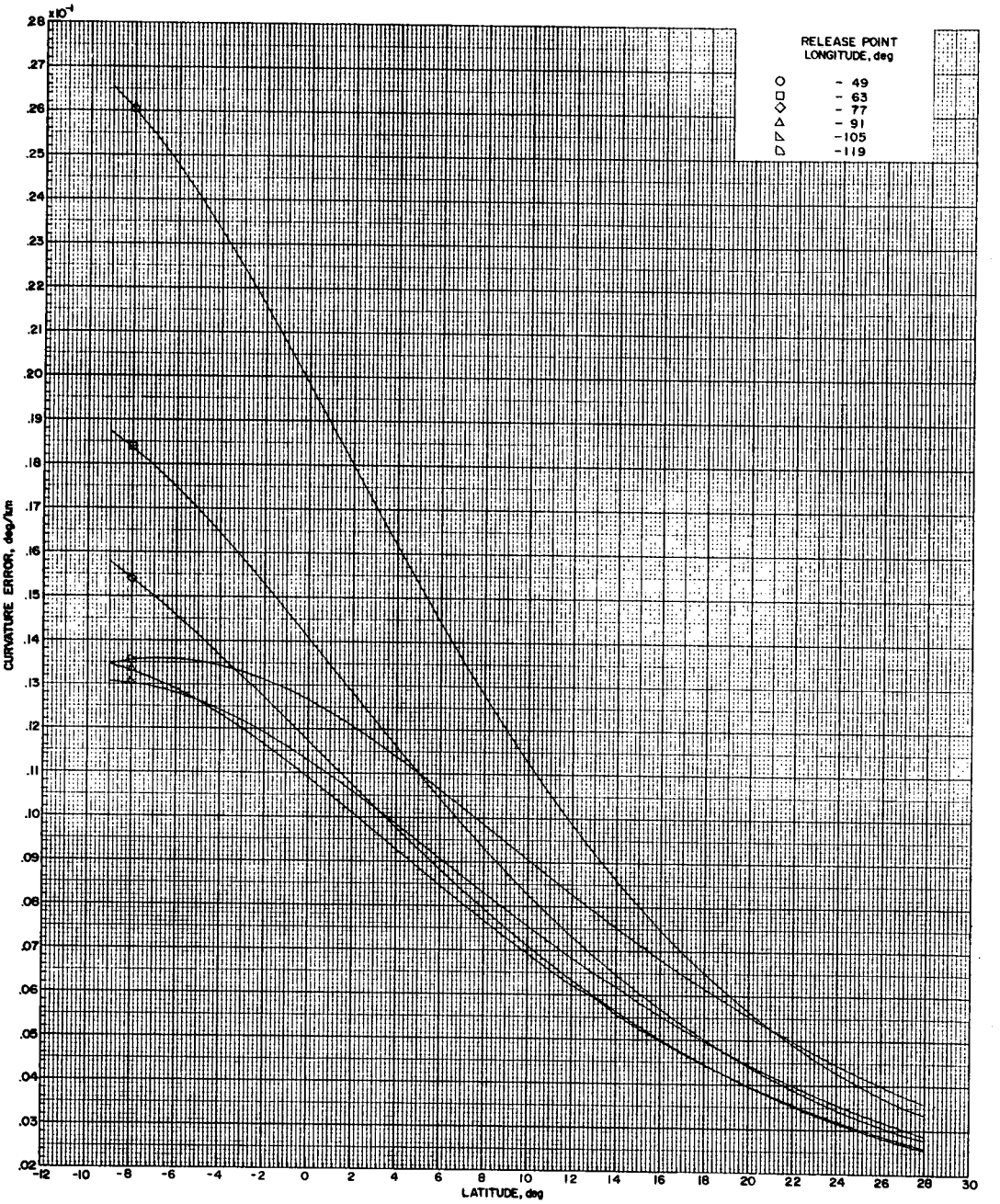

Figure 34.- Curvature pointing error as a function of latitude for the five-station case for different release points varying in longitude.

regions of - 63° and - 49° and that all of the pointing errors decrease as the cloud drifts westward into the longitudinal region of - 91°. As the cloud drifts farther westward into the longitudinal regions of - 105° and - 119°, the pointing errors increase or decrease depending on the cloud's position in latitude.

Pointing Errors as a Function of the Number of Input Data Points

Since the LaRC triangulation method requires for input data a number of points from the original azimuth-elevation curves from the observation stations, it was decided to determine just how many such raw data points are required to be read. It is recalled from the discussion of the LaRC method that the number of points NB_ℓ along the azimuth-elevation curve of arc length $sarc_\ell$ in degrees from station ℓ is given by equation 55

$$NB_\ell = \frac{sarc_\ell}{BN} , \tag{55}$$

where BN is the spacing in degrees between consecutive points along the curve. A convenient parameter for this determination is the spacing BN required between points instead of the actual number of points required to be read, as the arc lengths of the azimuth-elevation curves vary.

The LaRC method was tested for the following six different values of the spacing in degrees—BN = 0.28, 0.56, 1.12, 2.24, 4.48, and 8.96. Figures 35, 36, 37, 38, 39, 40, 41, and 42 are plots of the pointing errors—east-west displacement, north-south displacement, vertical

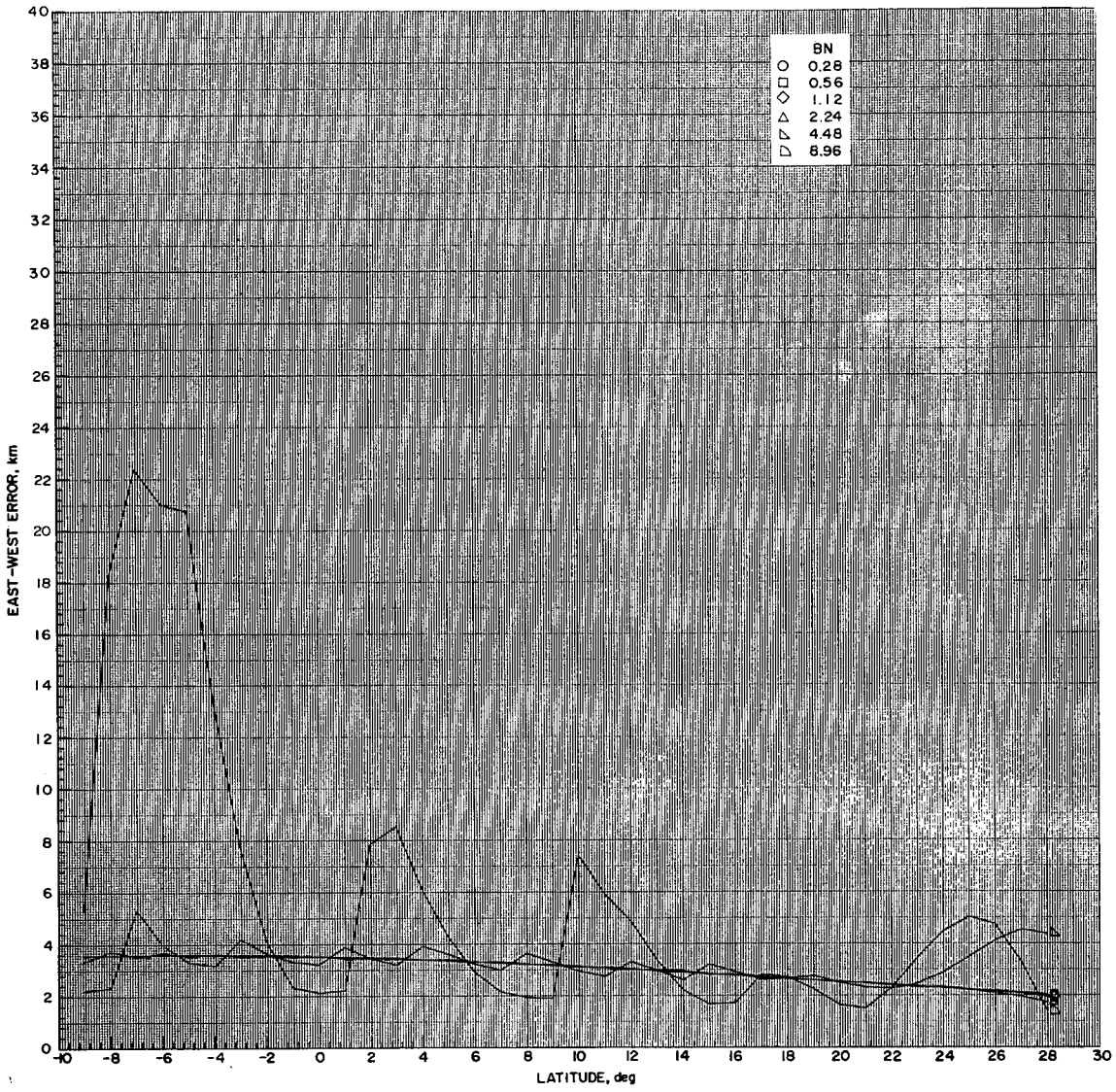

Figure 35.- East-west pointing displacement error as a function of latitude for the five-station case for different values of BN.

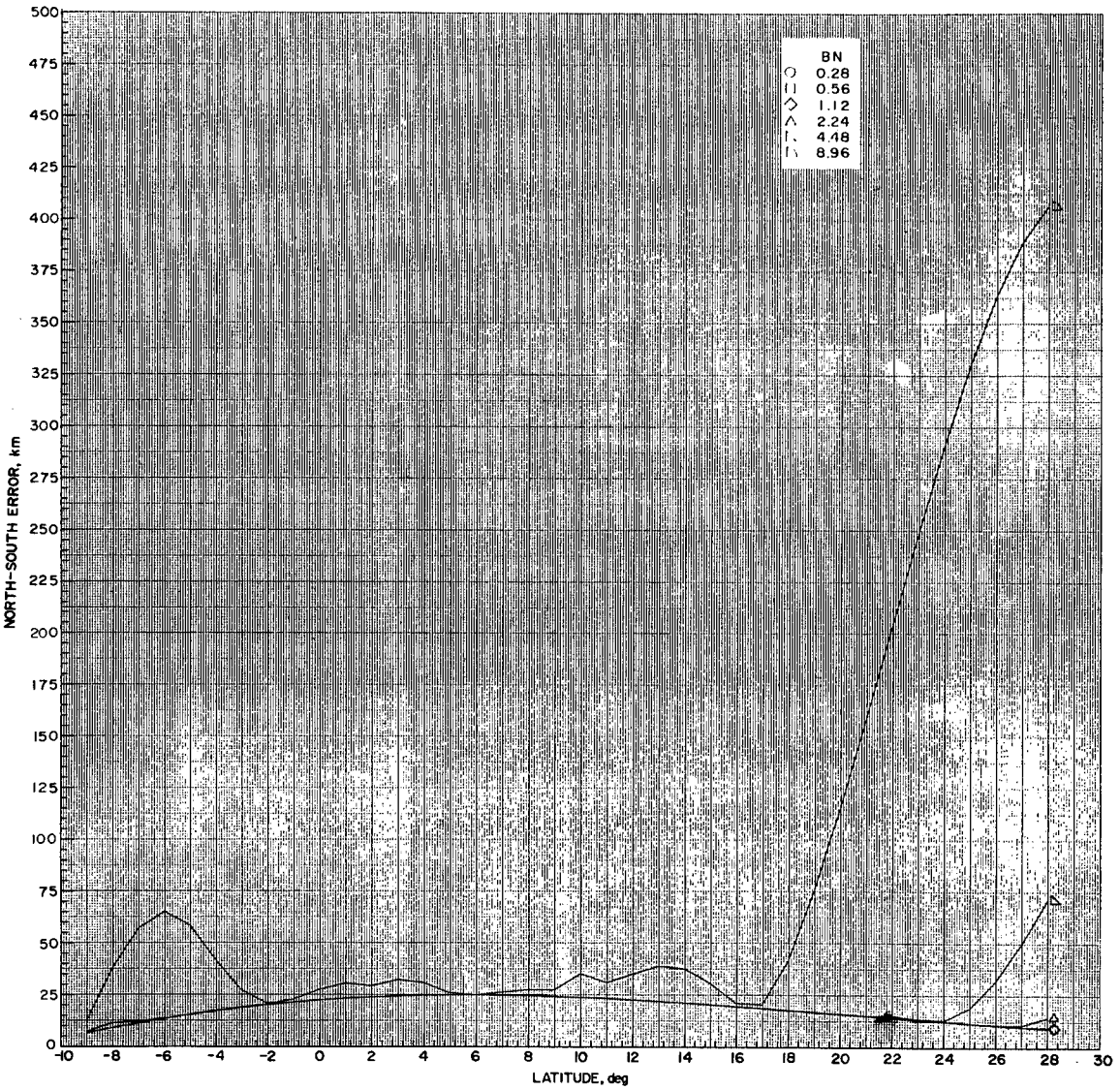

Figure 36.- North-south pointing displacement error as a function of latitude for the five-station case for different values of BN.

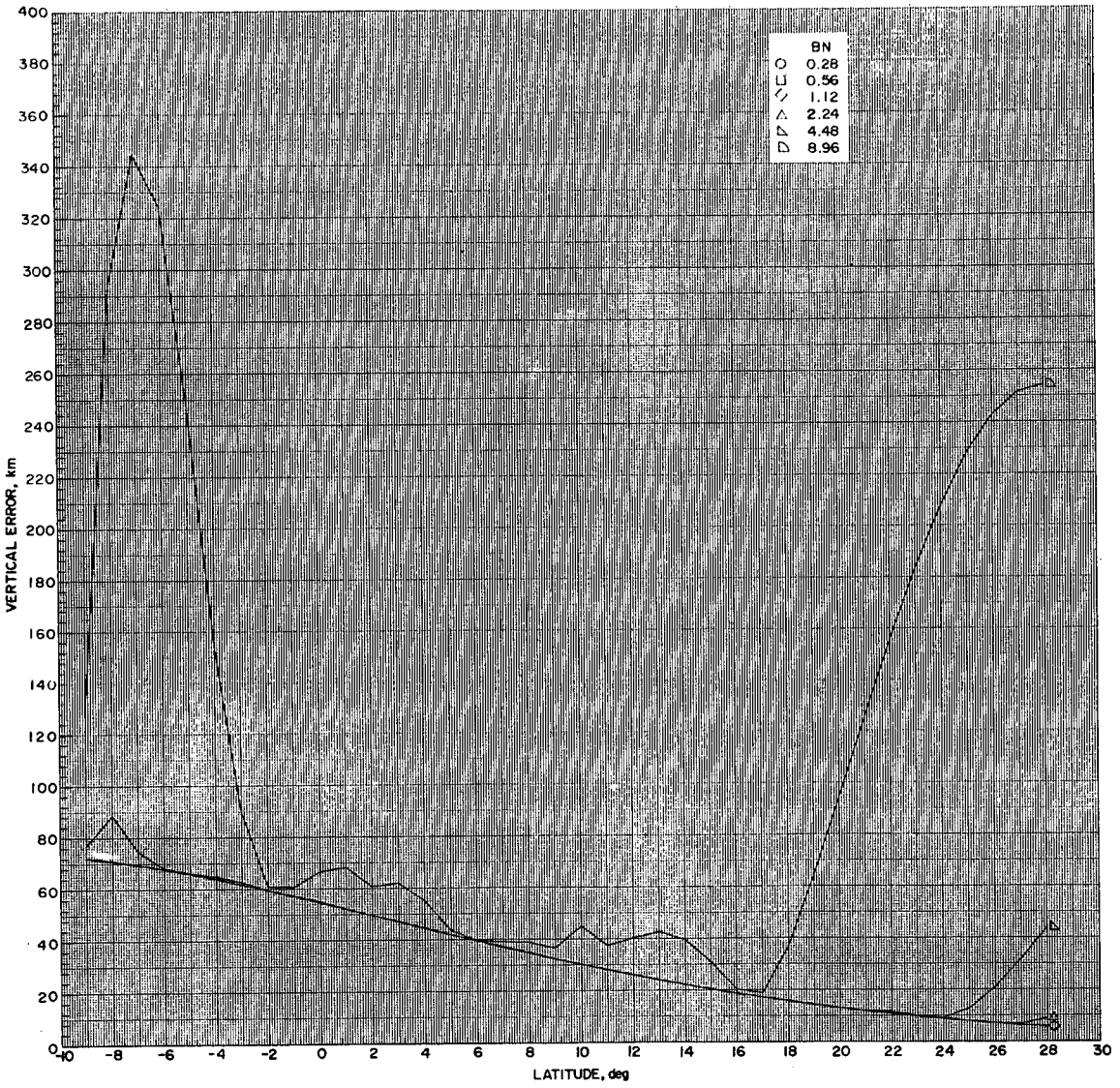

Figure 37.- Vertical pointing displacement error as a function of latitude for the five-station case for different values of BN.

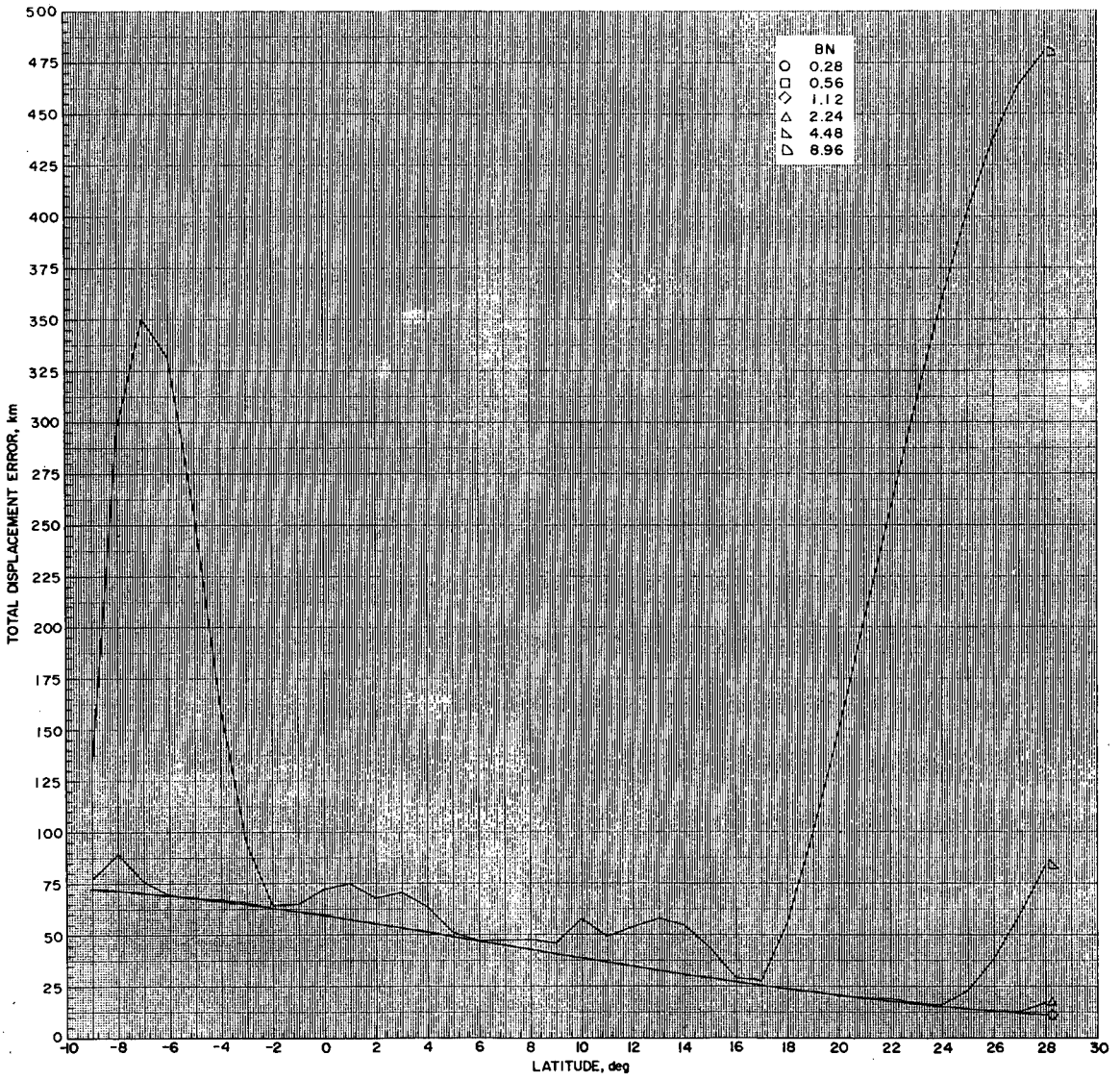

Figure 38.- Total pointing displacement error as a function of latitude for the five-station case for different values of BN.

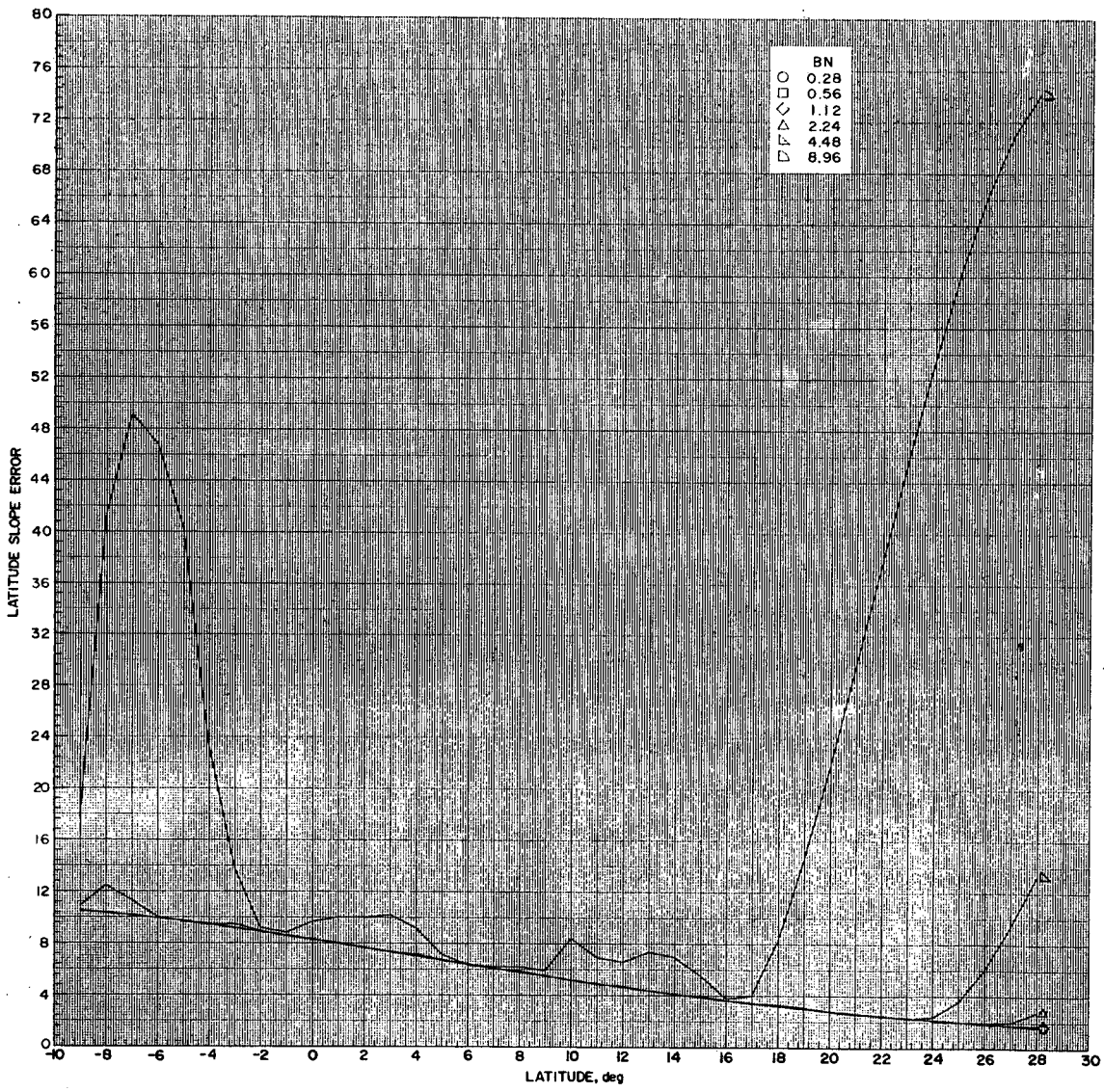

Figure 39.- Latitude pointing slope error as a function of latitude for the five-station case for different values of BN.

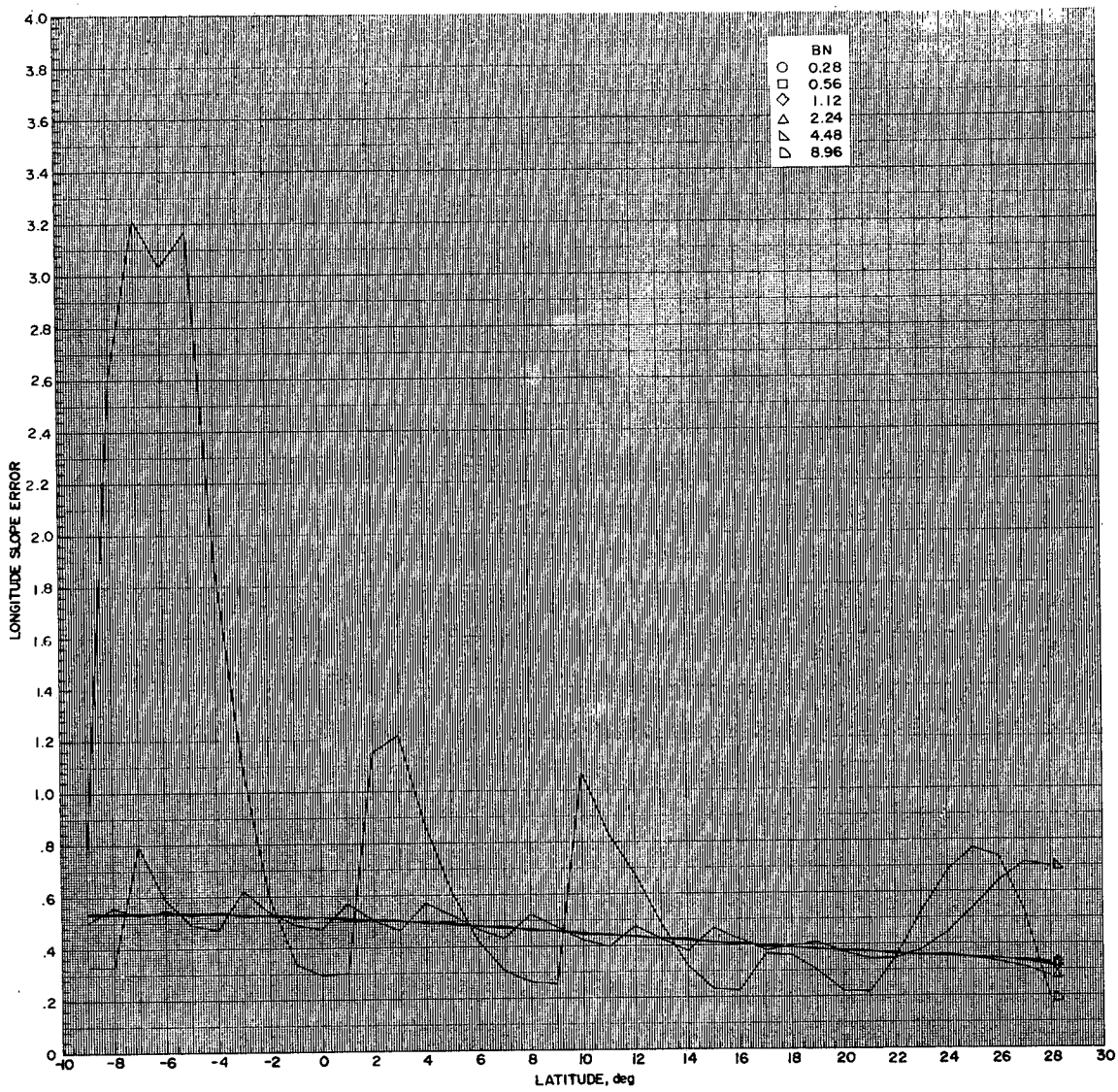

Figure 40.- Longitude pointing slope error as a function of latitude for the five-station case for different values of BN.

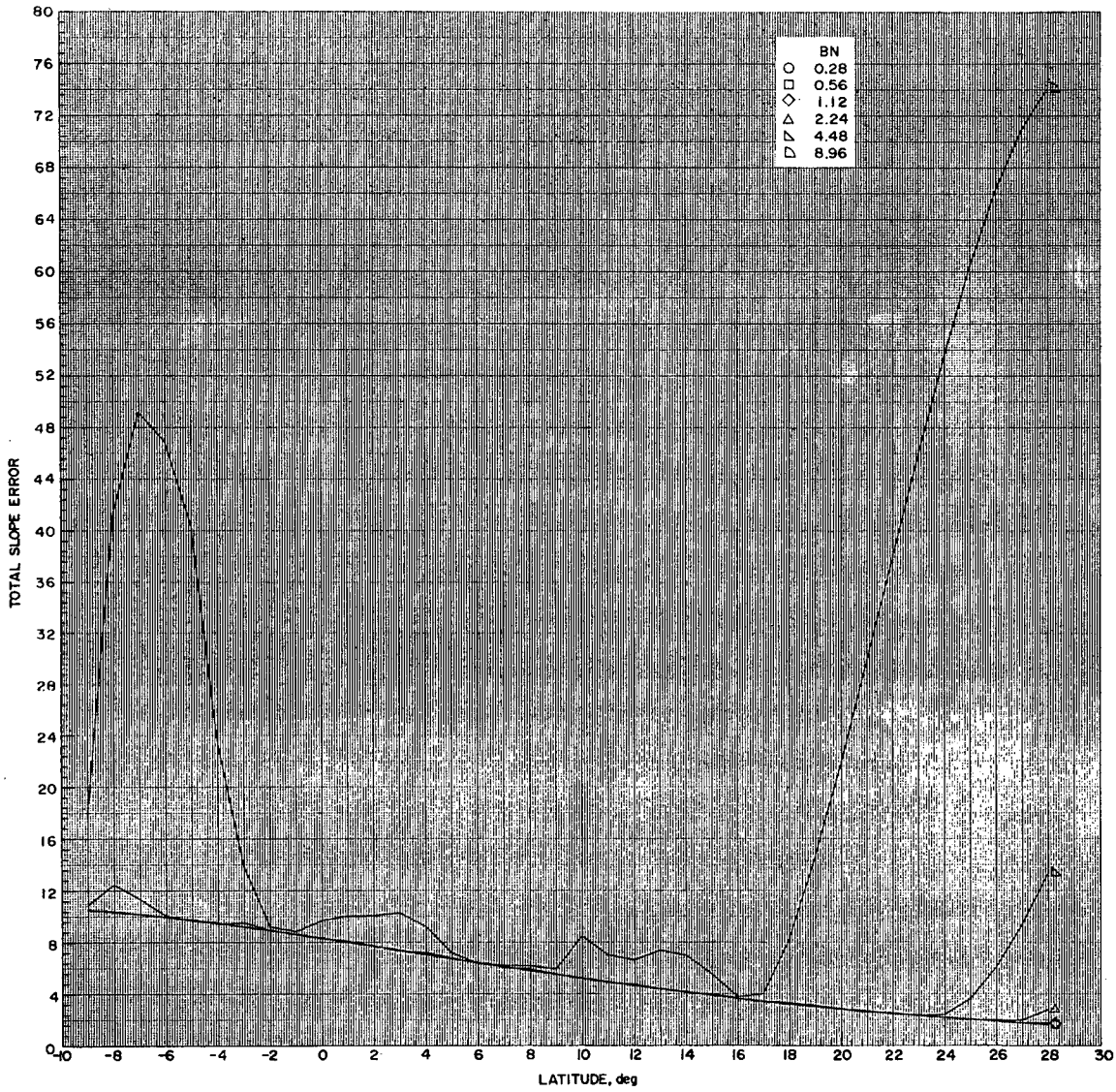

Figure 41.- Total pointing slope error as a function of latitude for the five-station case for different values of BN.

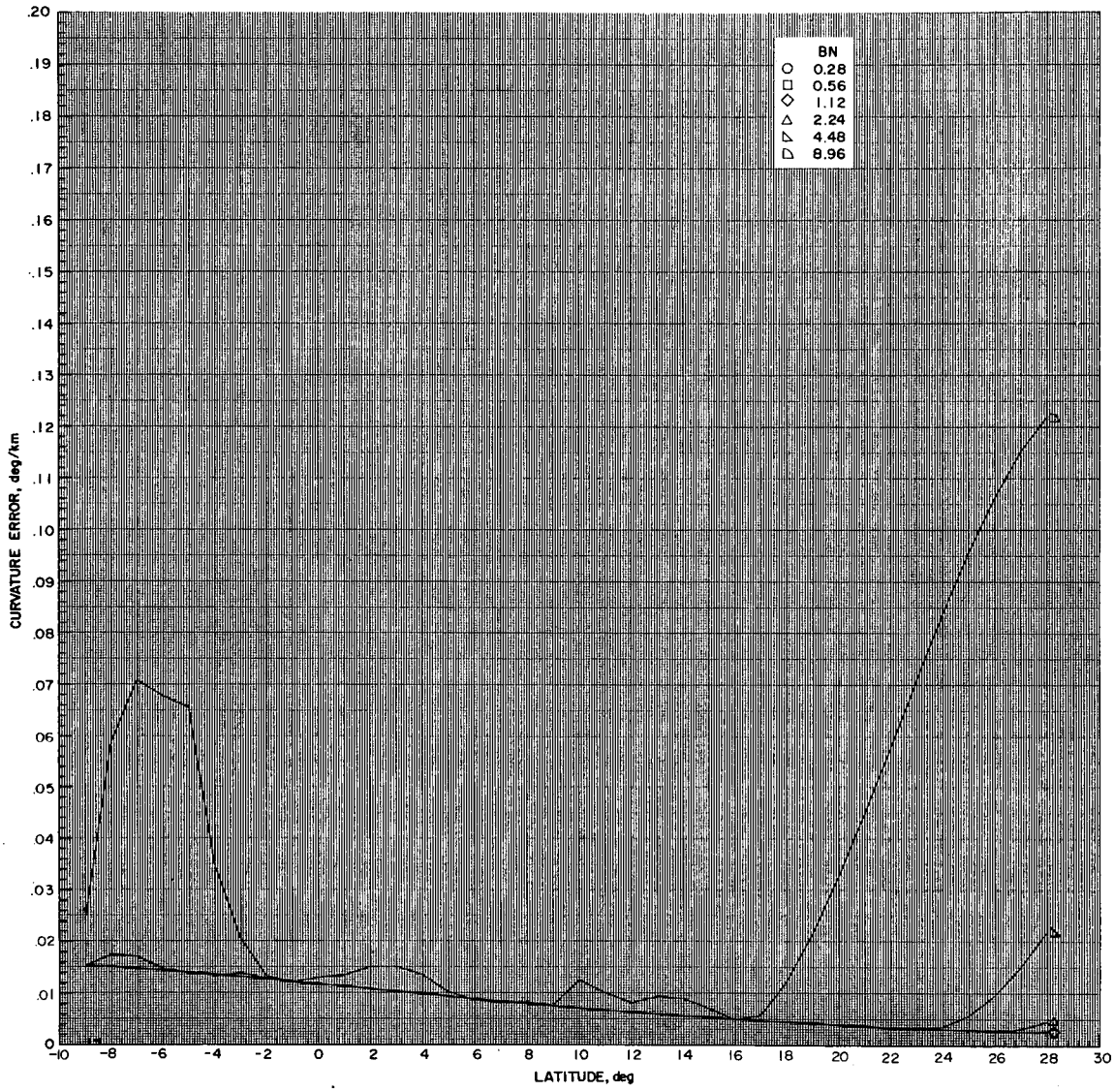

Figure 42.- Pointing curvature error as a function of latitude for the five-station case for different values of BN.

displacement, total displacement, latitude slope, longitude slope, total slope, and curvature, respectively—as functions of the latitude for the five-station case for these six different values of BN. As can be seen from the figures, the curves are nice and smooth for the shorter spacings of BN = 0.28, 0.56, and 1.12 degrees, whereas they are highly erratic for the longer spacings of BN = 4.48 and 8.96 degrees. The intermediate spacing of BN = 2.24 degrees produces only slightly erratic behavior. It is, therefore, recommended that the maximum spacing allowed between the input data points along the azimuth-elevation curves be BN = 1.12 degrees. For example, a reasonable arc length for a long barium cloud azimuth-elevation curve would be 37 degrees; using this maximum spacing of 1.12 degrees between points would require that at least 34 input data points be read from the curve.

Effects of Additional Cameras at a Particular Observation Station

From Figures 12, 13, 14, 15, 20, 21, 22, and 24 for the pointing errors, it was seen that case 8, which is composed of one camera at Cerro Morado and two cameras at Mt. Hopkins, gave significantly less errors than case 9, which is composed of just one camera at each of these same two stations. Therefore, adding a second camera to Mt. Hopkins in the two-station case improves the triangulation results.

It was decided to see if adding a second camera to Mt. Hopkins in the five-station case would also increase the accuracy. Table 3 gives the values of the pointing displacement errors as functions of the latitude

Table 3: Case 1 pointing displacement errors.

Latitude (deg)	E-W Error (km)	N-S Error (km)	Vertical Error (km)	Total Error (km)
-9	3.84	3.48	36.77	37.14
-8	3.87	4.74	36.52	37.02
-7	3.91	5.99	36.31	37.01
-6	3.94	7.20	35.99	36.91
-5	3.97	8.36	35.54	36.73
-4	3.97	9.38	34.70	36.17
-3	4.00	10.42	34.08	35.86
-2	4.02	11.37	33.33	35.45
-1	4.04	12.25	32.51	34.98
0	4.04	12.96	31.41	34.22
1	4.05	13.66	30.45	33.62
2	4.04	14.23	29.35	32.86
3	4.04	14.73	28.26	32.12
4	4.03	15.13	27.10	31.29
5	4.02	15.44	25.94	30.46
6	4.00	15.63	24.70	29.50
7	3.97	15.71	23.41	28.46
8	3.93	15.73	22.17	27.47
9	3.89	15.65	20.91	26.41
10	3.86	15.55	19.74	25.43
11	3.83	15.39	18.60	24.44
12	3.79	15.18	17.48	23.46
13	3.74	14.85	16.32	22.38
14	3.70	14.54	15.28	21.42
15	3.65	14.14	14.22	20.38
16	3.59	13.71	13.22	19.38
17	3.55	13.31	12.31	18.48
18	3.50	12.85	11.41	17.54
19	3.45	12.38	10.56	16.64
20	3.41	11.92	9.78	15.80
21	3.37	11.45	9.04	14.98
22	3.32	10.98	8.35	14.19
23	3.28	10.52	7.71	13.45
24	3.25	10.05	7.10	12.73
25	3.21	9.59	6.54	12.04
26	3.17	9.13	6.00	11.37
27	3.13	8.65	5.50	10.72
28	3.14	8.40	5.16	10.34

for case 1, the five-station case. Then a second camera was added to Mt. Hopkins, and this new case was denoted by case 1'. Table 4 gives the values of the pointing displacement errors as functions of the latitude for case 1'. The east-west component has remained the same or has decreased very slightly; but the north-south, vertical, and total pointing displacement errors have increased slightly. Then a third camera was added to Mt. Hopkins, and this case was denoted by case 1". Table 5 gives the values of the pointing displacement errors as functions of the latitude for this case. Once again the east-west component has remained the same or has decreased very slightly, while the north-south, vertical, and total pointing displacement errors have increased slightly. This process of adding an extra camera to Mt. Hopkins was continued up to the final case of twelve cameras at Mt. Hopkins; and each time the east-west component remained the same or decreased very slightly, while the north-south, vertical, and total pointing displacement errors increased slightly.

At first these increased errors might be a little alarming in view of the results found earlier for the two-station case, in which adding a second camera to Mt. Hopkins improved the accuracy. However, for the two-station case the intersection of the two conical-like surfaces in space defined by the respective azimuth-elevation curves from the two stations is unique; whereas, with three or more observation stations, especially with errors in pointing, the intersection of these surfaces is no longer unique. What happens when more and more cameras are added to one station in a case of three or more stations is that, in

Table 4: Case 1' pointing displacement errors.

Latitude (deg)	E-W Error (km)	N-S Error (km)	Vertical Error (km)	Total Error (km)
-9	3.83	3.76	39.72	40.08
-8	3.86	5.11	39.37	39.89
-7	3.90	6.45	39.07	39.79
-6	3.93	7.73	38.64	39.60
-5	3.97	8.96	38.08	39.32
-4	3.97	10.04	37.14	38.68
-3	4.00	11.13	36.40	38.27
-2	4.02	12.13	35.54	37.77
-1	4.04	13.04	34.60	37.20
0	4.03	13.77	33.38	36.34
1	4.04	14.49	32.31	35.64
2	4.04	15.07	31.08	34.77
3	4.04	15.57	29.87	33.93
4	4.03	15.97	28.60	33.01
5	4.02	16.27	27.33	32.06
6	4.00	16.45	25.98	31.01
7	3.96	16.50	24.58	29.87
8	3.93	16.49	23.25	28.77
9	3.89	16.38	21.89	27.61
10	3.86	16.25	20.63	26.54
11	3.83	16.06	19.40	25.47
12	3.79	15.81	18.20	24.40
13	3.74	15.43	16.97	23.24
14	3.70	15.09	15.85	22.20
15	3.64	14.64	14.73	21.08
16	3.59	14.17	13.66	20.01
17	3.55	13.74	12.70	19.04
18	3.50	13.24	11.75	18.04
19	3.45	12.73	10.86	17.09
20	3.41	12.24	10.04	16.19
21	3.36	11.73	9.26	15.32
22	3.32	11.23	8.54	14.50
23	3.28	10.74	7.87	13.71
24	3.25	10.25	7.24	12.96
25	3.21	9.76	6.65	12.24
26	3.17	9.27	6.10	11.54
27	3.12	8.77	5.57	10.85
28	3.14	8.50	5.22	10.46

Table 5: Case 1" pointing displacement errors.

Latitude (deg)	E-W Error (km)	N-S Error (km)	Vertical Error (km)	Total Error (km)
-9	3.83	3.90	41.13	41.49
-8	3.85	5.29	40.74	41.26
-7	3.89	6.67	40.39	41.12
-6	3.93	7.99	39.91	40.89
-5	3.96	9.25	39.30	40.57
-4	3.97	10.36	38.30	39.88
-3	3.99	11.47	37.50	39.42
-2	4.02	12.49	36.60	38.88
-1	4.04	13.41	35.60	38.26
0	4.03	14.16	34.33	37.35
1	4.04	14.89	33.19	36.60
2	4.04	15.47	31.90	35.69
3	4.04	15.98	30.64	34.79
4	4.03	16.37	29.32	33.82
5	4.02	16.67	28.00	32.83
6	4.00	16.83	26.59	31.73
7	3.96	16.87	25.15	30.54
8	3.93	16.86	23.76	29.39
9	3.89	16.73	22.35	28.19
10	3.86	16.58	21.05	27.07
11	3.83	16.38	19.78	25.97
12	3.79	16.11	18.55	24.85
13	3.74	15.71	17.27	23.65
14	3.70	15.35	16.13	22.57
15	3.64	14.88	14.97	21.42
16	3.59	14.40	13.88	20.31
17	3.55	13.94	12.89	19.31
18	3.50	13.42	11.92	18.29
19	3.45	12.90	11.01	17.30
20	3.41	12.39	10.16	16.38
21	3.36	11.87	9.37	15.49
22	3.32	11.35	8.63	14.64
23	3.28	10.84	7.94	13.84
24	3.24	10.34	7.30	13.07
25	3.21	9.84	6.71	12.33
26	3.17	9.33	6.14	11.61
27	3.12	8.83	5.61	10.92
28	3.14	8.55	5.25	10.51

effect, the data from this one station is receiving more and more weighting and the solution is becoming more and more constrained to lie on the surface originating from this one station. Hence, the triangulation errors should be expected to increase, as was seen in Tables 3-5.

Station Displacement Errors for the Aircraft Station

As was mentioned earlier the Wallops station is really an aircraft. The position of the moving aircraft contains some error, as the aircraft is tracked by radar and because of its particular flight path for the experiment there are times when it is outside of the range of the existing radar stations. This error in the Wallops station position produces errors in the triangulation results, called station errors, just as an error in the lines-of-sight from the different stations produces errors in the triangulation results, called pointing errors. A reasonable probable error to assume in the aircraft position is a three-kilometer sphere of uncertainty (a sphere of radius equalling three kilometers) about its position. This total uncertainty is denoted by σ_t. It is then reasonable to assume that this sphere of uncertainty is due to equal uncertainty in the three rectangular components—east-west, north-south, and vertical—of the aircraft. These three uncertainties are denoted by σ_{EW}, σ_{NS}, and σ_V, respectively, and are each equal to $\pm(3)^{1/2}$ km., as

$$\sigma_t = (\sigma_{EW}^2 + \sigma_{NS}^2 + \sigma_V^2)^{1/2} \tag{183}$$

$$\sigma_t = [(\pm \sqrt{3})^2 + (\pm \sqrt{3})^2 + (\pm \sqrt{3})^2]^{1/2}$$

$$= (3 + 3 + 3)^{1/2}$$

$$= (9)^{1/2}$$

$$= 3 \tag{184}$$

If Γ denotes the range of the aircraft, slat denotes its latitude, and σ_{slat}, σ_{slon}, and σ_Γ denote the uncertainties in its latitude, longitude, and range, respectively, then

$$\sigma_{EW} = \Gamma \cos (slat)\, \sigma_{slon} \tag{185}$$

$$\sigma_{NS} = \Gamma\, \sigma_{slat} \tag{186}$$

$$\sigma_V = \sigma_\Gamma \tag{187}$$

For computing the numerical values for σ_{slat} and σ_{slon}, the latitude and range used were those for the aircraft over Wallops. The latitude of Wallops is 37.9324 degrees. The aircraft flies at an altitude of 35,000 feet or higher. If 35,000 feet, which equals 10.6680 kilometers,

is assumed for the altitude of the aircraft, then the range of the aircraft is this altitude plus the earth's radius of 6371.2 kilometers; hence, Γ = 6381.9 kilometers. Solving for σ_{slon} in equation 185,

$$\sigma_{slon} = \frac{\sigma_{EW}}{\Gamma \cos (slat)} \tag{188}$$

$$\sigma_{slon} = \frac{\pm (3)^{1/2} \text{ km}}{(6381.9 \text{ km}) \cos (37.93240)}$$

$$= \pm 0.000343 \text{ radians} \tag{189}$$

Solving for σ_{slat} in equation 186,

$$\sigma_{slat} = \frac{\sigma_{NS}}{\Gamma} \tag{190}$$

$$\sigma_{slat} = \frac{\pm (3)^{1/2} \text{ km}}{(6381.9 \text{ km})}$$

$$= \pm 0.000271 \text{ radians} \tag{191}$$

And since the uncertainty in range is just equal to the uncertainty in the vertical component, as given by equation 187,

$$\sigma_{\Gamma} = \pm (3)^{1/2} \text{ km}$$

$$= \pm 1.732051 \text{ km} \tag{192}$$

The triangulation results were again computed using the magnetic

field line data through the BIC nominal release point for the input data - only this time instead of introducing the probable error ed = 0.01° into the lines-of-sight from each station, one at a time, the uncertainties σ_{slat}, σ_{slon}, and σ_{Γ} were introduced into the aircraft coordinates over Wallops, one at a time. The four station displacement errors due to the uncertainties σ_{slat}, σ_{slon}, and σ_{Γ} - given by equations 191, 189, and 192, respectively - were calculated, using an analogous procedure to that used earlier for calculating the four pointing displacement errors due to the probable error ed. Figures 43, 44, 45, and 46 are plots of the station displacement errors - east-west, north-south, vertical, and total, respectively - as functions of the latitude due to the uncertainties σ_{slat}, σ_{slon}, and σ_{Γ} in the coordinates of the aircraft over Wallops. Only the cases 1, 3, 4, and 6, which are defined in Table 2, were considered, as these are the only cases which include the Wallops station.

It is seen from Figures 44, 45, and 46 for the north-south, vertical, and total station displacement errors, respectively, that the errors for case 3, composed of four stations, are less than the errors for case 1, composed of five stations, and also that the errors for case 6, composed of three stations, are less than the errors for case 4, composed of four stations. At first this might be a little alarming in view of the fact that reference 4, even though it is for an idealized situation, indicates that the triangulation error decreases as the number of observation stations increases. However, it is noticed when looking back to Table 2 that

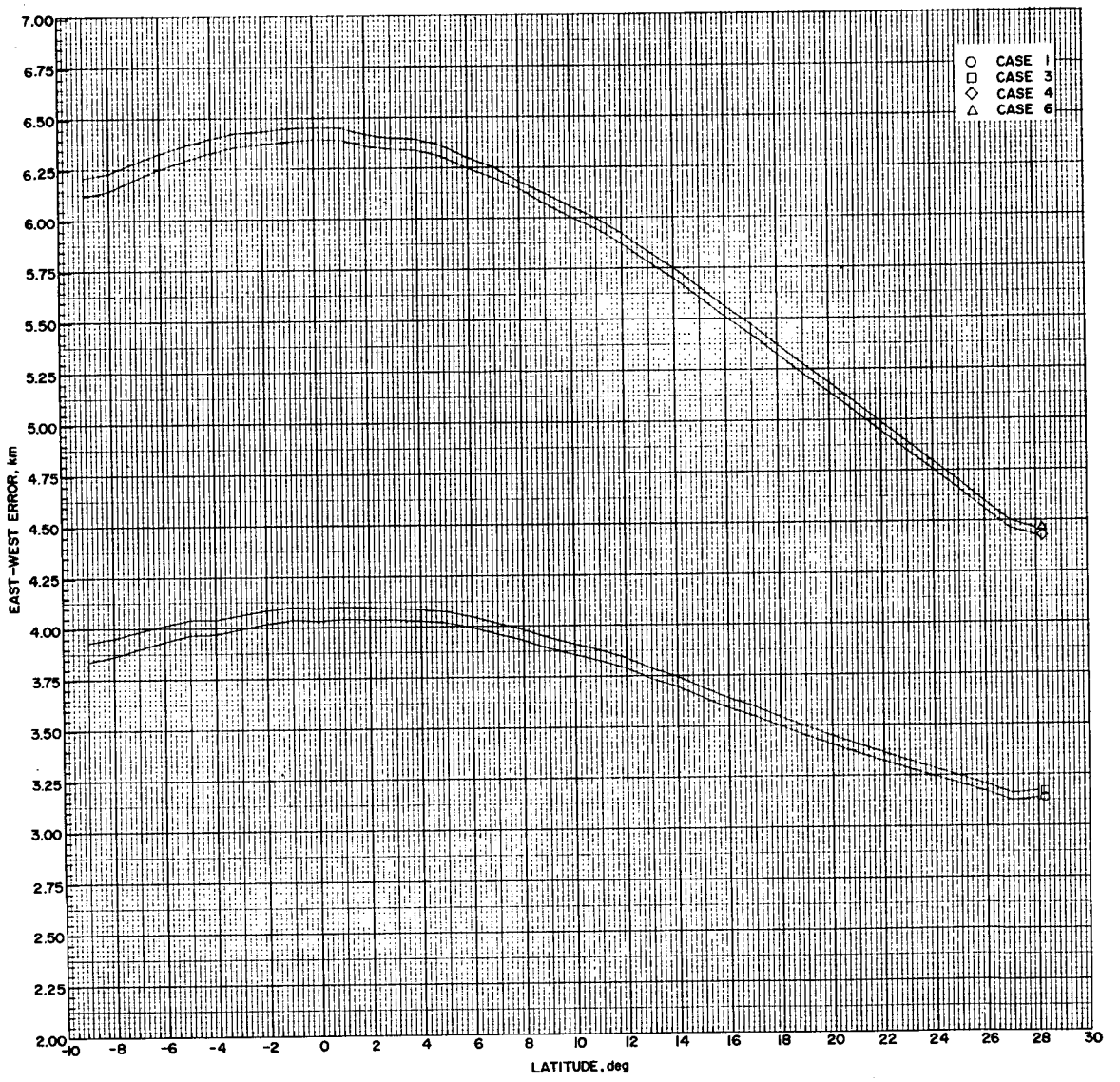

Figure 43.- East-west station displacement error as a function of latitude for the station cases containing the aircraft.

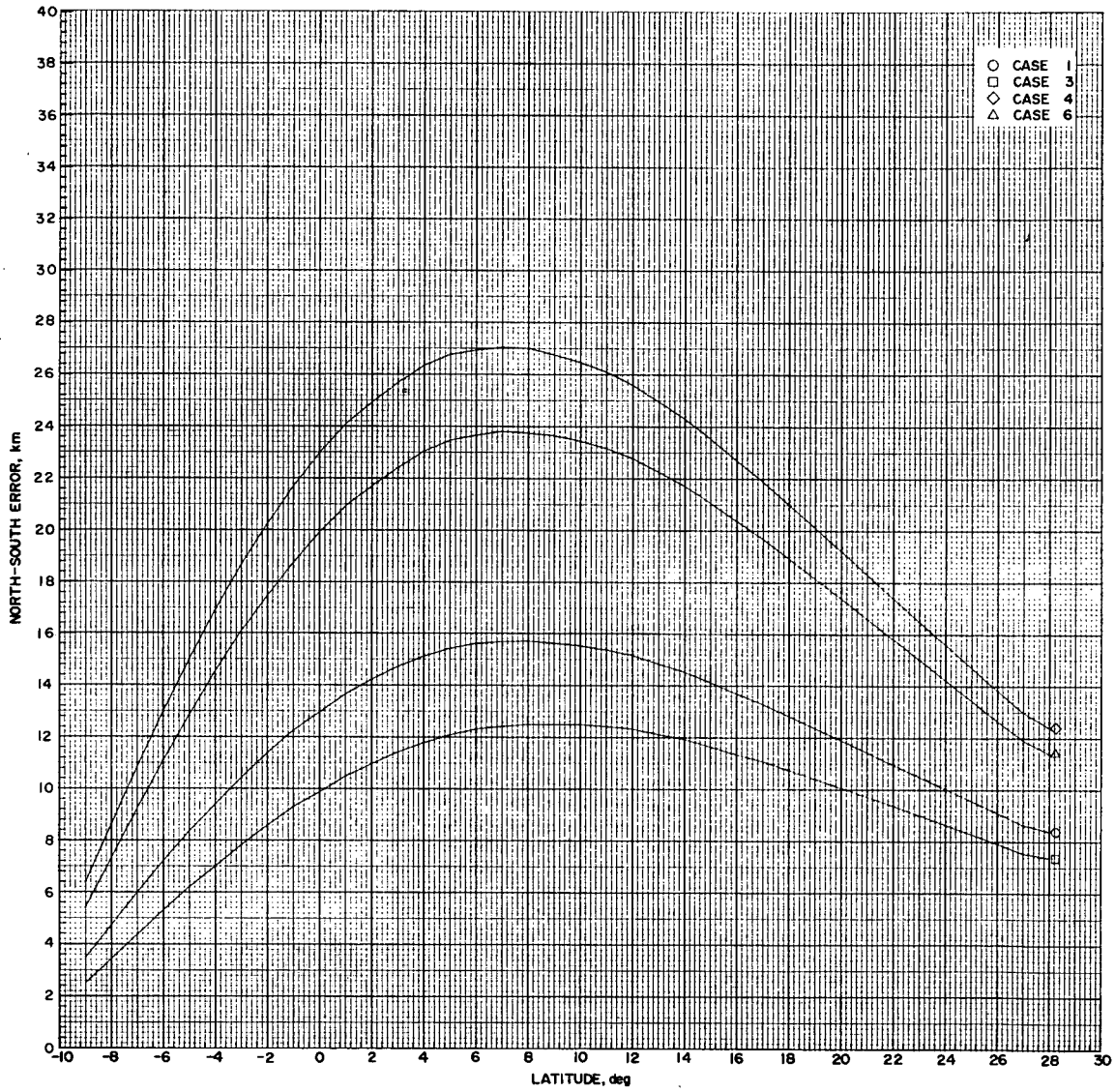

Figure 44.- North-south station displacement error as a function of latitude for the station cases containing the aircraft.

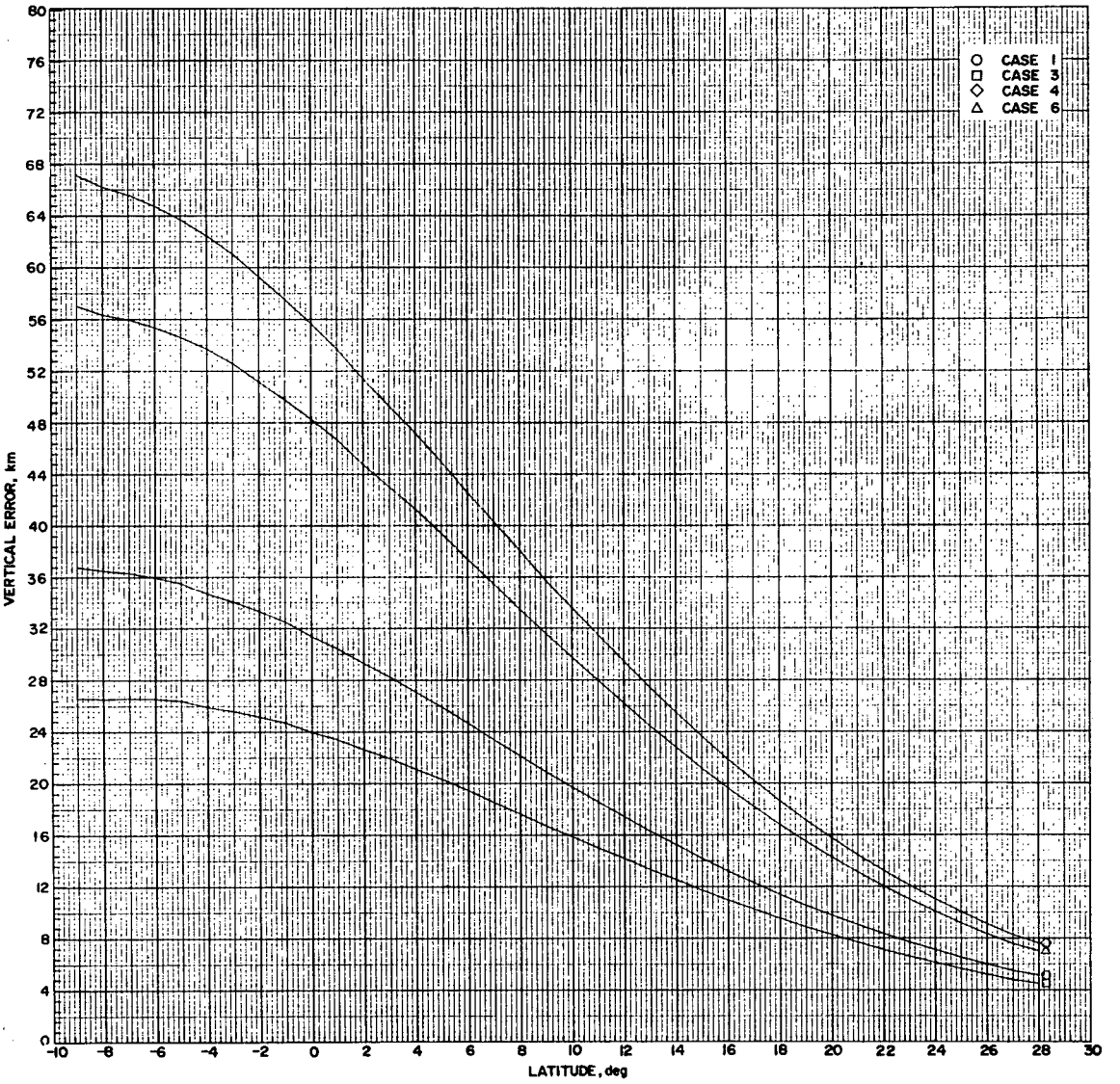

Figure 45.- Vertical station displacement error as a function of latitude for the station cases containing the aircraft.

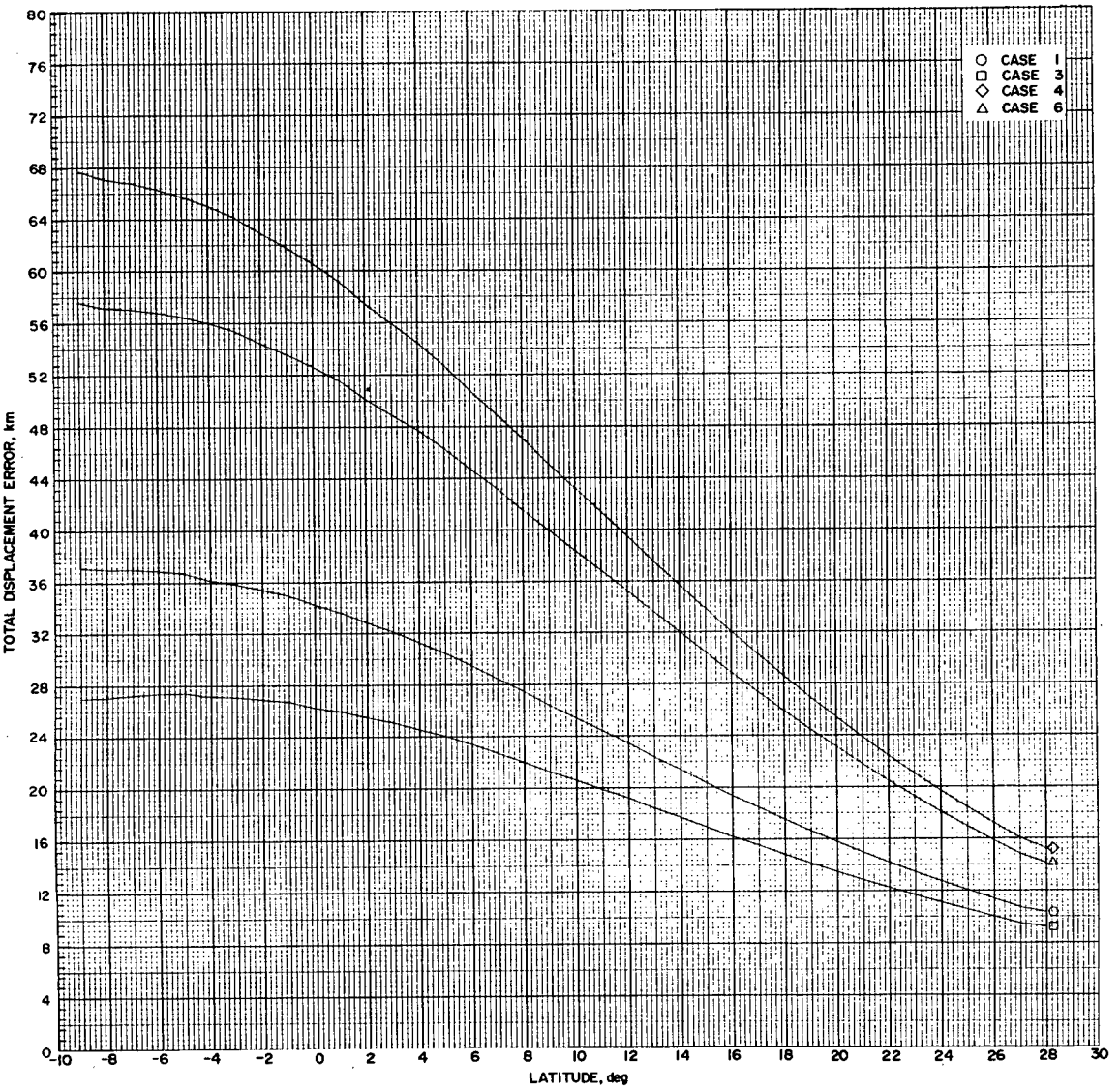

Figure 46.- Total station displacement error as a function of latitude for the station cases containing the aircraft.

case 1 is equal to case 3 with White Sands added and that also case 4 is equal to case 6 with White Sands added. From Table 1 it is noticed that the coordinates of White Sands are almost the same as the coordinates of Mt. Hopkins. Hence, case 1 is approximately the same as case 3 with a second camera added to Mt. Hopkins and also case 4 is approximately the same as case 6 with a second camera added to Mt. Hopkins. It is recalled from the previous discussion on the effects of additional cameras at a particular observation station that adding a second camera to Mt. Hopkins in case 1 causes the north-south, vertical, and total pointing displacement errors to increase slightly. As was explained just previously, for three or more observation stations, especially with errors present, the intersection of the conical-like surfaces in space defined by the respective azimuth-elevation curves from the stations is not unique and that when a second camera is added to one station that station's data essentially receives a higher weighting and the solution is more constrained to lie on the surface from that one station. Hence, the results of Figures 44, 45, and 46 for the north-south, vertical, and total station displacement errors, respectively, are not as alarming as they first might seem.

In the situation of the pointing displacement errors, however, when White Sands was added to a given station case not originally containing it these results did not occur. Hence, the north-south, vertical, and total station displacement errors are more sensitive to this phenomenon than their corresponding pointing displacement errors.

Resultant Displacement Errors for the Aircraft Station

The resultant displacement errors, defined as the square root of the sum of the squares of the corresponding components of the pointing displacement errors and the station displacement errors, were calculated. Then, the per cent differences between the resultant displacement errors and their corresponding pointing displacement errors were calculated.

These resultant displacement errors and these per cent differences between the resultant displacement errors and their corresponding pointing displacement errors are shown in Tables 6, 7, 8, and 9 for the cases 1, 3, 4, and 6, respectively. From these tables it is seen that the per cent differences between the resultant displacement errors and their corresponding pointing displacement errors are indeed significant.

Aircraft Data Weighting Factors

Since the coordinates of the moving aircraft contain uncertainties - which are manifested in the triangulation as station displacement errors, in addition to any pointing displacement errors, rendering resultant displacement errors whose per cent differences with the corresponding pointing displacement errors are significant - it was decided that the data from the moving aircraft should not be weighted as heavily as the data from the fixed, ground-based stations. Some scheme of weighting the data from the different observation stations needed to be devised.

Table 6: Case 1 resultant displacement errors.

Latitude (deg)	E-W Error (km)	% difference with E-W Pointing Error only	N-S Error (km)	% difference with N-S Pointing Error only	Vertical Error (km)	% difference with Vertical Pointing Error only	Total Error (km)	% difference with Total Pointing Error only
-9	5.25	32	7.74	11	80.95	11	81.49	11
-8	5.28	32	10.43	11	79.76	11	80.60	11
-7	5.31	32	13.00	11	78.38	11	79.63	11
-6	5.34	33	15.43	12	76.77	12	78.48	12
-5	5.35	33	17.70	12	74.93	12	77.18	12
-4	5.35	33	19.75	12	72.77	12	75.59	12
-3	5.37	33	21.65	12	70.58	12	74.01	13
-2	5.37	34	23.35	13	68.23	13	72.32	13
-1	5.38	34	24.85	13	65.78	13	70.52	13
0	5.36	34	26.10	13	63.10	13	68.50	13
1	5.35	35	27.19	14	60.47	14	66.51	14
2	5.33	35	28.05	14	57.73	14	64.40	14
3	5.31	35	28.72	14	54.99	14	62.26	14
4	5.27	36	29.20	14	52.21	15	60.06	15
5	5.24	36	29.50	15	49.46	15	57.83	15
6	5.20	36	29.61	15	46.70	15	55.54	15
7	5.15	36	29.54	15	43.95	15	53.20	16
8	5.09	36	29.33	16	41.29	16	50.91	16
9	5.02	37	28.98	16	38.66	16	48.58	16
10	4.97	37	28.53	16	36.16	16	46.33	16
11	4.91	37	27.97	17	33.74	17	44.10	17
12	4.85	38	27.32	17	31.41	17	41.91	17
13	4.78	38	26.54	17	29.14	17	39.70	17
14	4.71	38	25.73	17	27.01	18	37.60	18
15	4.63	38	24.83	18	24.95	18	35.50	18
16	4.55	39	23.89	18	23.01	18	33.47	18
17	4.48	39	22.94	19	21.19	19	31.56	19
18	4.40	39	21.95	19	19.47	19	29.67	19
19	4.33	40	20.93	19	17.85	19	27.86	20
20	4.26	40	19.94	20	16.35	20	26.14	20
21	4.19	41	18.93	20	14.94	20	24.49	21
22	4.11	41	17.93	21	13.64	21	22.90	21
23	4.04	42	16.97	22	12.43	22	21.42	22
24	3.98	42	16.00	22	11.31	22	20.00	23
25	3.91	43	15.07	23	10.27	23	18.65	24
26	3.84	44	14.15	24	9.31	24	17.37	24
27	3.77	44	13.25	24	8.43	24	16.15	25
28	3.74	46	12.53	26	7.70	26	15.17	27

Table 7: Case 3 resultant displacement errors.

Latitude (deg)	E-W Error (km)	% difference with E-W Pointing Error only	N-S Error (km)	% difference with N-S Pointing Error only	Vertical Error (km)	% difference with Vertical Pointing Error only	Total Error (km)	% difference with Total Pointing Error only
-9	4.96	27	8.75	4	91.22	4	91.79	4
-8	5.37	33	11.77	4	89.80	4	90.74	5
-7	5.39	33	14.66	5	88.15	5	89.52	5
-6	5.41	33	17.37	5	86.22	5	88.11	5
-5	5.43	34	19.88	5	84.05	5	86.53	5
-4	5.43	34	22.18	5	81.57	5	84.71	5
-3	5.43	34	24.27	5	79.00	5	82.82	5
-2	5.44	34	26.13	6	76.25	6	80.79	6
-1	5.44	35	27.76	6	73.39	6	78.65	6
0	5.42	35	29.13	6	70.36	6	76.34	6
1	5.40	35	30.31	6	67.31	6	74.02	6
2	5.38	35	31.23	6	64.19	6	71.59	7
3	5.36	36	31.94	7	61.06	7	69.12	7
4	5.33	36	32.42	7	57.90	7	66.49	7
5	5.30	36	32.71	7	54.78	7	64.02	7
6	5.24	36	32.81	7	51.67	7	61.44	8
7	5.19	37	32.70	8	48.60	8	58.80	8
8	5.14	37	32.44	8	45.60	8	56.20	8
9	5.08	37	32.02	8	42.68	8	53.60	8
10	5.02	37	31.49	8	39.88	8	51.06	8
11	4.96	38	30.83	8	37.16	9	48.53	9
12	4.90	38	30.08	9	34.56	9	46.08	9
13	4.82	38	29.20	9	32.04	9	43.62	9
14	4.76	38	28.27	9	29.67	9	41.25	10
15	4.68	39	27.27	10	27.38	10	38.92	10
16	4.60	39	26.21	10	25.22	10	36.66	10
17	4.53	39	25.14	10	23.21	10	34.51	11
18	4.45	40	24.02	11	21.29	11	32.41	11
19	4.38	40	22.89	11	19.50	11	30.39	11
20	4.30	40	21.76	11	17.83	11	28.46	12
21	4.23	41	20.64	12	16.28	12	26.62	12
22	4.16	41	19.52	12	14.84	12	24.87	13
23	4.09	42	18.42	13	13.50	13	23.19	14
24	4.02	43	17.35	13	12.26	14	21.62	14
25	3.95	43	16.29	14	11.11	14	20.11	15
26	3.88	44	15.28	15	10.06	15	18.69	16
27	3.81	44	14.28	15	9.08	15	17.34	16
28	3.78	46	13.44	16	8.25	16	16.22	18

Table 8: Case 4 resultant displacement errors.

Latitude (deg)	E-W Error (km)	% difference with E-W Pointing Error only	N-S Error (km)	% difference with N-S Pointing Error only	Vertical Error (km)	% difference with Vertical Pointing Error only	Total Error (km)	% difference with Total Pointing Error only
-9	7.62	41	10.03	23	105.18	23	105.93	23
-8	7.64	41	13.51	23	103.56	23	104.72	23
-7	7.69	41	16.87	23	101.91	24	103.59	24
-6	7.73	41	20.05	24	99.95	24	102.23	24
-5	7.77	42	23.03	24	97.70	24	100.68	24
-4	7.79	42	25.80	24	95.18	25	98.91	25
-3	7.81	42	28.31	25	92.41	25	96.96	25
-2	7.81	42	30.53	25	89.34	25	94.74	25
-1	7.80	43	32.53	25	86.21	26	92.48	26
0	7.80	43	34.25	26	82.92	26	90.05	26
1	7.77	43	35.71	26	79.51	26	87.51	26
2	7.72	43	36.83	26	75.88	27	84.70	27
3	7.69	44	37.74	27	72.32	27	81.95	27
4	7.66	44	38.46	27	68.84	27	79.23	27
5	7.60	44	38.88	28	65.24	28	76.33	28
6	7.52	44	39.01	28	61.57	28	73.27	28
7	7.45	45	38.97	28	58.04	28	70.30	28
8	7.37	45	38.74	28	54.57	29	67.32	29
9	7.28	45	38.26	29	51.10	29	64.25	29
10	7.18	45	37.68	29	47.79	29	61.28	29
11	7.09	46	36.96	29	44.62	29	58.37	30
12	7.00	46	36.09	30	41.54	30	55.47	30
13	6.88	46	35.07	30	38.53	30	52.55	30
14	6.77	46	33.99	30	35.70	30	49.76	30
15	6.65	46	32.79	30	32.98	31	46.98	31
16	6.53	47	31.54	31	30.39	31	44.28	31
17	6.41	47	30.26	31	27.98	31	41.71	31
18	6.28	47	28.93	31	25.68	31	39.18	32
19	6.16	47	27.57	32	23.52	32	36.76	32
20	6.03	48	26.23	32	21.52	32	34.46	33
21	5.92	48	24.86	32	19.63	33	32.23	33
22	5.79	48	23.51	33	17.88	33	30.10	33
23	5.66	49	22.17	33	16.25	33	28.07	34
24	5.54	49	20.86	34	14.75	34	26.14	34
25	5.41	49	19.57	34	13.35	34	24.32	35
26	5.29	50	18.32	35	12.07	35	22.56	35
27	5.16	50	17.11	35	10.87	35	20.92	36
28	5.08	51	16.12	36	9.90	36	19.58	37

Table 9: Case 6 resultant displacement errors.

Latitude (deg)	E-W Error (km)	% difference with E-W Pointing Error only	N-S Error (km)	% difference with N-S Pointing Error only	Vertical Error (km)	% difference with Vertical Pointing Error only	Total Error (km)	% difference with Total Pointing Error only
-9	7.70	41	10.57	14	110.53	14	111.31	14
-8	7.73	41	14.23	14	108.84	14	110.03	15
-7	7.77	41	17.75	15	107.01	15	108.75	15
-6	7.81	42	21.07	15	104.86	15	107.24	15
-5	7.84	42	24.18	15	102.39	15	105.50	16
-4	7.86	42	27.05	16	99.66	16	103.57	16
-3	7.87	42	29.66	16	96.68	16	101.43	16
-2	7.86	43	31.96	16	93.40	16	99.02	16
-1	7.87	43	34.01	17	90.03	17	96.56	17
0	7.85	43	35.79	17	86.52	17	93.96	17
1	7.83	44	37.28	17	82.91	17	91.24	18
2	7.77	44	38.42	17	79.08	18	88.26	18
3	7.74	44	39.35	18	75.32	18	85.34	18
4	7.70	44	40.05	18	71.62	18	82.42	19
5	7.65	45	40.46	19	67.83	19	79.35	19
6	7.57	45	40.58	19	64.00	19	76.16	19
7	7.50	45	40.52	19	60.29	19	73.03	19
8	7.41	45	40.21	19	56.58	19	69.81	20
9	7.33	45	39.75	20	53.00	20	66.69	20
10	7.23	46	39.12	20	49.59	20	63.59	20
11	7.14	46	38.35	20	46.26	20	60.53	21
12	7.04	46	37.45	21	43.07	21	57.50	21
13	6.93	46	36.37	21	39.94	21	54.46	21
14	6.82	46	35.24	21	37.00	21	51.55	22
15	6.70	47	33.99	22	34.17	22	48.66	22
16	6.58	47	32.69	22	31.47	22	45.85	22
17	6.46	47	31.35	22	28.97	22	43.17	23
18	6.33	47	29.96	23	26.58	23	40.55	23
19	6.21	48	28.55	23	24.34	23	38.02	23
20	6.09	48	27.14	23	22.26	23	35.63	24
21	5.95	48	25.72	24	20.30	24	33.31	24
22	5.84	48	24.31	24	18.48	24	31.09	25
23	5.71	49	23.16	25	16.79	25	28.98	25
24	5.58	49	21.55	25	15.23	25	26.97	26
25	5.46	49	20.21	25	13.78	25	25.06	26
26	5.32	50	18.91	26	12.45	26	23.26	27
27	5.19	50	17.64	26	11.22	26	21.55	27
28	5.12	51	16.59	27	10.19	27	20.12	29

The per cent difference for the $i^{\underline{th}}$ case, $j^{\underline{th}}$ component, and $NA^{\underline{th}}$ point is denoted by $PD_{i,j,NA}$, where i = 1, 3, 4, 6 and denotes the particular combination of observation stations employed and j = east-west, north-south, vertical, or total and denotes the particular displacement error of interest and NA = 1, 2,..., NT, where NT is the total number of solution points. The average per cent difference $(PD_{i,j})_{AV}$ for the $i^{\underline{th}}$ case and the $j^{\underline{th}}$ component is then

$$(PD_{i,j})_{AV} = \frac{\sum_{NA=1}^{NT} PD_{i,j,NA}}{NT} \tag{193}$$

If the weighting factors for the data from all of the fixed, ground-based observation stations are chosen as unity, then it seems appropriate to choose for the aircraft data the weighting factors $w_{i,j}$ given by

$$w_{i,j} = 1 - (PD_{i,j})_{AV}, \tag{194}$$

where i = 1, 3, 4, 6 and j = east-west, north-south, vertical, or total and $(PD_{i,j})_{AV}$ is given by equation 193. Table 10 lists the aircraft data weighting factors for these displacement errors and these station cases containing the aircraft, as calculated using equation 194.

The median per cent difference $(PD_{i,j})_{MED}$, the per cent difference for the solution point with latitude equal to nine degrees, is identical to the average per cent difference in nine instances and differs only by one per cent from the average per cent difference in the remaining seven instances (the four cases times the four components give the

Table 10: Aircraft data weighting factors for the displacement errors for different station cases.

Case #	E - W	N - S	Vertical	Total
1	.63	.85	.83	.83
3	.62	.91	.91	.91
4	.55	.71	.71	.71
6	.54	.80	.80	.80

sixteen instances). Hence, the median per cent difference can be used instead of the average per cent difference, thereby omitting the calculation of the per cent differences for (NA-1) of the solution points and the calculation of the average per cent difference. Hence, a second equation for the aircraft data weighting factors $w_{i,j}$ is then

$$w_{i,j} = 1 - (PD_{i,j})_{MED} \tag{195}$$

Also, for any given case and any given component, the weighting factor as calculated by equation 194 is numerically equal to the average of the ratios of the pointing displacement errors to their corresponding resultant displacement errors. If $PE_{i,j}$ denotes the $j^{\underline{th}}$ component of the pointing displacement error for the $i^{\underline{th}}$ case and $RE_{i,j}$ denotes the $j^{\underline{th}}$ component of the resultant displacement error for the $i^{\underline{th}}$ case, then a third equation for the aircraft data weighting factors is

$$w_{i,j} = \left(\frac{PE_{i,j}}{RE_{i,j}}\right)_{AV}, \tag{196}$$

where the average is again taken over the NT solution points.

Just as the median per cent difference is almost identical to the average per cent difference, the median of the ratios of the pointing displacement errors to their corresponding resultant displacement errors is almost identical to the average of the ratios of the pointing displacement errors to their corresponding resultant displacement errors. Hence, a final equation for the weighting factors for the aircraft data

is just

$$w_{i,j} = \left(\frac{PE_{i,j}}{RE_{i,j}} \right)_{MED} , \qquad (197)$$

where $PE_{i,j}$ is the $j^{\underline{th}}$ component of the pointing displacement error for the $i^{\underline{th}}$ case, $RE_{i,j}$ is the $j^{\underline{th}}$ component of the resultant displacement error for the $i^{\underline{th}}$ case, i = 1, 3, 4, 6 and denotes the particular combination of observation stations employed, j = east-west, north-south, vertical, or total and denotes the particular displacement error of interest, and the subscript MED means that the ratio is for the solution point with latitude equal to nine degrees.

Summary and Conclusions

The single-point two-station triangulation problem, line and multistation triangulation considerations, and the LaRC triangulation method - developed specifically for the Barium Ion Cloud (BIC) Project at the NASA, Langley Research Center - were discussed.

Expressions for the four pointing displacement errors, the three pointing slope errors, and the pointing curvature error in the triangulation solution due to a probable error in the lines-of-sight from the observation stations to the points on the cloud were derived. For a probable error of 0.01 degrees in the lines-of-sight, the pointing displacement, slope, and curvature errors were plotted as functions of the latitude for the nine different combinations of the observation stations chosen for the BIC Project to determine the effect of the number and location of the observation stations on these pointing

errors. It was concluded that the pointing errors are the smallest for the five-station case and are the largest for the two-station case, with the combinations of four and three stations giving intermediate values.

The four pointing displacement errors were plotted for comparison on a single plot and also the three pointing slope errors were plotted for comparison on a single plot as functions of the latitude for the five-station case. It was concluded that the vertical component is the dominant component of the total pointing displacement error throughout the latitudinal region of -9° to 15°, whereas the north-south component is the dominant component of the total pointing displacement error over the latitudinal region of 16° to 28°. It was concluded that the latitude component is the dominant component of the total pointing slope error.

The pointing errors were examined for the observation durations of 10,000 sec, 6,000 sec, and 1,000 sec. It was concluded that the east-west pointing displacement error and the longitude pointing slope error practically remain constant throughout the three observation durations; that the north-south pointing displacement error increases toward the lower-latitude end and decreases toward the higher-latitude end over the 1,000-sec observation duration and first increases and then decreases toward the lower-latitude end and decreases toward the higher-latitude end over the 6,000-sec and 10,000-sec observation durations; and that the vertical and total pointing displacement errors, the latitude and total pointing slope errors, and the pointing curvature error increase toward the lower-latitude end and decrease toward the

higher-latitude end over all three of the observation durations.

The pointing errors were plotted as functions of the latitude for different release points varying in longitude to determine the effect of east-west cloud drift on the pointing errors. It was concluded that for the chosen BIC nominal release point - latitude = 9.229°, longitude = -75.000°, and altitude = 31,633.008 km - the pointing errors increase as the cloud drifts eastward into the longitudinal regions of -63° and -49° and decrease as the cloud drifts westward into the longitudinal region of -91°; as the cloud drifts farther westward into the longitudinal regions of -105° and -119°, the pointing errors increase or decrease depending on the cloud's position in latitude.

The pointing errors were plotted as functions of the latitude for different spacings between the points along the azimuth-elevation curves from the observation stations to determine the effect of the number of input data points on the pointing errors. It was concluded that the spacing between the input data points along the azimuth-elevation curves from the observation stations should be no greater than 1.12 degrees.

The pointing errors were plotted as functions of the latitude for the two-station case with an extra camera added to the Mt. Hopkins station. It was concluded that for the two-station case adding an extra camera to Mt. Hopkins decreases the pointing errors. The pointing displacement errors were calculated for the five-station case with from one to eleven extra cameras added to Mt. Hopkins. It was

concluded that for the five-station case adding extra cameras to Mt. Hopkins increases the north-south, vertical, and total pointing displacement errors.

The four station displacement errors in the triangulation solution due to a probable error of three kilometers in the position of the moving Wallops aircraft station were calculated, using an analogous procedure to that used for calculating the four pointing displacement errors. The station displacement errors were plotted as functions of the latitude for the station cases containing the Wallops aircraft. It was concluded that the north-south, vertical, and total station displacement errors increase when an extra fixed station whose coordinates are close to those of Mt. Hopkins is added. The resultant displacement errors, which are the resulting errors of the corresponding components of the pointing and station displacement errors, and the per cent differences between the corresponding resultant and pointing displacement errors were calculated for the aircraft. It was concluded that the station displacement errors were significant enough to warrant reduced weighting of the aircraft data. Expressions for the weighting factors were derived, and the weighting factors for the Wallops aircraft data were calculated.

LIST OF REFERENCES

1. Justus, C. G.; Edwards, H. D.; and Fuller, R. N.: Analysis Techniques for Determining Mass Motions in the Upper Atmosphere from Chemical Releases. AFCRL-64-187, 1964, pp. 1-16.

2. Whipple, Fred L.; and Jacchia, Luigi G.: Reduction Methods for Photographic Meteor Trails. Smithsonian Contrib. Astrophys., vol. 1, no. 2, 1957, pp. 183-206.

3. Hogge, John E.: Three Ballistic Camera Data Reduction Methods Applicable to Reentry Experiments. NASA TN D-4260, 1967.

4. Long, Sheila Ann T.: Analytical Study to Minimize the Triangulation Error for an Idealized Observation Site Arrangement. NASA TN in preparation.

5. Long, Sheila Ann T.: Comparison of Three Triangulation Methods Applicable to the Barium Ion Cloud Project. NASA TN in preparation.

6. Fricke, Clifford L.: Triangulation of Multistation Camera Data to Locate an Elongated Barium Cloud. NASA, Langley Research Center computer program, 1971.

7. Long, Sheila Ann T.: A Transformation from Geocentric to Geodetic Coordinates and Vice Versa in Powers of the Earth's Flattening. NASA TN in preparation.

Appendix. Transformation from Latitude, Longitude, Altitude to Azimuth, Elevation, Range Coordinates

If the geodetic coordinates of an observation station and of a point in space are known, the line-of-sight from the station to the point in space in azimuth, elevation, and range coordinates can be computed.

The coordinate system of Figure 47 is a local coordinate system centered at the station S. The x axis points east, the y axis points north, and the z axis is vertical (or radial). The azimuth az is measured in the north-east plane, the elevation el is measured out of the north-east plane, and the range r_a is the distance from the station S to the point P in space.

First, the geodetic coordinates of the station and of the point in space are transformed to geocentric coordinates according to equations derived in reference 7.

The latitude, longitude, and range of the station are denoted by ϕ_S, θ_S, and r_S, respectively; the latitude, longitude, and range of the point in space, by ϕ_P, θ_P, and r_P, respectively. From Figure 48 it is seen that the rectangular coordinates of the station S - denoted by x_S, y_S, and z_S - are

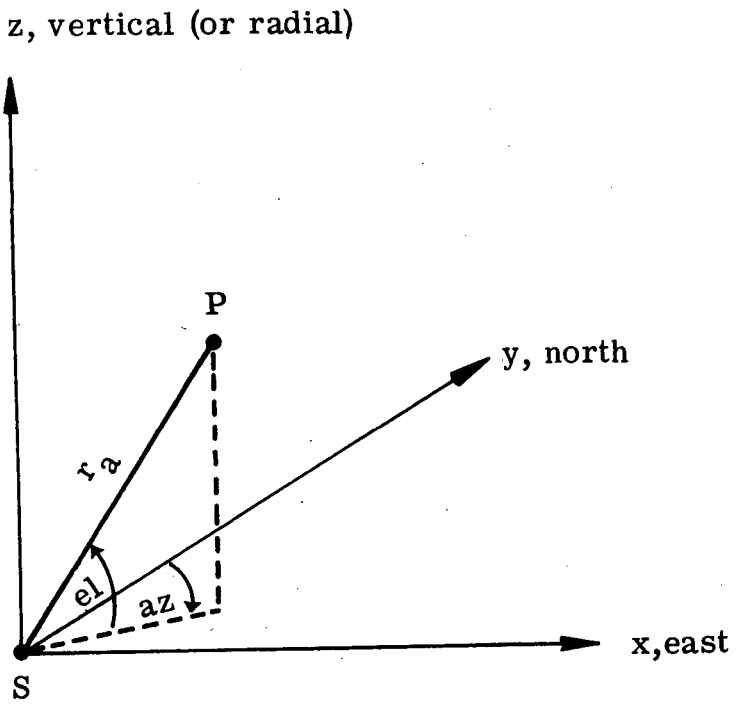

Figure 47.- The azimuth, elevation, and range coordinates of the line-of-sight from an observation station S to a point in space P.

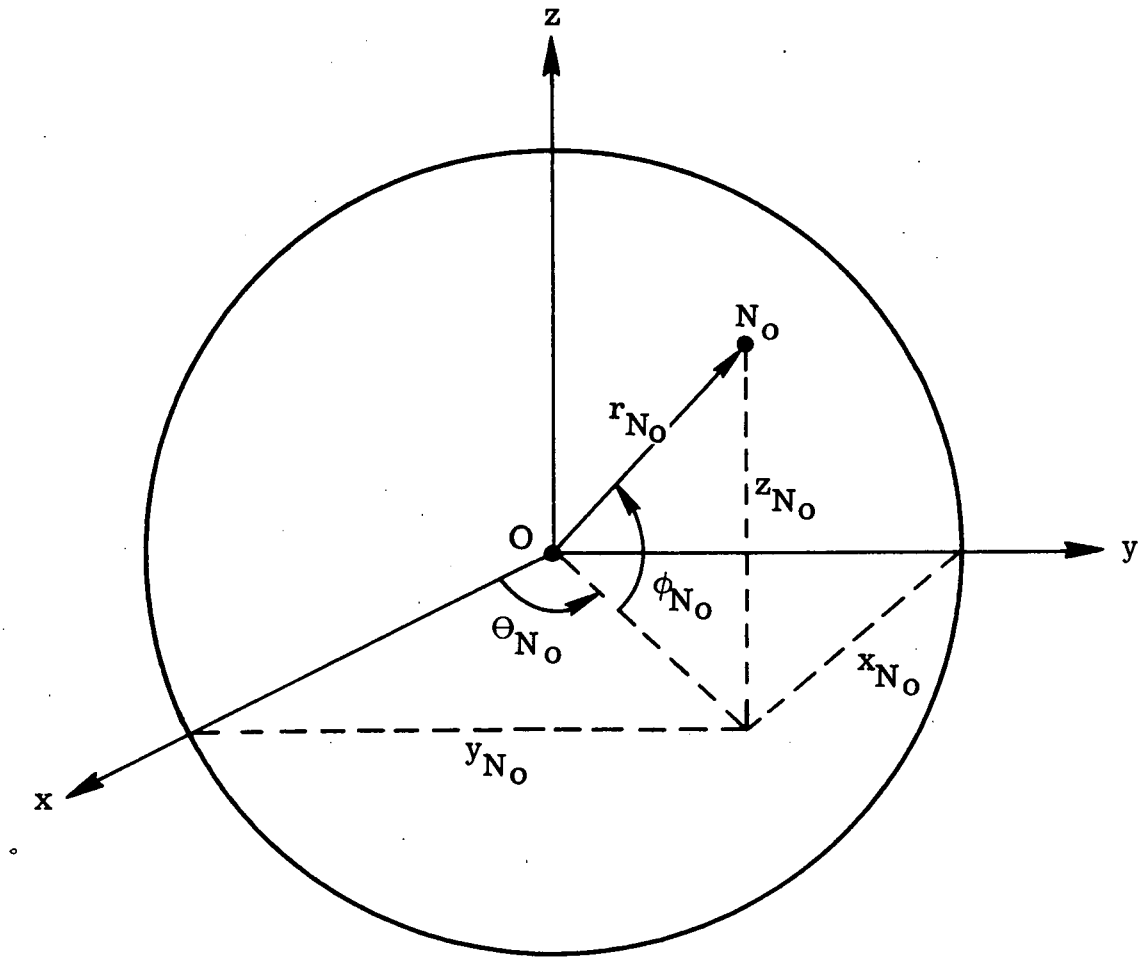

Figure 48.- The geocentric latitude, longitude, and range coordinates of a point N_o.

$$x_S = r_S \cos \phi_S \cos \theta_S \tag{198}$$

$$y_S = r_S \cos \phi_S \sin \theta_S \tag{199}$$

$$z_S = r_S \sin \phi_S \tag{200}$$

And, also from Figure 48, the rectangular coordinates of the point P in space - denoted by x_P, y_P, and z_P - are

$$x_P = r_P \cos \phi_P \cos \theta_P \tag{201}$$

$$y_P = r_P \cos \phi_P \sin \theta_P \tag{202}$$

$$z_P = r_P \sin \phi_P \tag{203}$$

The differences - denoted by x_a, y_a, and z_a - between the respective x, y, z components of the point in space and the station are just

$$x_a = x_P - x_S \tag{204}$$

$$y_a = y_P - y_S \tag{205}$$

$$z_a = z_P - z_S \tag{206}$$

The azimuth az and the elevation el of the line-of-sight from the observation station to the point in space are given by

$$az = \tan^{-1}\left(\frac{x_t}{y_t}\right) \tag{207}$$

$$el = \tan^{-1}\left[\frac{z_t}{\left((x_t)^2 + (y_t)^2\right)^{1/2}}\right], \tag{208}$$

where

$$x_t = - x_a \sin \theta_S + y_a \cos \theta_S \tag{209}$$

$$y_t = - x_a \sin \phi_S \cos \theta_S - y_a \sin \phi_S \sin \theta_S + z_a \cos \phi_S \tag{210}$$

$$z_t = x_a \cos \phi_S \cos \theta_S + y_a \cos \phi_S \sin \theta_S + z_a \sin \phi_S \tag{211}$$

And, the range r_a of the line-of-sight from the observation station to the point in space is given by

$$r_a = (x_a^2 + y_a^2 + z_a^2)^{1/2} \tag{212}$$